United States
Environmental Protection
Agency

Environmental Monitoring
Systems Laboratory
P.O. Box 15027
Las Vegas NV 89114

EPA-600/4-80-019
March 1980

Research and Development

EPA

Multispectral Techniques for Remote Monitoring of Sediment in Water:

A Feasibility Investigation

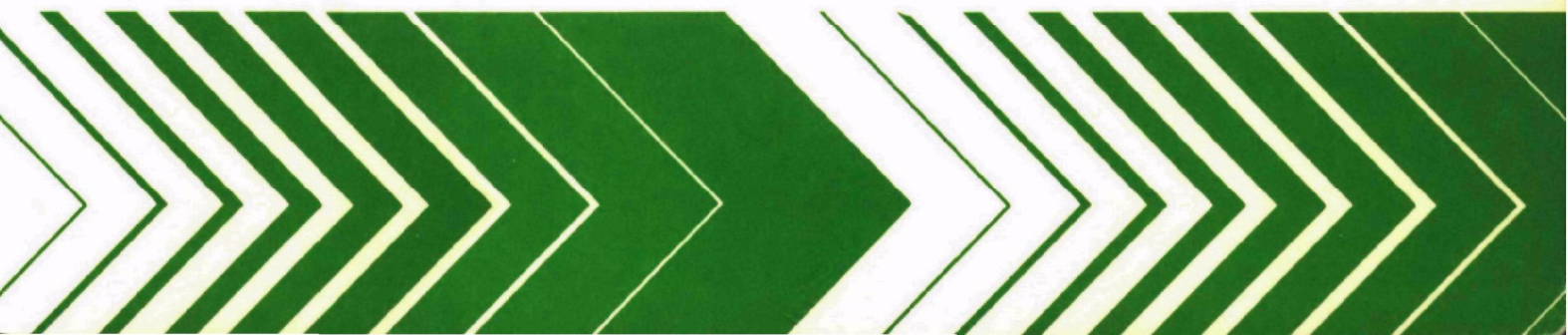

EPA-600/4-80-019
March 1980

MULTISPECTRAL TECHNIQUES FOR REMOTE MONITORING OF SEDIMENT IN WATER: A Feasibility Investigation

by

Ronald J. Holyer
Lockheed Electronics Company, Inc.
Remote Sensing Laboratory
Las Vegas, Nevada 89114

Contract No. EPA 68-03-2153

Project Officer

Gary A. Shelton
Advanced Monitoring Systems
Environmental Monitoring Systems Laboratory
Las Vegas, Nevada 89114

U.S. ENVIRONMENTAL PROTECTION AGENCY
OFFICE OF RESEARCH AND DEVELOPMENT
ENVIRONMENTAL MONITORING SYSTEMS LABORATORY
LAS VEGAS, NEVADA 89114

DISCLAIMER

This report has been reviewed by the Environmental Monitoring Systems Laboratory--Las Vegas, U.S. Environmental Protection Agency, and approved for publication. Approval does not signify that the contents necessarily reflect the views and policies of the U.S. Enviormmental Protection Agency, nor does mention of trade names or commercial products constitute endorsement or recommendation for use.

FOREWORD

Protection of the environment requires effective regulatory actions based on sound technical and scientific information. This information must include the quantitative description and linking of pollutant sources, transport mechanisms, interactions, and resulting effects on man and his environment. Because of the complexities involved, assessment of exposure to specific pollutants in the environment requires a total systems approach that transcends the media of air, water, and land. The Environmental Monitoring Systems Laboratory--Las Vegas contributes to the formation and enhancement of a sound monitoring data base for exposure assessment through programs designed to:

- develop and optimize systems and strategies for monitoring pollutants and their impact on the environment
- demonstrate new monitoring systems and technologies by applying them to fulfill special monitoring needs of the Agency's operating programs

This report considers a method of remotely measuring suspended sediment concentrations in water using multispectral techniques having sufficient accuracy to be feasible for regulatory purposes without the need for continual ground truth support. Federal and state agencies should find this approach promising for large area coverage with a minimum of cost and time. Further information can be obtained from the Remote Sensing Operations Branch of the Environmental Monitoring Systems Laboratory in Las Vegas, Nevada.

George B. Morgan

George B. Morgan
Director
Environmental Monitoring Systems Laboratory
Las Vegas

ABSTRACT

A data acquisition and analysis program has been undertaken to demonstrate the feasibility of remote multispectral techniques for monitoring suspended sediment concentrations in natural water bodies. Two hundred surface albedo measurements (400 to 1,000 nanometers) were made at Lake Mead with coincident water sampling for laboratory analysis. Water volume spectral reflectance was calculated from the recorded surface albedo, and volume reflectance-suspended sediment relationships were investigated. Statistical analysis has shown that quantitative estimates of nonfilterable residue - 105°C and nephelometric turbidity can be made from volume spectral reflectance data with sufficient accuracy to make the multispectral technique feasible for sediment monitoring.

CONTENTS

Foreword		iii
Abstract		iv
Figures		vii
Tables		xi
Abbreviations and Symbols		xii
Acknowledgments		xiii
I	Introduction	1
	Statement of the problem	1
	State-of-the-art overview	2
	Significance of this study as related to previous work	4
	EPA guidelines	5
II	Summary and Recommendations	7
	Conclusion regarding feasibility	7
	Recommendations	8
III	Turbidity	10
	Definition	10
	Methods of measurement	12
IV	Peripheral Effects	14
	General discussion	14
	Mathematical discussion	15
	Magnitude of peripheral effects	32
V	Instrumentation	36
	Spectrometer	36
	Spectrometer mounting	38
	Calibrated reflectance standards	38
VI	Error Analysis	43
	Instrumental uncertainties	43
	Conceptual uncertainties	57
	Laboratory accuracy	67
	Error summary	69
VII	Data Acquisition	72
	Lake Mead test sites	72
	Sampling stations	75
	Field procedures	75
	Data reduction	80
VIII	Data Description	85
	Suspended sediment concentrations	85
	Variability of sediment types	85
	Color interferences	88

CONTENTS (Continued)

IX Data Analysis. 94
Introduction to data analysis 94
Verification of the particle size hypothesis. 97
Polynomial fits to residue/turbidity vs. volume reflectance. 100
A statistical method for obtaining multispectral quadratic algorithms. 109
Evaluation of statistical algorithms. 114
Single channel algorithms for verification of error analysis results 115
Multispectral algorithms. 119
Signature transferability 126
Universal nephelometric turbidity algorithms. 127

X References 132

Appendix A - Conversion Table 135
Appendix B - VOLREF Program Listing 136
Appendix C - ALGOR Program Listing. 153

FIGURES

Number		Page
1	Geometry of measurement points and definition of variables used in removing peripheral effects.	17
2	Correction factor to be applied to approximate alpha for sunlight on a flat water surface	22
3	Surface slope distribution function for several wind velocities	24
4	Mean α correction factors as a function of wind velocity for several sun zenith angles and for skylight	25
5	Radiance distribution for a clear sky (Jerlov, 1968)	28
6	Percent of total underwater energy density attributable to skylight.	33
7	Comparison of surface albedo and calculated water volume reflectances for a typical overcast sky.	34
8	Comparison of surface albedo and calculated water volume reflectances for a typical clear sky	35
9	Spectrometer head, periscope, mounting platform, and reflectance panel holder installed on boat	39
10	Reflectance panel holder in use.	40
11	Typical reflectance values for MgO, Kodak neutral test cards, and painted calibration panels.	42
12	Experimental setup for measuring water reflectance	44
13	Spectral reflectance data for Krylon Gray Primer calibration panels	47
14	Experimental setup for measuring gain of last amplification stage of spectrometer electronics.	48
15	Variance in gain measurements as a function of wavelength. . . .	50

FIGURES (Continued)

Number		Page
16	Average strip chart deflection as a function of wavelength for data used in calculating σ_G^2.	51
17	Variance in illumination and spectrometer electronics as a function of wavelength	52
18	Typical volume spectral reflectance curves for water containing suspended sediment concentrations of 25 and 250 mg/l	54
19	Normalized variance in volume spectral reflectance resulting from instrumental uncertainties	55
20	Sensitivity of reflectance to changes in sediment concentration as a function of wavelength	56
21	Instrumental uncertainties expressed in units of sediment concentration for 25 mg/l water.	57
22	Instrumental uncertainties expressed in units of sediment concentration for 250 mg/l water	58
23	Instrumental uncertainties expressed in units of nephelometric turbidity for 15 and 150 NTU water.	59
24	Maximum depth of water penetration by sunlight assuming reflectance from a panel with a typical sediment spectral reflectance and a two percent return to the surface	62
25	Least-squares linear fits to filterable and non-filterable residue values from the analysis of the Lake Mead water samples	64
26	Albedos, peripheral effects, and volume reflectances of a clear and an overcast day at station MV1.	66
27	Uncertainties in the Lake Mead data as a function of residue and turbidity values.	71
28	Lake Mead test sites.	73
29	Sampling stations at the Colorado River site.	76
30	Sampling stations at the Las Vegas Wash and Government Wash sites	77

FIGURES (Continued)

Number		Page
31	Sampling stations at the Virgin River and Muddy River sites.	78
32	Casting a shadow on the calibration panel.	79
33	Field observations form filled out at each sampling station	81
34	Spectrometer video outputs as recorded on strip chart for sample 35175-1	82
35	Computer printout for the data shown in Figure 34.	83
36	Histogram of nonfilterable residue (105°C) values in the 200 Lake Mead samples	86
37	Spectral reflectance curves for the moistened sediment samples	87
38	Nonfilterable residue (105°C) vs. nephelometric turbidity for all Lake Mead samples in the 50 to 500 mg/l range.	89
39	Spectral absorption curve of a natural phytoplankton population (Yentsch, 1960)	91
40	Statistical estimates of volume spectral reflectance for 0 and 20 NTU turbidity levels.	92
41	Six "best fit" curves for volume reflectance at 652 nm vs. nonfilterable residue (105°C) for silt-sized particles in Lake Mead	96
42	Typical nonfilterable residue-nephelometric turbidity relationships for various particle sizes	98
43	Particle size distribution for Muddy, Virgin, and Colorado River sediment samples.	101
44	Particle size distribution for Las Vegas and Government Wash sediment samples.	102
45	Volume reflectance at 480 nm as a function of nonfilterable residue (105°C).	104

FIGURES (Continued)

Number		Page
46	Volume reflectance at 550 nm as a function of nonfilterable residue (105°C).	105
47	Volume reflectance at 652 nm as a function of nonfilterable residue (105°C).	106
48	Volume reflectance at 782 nm as a function of nonfilterable residue (105°C).	107
49	Volume reflectance at 480 nm as a function of nephelometric turbidiy	108
50	Volume reflectance at 550 nm as a function of nephelometric turbidity.	109
51	Volume reflectance at 652 nm as a function of nephelometric turbidity.	110
52	Volume reflectance at 782 nm as a function of nephelometric turbidity.	111
53	Effects of random noise addition on training set and test set accuracy evaluations.	116
54	Uncertainties in remote measurements based on red or near-IR volume reflectance	118
55	Accuracies of multispectral algorithms for predicting nonfilterable residue (105°C).	124
56	Accuracies of multispectral algorithms for predicting nephelometric turbidity.	125
57	Comparison between accuracies of correct and misapplied six-wavelength algorithms.	129
58	Expected accuracy of universal nephelometric turbidity algorithms	131

TABLES

Number		Page
1	Turbidity-Related Parameters Used in EPA Permits	12
2	JPL Supplied Filter Data	37
3	Size Ranges of Various Particulates	60
4	Sky and Water Condition at Station MV1 on 8/8/75 and 11/14/75	65
5	Uncertainties in Laboratory Analysis Results	68
6	Summary of Uncertainties in the Lake Mead Data in Units of Suspended Sediment	69
7	Summary of Uncertainties in the Lake Mead Data in Units of Nephelometric Turbidity	69
8	Platinum-Cobalt Color Averages by Site	90
9	Grouping of Samples by Site and Particle Size	99
10	Single-Wavelength Algorithms - Particle Size Known	117
11	Multispectral Algorithm Coefficients Fine Sand - Nonfilterable Residue (105°C)	120
12	Multispectral Algorithm Coefficients Silt - Nonfilterable Residue (105°C)	121
13	Multispectral Algorithm Coefficients Fine Sand - Nephelometric Turbidity	122
14	Multispectral Algorithm Coefficients Silt - Nephelometric Turbidity	123
15	Multispectral Algorithm - Nonfilterable Residue (0 to 50 mg/l Silt)	128
16	Multispectral Algorithm - Nephelometric Turbidity (0 to 40 NTU Silt)	128
17	Universal Nephelometric Turbidity Algorithms	130

ABBREVIATIONS AND SYMBOLS

APHA	American Public Health Association
ASTM	American Society for Testing and Materials
AWWA	American Water Works Association
deg.,	degree
EIFAB	European Inland Fisheries Advisory Board
EMSL/LV	Environmental Monitoring and Support Laboratory—Las Vegas
EPA	U.S. Environmental Protection Agency
FET	Field Effect Transistor
IR	infrared
JPL	Jet Propulsion Laboratory of the University of California
mg/l	milligrams per liter
m/sec	meters per second
MΩ	Megohm
N/A	Not available
nm	nanometers
NOIC	National Oceanographic Investigation Committee
NTU	nephelometric turbidity units
OEGC	Office of Enforcement General Counsel
Pt-Co	platinum-cobalt
rms	root mean square
SCS	Scene Color Standard
USDI	U.S. Department of the Interior
VAC	Volts, Alternating Current
VDC	Volts, Direct Current
WPCF	Water Pollution Control Federation

ACKNOWLEDGMENTS

Recognition is given to Mr. John Novotny and Mr. Chuck Lanska of Lockheed Electronics Company, Inc. who redesigned and modified several portions of the EPA spectrometer to increase its sensitivity and reliability to levels acceptable for the requirements of this project.

The quality of the data acquired in the field, and hence the success of this study, was greatly dependent upon proper care in exercising field procedures and upon careful attention to assure proper spectrometer operation. Messrs. Mike Ensminger, Chuck Lanska, and Wilbur McAllister of Lockheed are thanked for their conscientious efforts in assisting the author in performing the field work reported here.

SECTION I

INTRODUCTION

STATEMENT OF THE PROBLEM

Sediment has been defined as soil material which erodes from the surface of the land and is transported to streams and reservoirs by runoff water (USEPA 1973). Suspended sediment is that part of the total fluvial sediment which remains in suspension in water owing to the upward components of turbulent currents or by colloidal suspension (USDI 1959). Suspended sediment in natural water bodies is an environmental problem of major consequence for many reasons. The following are among the more significant effects:

Suspended sediment directly affects light penetration, water temperature, and oxygen transfer which in turn can create unfavorable habitats for aquatic life.

Suspended sediment serves as a mechanism of transport for sorbed minerals and organic substances including many toxic materials.

The aesthetic and recreational value of a water body is reduced by the turbidity resulting from suspended sediment.

Agriculture, silviculture, construction, and mining are among the more important activities of man that contribute sediment to waterways. These sources of sediment loading are not point sources but can involve processes occurring over an entire watershed. This type of nonpoint source pollution is not easily monitored by conventional ground-based sampling techniques. Thus aerial remote sensing techniques are drawing increased attention from the United States Environmental Protection Agency (EPA) as useful tools for monitoring nonpoint source surface water pollution. It has been suggested (USEPA 1975) that remote sensing techniques for measuring suspended sediment concentration could be valuable aids in the following areas:

Identification of sources and potential sources of sediment loading.

Determination of the extent of areas affected.

Quantitative assessment of the distribution of sediment in waterways.

Assessment of the contributions of sediment to waterways from various point and nonpoint sources.

Study of relationships between sediment loading rates and land use practices.

This report covers the first phase of a long-range study the ultimate objective of which is the development of remote sensing techniques for the routine monitoring of suspended sediments. The work performed in this first phase consists of the acquisition of coincident spectral reflectance data and water samples from five sites in Lake Mead, Nevada-Arizona, and the analysis of that data to determine the feasibility of monitoring suspended sediments remotely. Speaking in broad terms, the problem of determining feasibility is thought to consist of the following:

From the Lake Mead data, statistically define the relationships between sediment concentration and the spectral reflectance of the water body.

Based on these statistical relationships, estimate the accuracy, precision, analytical range, and other parameters describing the confidence levels to be expected in remote measurements.

Determine the degree of variability of the reflectance/suspended sediment relationships from site to site in order to evalute the possibility of developing universally applicable multispectral algorithms which would estimate sediment concentrations without the need for extensive ground truth at each monitoring site.

STATE-OF-THE-ART OVERVIEW

The relationship between water spectral reflectance and suspended solids has been the topic of numerous investigations. Conventional and multispectral photography, spectrometers, multispectral scanners, and LANDSAT have all been used as remote sensing systems for previous studies. A small representative sample of some recent work in this field is briefly summarized in the following paragraphs.

Photographic Studies

Color-infrared photography was employed by Rosgen (1975) in a study of the West Fork of the Madison River in southwestern Montana. The concentrations and sources of sediment produced during peak snowmelt runoff were determined by photo densitometric analysis coupled with specifically located ground-truth stations. His conclusion was that, with proper attention to the controls necessary to minimize spectral variability in photographic procedures and microdensitometer analysis, reliable sediment concentrations may be obtained

through photo analysis. He reports a 71.5-milligrams-per-liter (mg/l) standard error in his statistical estimates of suspended sediment concentrations which ranged from 22 to 660 mg/l.

The Upper Truckee River sediment plume in Lake Tahoe was the subject of a recent remote sensing study by Goldman (1974). Aerial color and multispectral photography and simultaneous ground-truth measurements in the lake were subjected to a statistical analysis. Their procedure was to assign a four- or five-level visual density scale to the imagery of the plume. It was found that the correlation coefficients were high between these density values and surface measurements of suspended sediment.

Another recent study involving color-infrared photographs and simultaneous water sampling was performed by Lillesand et al. (1975) in the mixing zone resulting from the discharge of paper mill effluent. The objective was to quantitatively delineate the mixing zone by photographic photometry. It was concluded that, if predicated on a limited amount of ground sampling, these methods could be used to measure and delineate waste distributions as reliably as conventional surface-measuring techniques. Although the authors made no specific statements concerning accuracy, data from this paper have been used to infer a variance at the 25-mg/l level of approximately 0.16. They stated that variations between observed and modeled concentrations could be attributed to the experimental error inherent in collecting and processing the suspended solids ground truth.

The Ross Barnett Reservoir near Jackson, Mississippi, was the test site for a study in which multispectral photography and ground-truth were combined to give a model relating measured turbidities with the spectral responses at the various sample sites. Data from two areas within the reservoir were analyzed and it was noted that the spectral response-turbidity relationship was not the same for both sites.

Other photographic studies include Klooster and Scherz (1974) and Lillesand (1973).

Spectrometer Studies

Ritchie et al. (1974) conducted an in situ measurements program of special interest because of its similarity with the present study. The reflected solar radiation from the surface waters of six northern Mississippi lakes was measured using a portable spectrometer. Their objective was to determine the relationship between the reflected solar radiation and the concentration of total solids in the surface waters. This study indicated that a quantitative relationship existed, but the relationships apparently were not the same for all six lakes. The need is pointed out for further studies to determine if separate regression models are needed for each lake or if a composite model could be used on all lakes.

Multispectral Scanner Studies

An aircraft-borne multispectral scanner study has been conducted by Pionke and Blanchard (1975) leading to the conclusion that the suspended sediment concentrations of 14 Oklahoma impoundments were related to spectral reflectance. They investigated the transferability of the relationships from one area to another and concluded that a relationship can be applied to other areas providing sediment characteristics controlling reflectance are similar. Soil color or geologic origin were thought to be the most important factors influencing transferability and that textural differences are of little significance.

LANDSAT Studies

Klemas et al. (1974) related ground-truth sediment concentration values to LANDSAT band 5 radiance values with an exponential function and found good correlation between modeled and ground-truth values. They go on to state that such a method promises not only to yield a mathematically expressible relationship between concentration and radiance but also, by identification of typical spectral signatures, allows identification of sediment and certain pollutants. If this method is refined by using a greater number of bands, they feel it may even be capable of distinguishing between different sediment types.

LANDSAT data have been widely used in studies of such water clarity indicators as secchi disc extinction depth, Jackson candle turbidity, and the mass/volume of suspended solids. Other investigators applying LANDSAT data to these types of problems include Kritikos et al. (1974), and Bowker et al. (1975).

SIGNIFICANCE OF THIS STUDY AS RELATED TO PREVIOUS WORK

Most previous studies, including those just cited, share a common "case study" approach to the sediment/water reflectance problem. This approach consists of the coincident acquisition of remote and ground-truth data. Remote statistical algorithms are derived based on the ground-truth and then applied back to that same data set to evaluate performance. The result is a case study demonstrating the existence of relationships between suspended solids and reflected radiance.

The desire of EPA to use remote sensing techniques as routine monitoring tools demands a departure from the traditional case study approach to a more universal understanding of the reflectance properties of sediment-bearing water-bodies. If extensive ground truth is required at each monitoring site for purposes of calibrating the remote algorithm, the use of remote methods would be greatly reduced. The objective of this study is to examine the variability of sediment/reflectance relationships to determine the need for local calibration of remote algorithms.

Ritchie et al. (1974), Pionke and Blanchard (1975), and Blanchard and Leamer (1973) have investigated the transferability of signatures but not in sufficient depth to evaluate realistically the feasibility of remote methods for EPA monitoring. Thus the present study is seen as a logical and significant extension of the state-of-the-art from a case study understanding toward a more general knowledge of suspended sediment signatures which would permit quantitative remote monitoring with little or no ground truth.

EPA GUIDELINES

The feasibility of a remote technique for some specific application is generally not a case of yes or no; the answer lies in a set of trade-off relationships between many variables. Sensitivity, accuracy, ground-truth requirements, spatial resolution, cost effectiveness, data processing requirements and many other variables can normally be improved at the expense of one or more of the others. The complexity of the trade-off relationships can be reduced if a priori knowledge is available concerning acceptable limits on some of the variables. Therefore, it is necessary to consider certain guidelines which have been established by the EPA.

Requirements have been issued (USEPA 1975) for four parameters related to the problem of remote monitoring of suspended sediments. One of these, spatial resolution, is not considered in the present study, but the other three, which are discussed briefly below, are related to the problem at hand.

Sensitivity

The sensitivity criterion is based on the philosophy that suspended sediments should be detectable down to the lowest concentration at which a measurable effect on water uses or aquatic life is first produced. The European Inland Fisheries Advisory Board reports the minimum level which has any harmful effects on fisheries is 25 mg/l (EIFAB 1965). This level has, therefore, been established as the detection threshold for suspended sediment.

Accuracy and Precision

Accuracy is a measurement of how close the result of an experiment comes to the "true" value. Precision is a measure of the spread of sample values about their own mean. If there is no bias in experimental and estimation procedures, accuracy and precision can be considered synonymous.

The EPA (USEPA 1975) requirement does not establish values for accuracy and precision individually because the "true" value of sediment measurements is difficult to determine. Therefore, the guideline is that the sum of the inaccuracy and imprecision shall result in a variance of the remote estimate not to exceed 0.05. It is assumed that this value is a normalized variance which is not to be exceeded over the entire analytical range down to the

25-mg/l detection threshold. To prevent any ambiguity, the EPA accuracy requirement, as interpreted for purposes of this project, can be expressed mathematically as

$$\frac{N^2}{(N-1)} \sum_{i=1}^{N} (s_i - s_i')^2 \left(\sum_{i=1}^{N} s_i \right)^{-2} < 0.05 \qquad (1)$$

where s_i is the ith remote estimate of suspended sediment concentration

s_i' is the ground truth value at the ith point

N is the number of estimates.

This requirement corresponds to a ±5.6-mg/l standard deviation in remote estimates at a 25-mg/l concentration.

Laboratory measurements of nonfilterable residues in the 25-mg/l range have uncertainties ranging from ±4.3 to ±8.2 mg/l depending on the drying temperature (see Table 7). Thus the accuracy guideline for remote measurements is comparable to the accuracy of standard laboratory techniques. This requirement may be too stringent to lie within the capability of a remote sensing system. The question arises as to whether this type of accuracy is really needed when evaluated in the light of the intended applications for remote sediment monitoring systems.

SECTION II

SUMMARY AND RECOMMENDATIONS

CONCLUSION REGARDING FEASIBILITY

The objective of this study was to demonstrate the feasibility of multispectral techniques for remote monitoring of sediment in water. The introductory section of this report stated that feasibility would be demonstrated by following a three-part approach consisting of defining relationships, estimating accuracies, and investigating signature transferability. Each of these three study areas is dealt with in Section IX of this report. The findings regarding each question are summarized in general terms below:

> Quadratic least-squares fits relating volume spectral reflectance to nephelometric turbidity and nonfilterable residue (105°C) have been statistically defined for single and multiple wavelengths. Thus the existence of sediment-reflectance relationships has been demonstrated.
>
> These statistically defined relationships were cast into a form suitable for predicting nephelometric turbidity and nonfilterable residue values from spectral reflectance data. The accuracy of these prediction algorithms depended upon which parameter was being predicted, number of wavelengths used, range of parameter values, etc. However, in most cases accuracy evaluations resulted in values close to the $\sigma^2 = 0.05$ EPA requirement.
>
> It was discovered that nonfilterable residue algorithms could be transferred among sites with a relatively small reduction in accuracy if the size of the suspended particles was known. However, nephelometric turbidity algorithms were found to be transferable between all Lake Mead test sites with virtually no loss in accuracy and without knowing particle size. Thus the possibility seems promising for operational implementation of remote techniques without the need for continual ground truth support.

Answers in each of these three fundamental question areas were encouraging. It is concluded that the evidence presented here speaks strongly in favor of the feasibility of remote multispectral techniques for EPA monitoring purposes.

RECOMMENDATIONS

Promotion of Nephelometric Turbidity

One of the more important results of this study has been the emergence of nephelometric turbidity as a much more desirable parameter for remote monitoring than is nonfilterable residue which is now the most widely used measurement. It is expected that EPA will concur with the conclusions of this report and pursue a long-range program to bring remote multispectral techniques to an operational status. If this be the case, it is strongly recommended that nephelometric turbidity be promoted within the environmental community as the primary suspended sediment related parameter.

In some situations the mass/volume value may be important and it may not be possible to substitute nephelometric turbidity for nonfilterable residue. However, it is suspected that nonfilterable residue is often specified in discharge permits because it is traditional to do so and not because the mass/volume is really significant. In these cases if permits could be written in units of nephelometric turbidity it would definitely facilitate the eventual implementation of remote monitoring.

The big advantage of nephelometric turbidity is its signature transferability. However, there are several other important advantages associated with this parameter.

This study has shown that nephelometric turbidity is more accurately related to volume spectral reflectance than is nonfilterable residue.

Nephelometric turbidity can also be more accurately measured on the water samples collected for accuracy verification.

Nephelometric turbidity can be measured in the field using an inexpensive turbidimeter, whereas, nonfilterable residue necessitates sample storage, transportation, and laboratory analysis.

Future Studies

The study reported here was only a first step toward the long-range objective of operational remote monitoring of suspended sediment. The feasibility of this goal has been demonstrated, but continuing study will be required to gain the additional knowledge necessary for upgrading these techniques to the status of an operational monitoring tool. Many areas need further investigation but there are two of primary importance that are recommended for the next phase of study.

Geographical Expansion of the Data Base

The conclusions resulting from this study are significant if they are true in general and not just a peculiarity of Lake Mead. To verify these conclusions in the general sense it is recommended that additional data acquisition be performed at several other water bodies in geographically diverse locations.

Atmospheric Effects

Data acquisition for this project was performed from a boat. Therefore, we could not investigate the effects that the intervening atmosphere would have on a remotely sensed surface albedo. Indications are that the magnitude of atmospheric effects can be larger than the surface albedo itself. Thus accurate removal of atmospheric effects from airborne data will be a necessity.

It is recommended that the extension of data acquisition to other geographical locations be accomplished from an airborne platform so that the resulting data can serve as input to the analysis of the atmospheric effects problem.

SECTION III

TURBIDITY

DEFINITION

Light scattered by sediment particles gives water a cloudy or turbid appearance. In discussing the optical properties associated with the presence of particles in water, the term "turbidity" arises constantly. Unfortunately the topic of water turbidity is not clearly defined. There are three authoritative sources of guidelines for the measurement and definition of turbidity: American Public Health Association's (APHA) "Standard Methods ..." (1971); EPA's "Methods ..." (1973); ASTM's "Annual Book of ..." (1973). These sources do not agree with each other in all respects and often a single source will contain internal ambiguities.

In May of 1974 the National Oceanographic Instrumentation Center (NOIC) sponsored an interdisciplinary workshop on turbidity to identify the various applications for turbidity data and to determine techniques for turbidity measurement. The proceedings of that workshop were published and conclusions and recommendations were made (Proceedings, NOIC ..., 1974). A complete treatment of the topic of water turbidity is beyond the scope of this report. The interested reader is referred to the aforementioned proceedings and to a recent review paper (Pijanowski 1975) for a more complete discussion.

One recommendation of the NOIC workshop, which will be followed in this report, was that turbidity should be defined as a qualitative and relative appearance descriptor of water clarity. To illustrate this definition the analogy was drawn between turbidity and "warmth" which is also a qualitative and relative term. One does not measure warmth; one measures temperature. Likewise one does not measure turbidity; one measures beam transmittance, scattering coefficient, or some other quantitative parameter.

An attempt has been made to compile a composite and consistent set of definitions of turbidity-related parameters from the three references previously cited. Because of the ambiguous nature of the topic this attempt is not completely successful. However, for purposes of this report, terminology will be used according to the definitions given below.

> Absolute Turbidity--the fractional decrease of incident monochromatic light through the sample, integrating both scattered and transmitted light.

Apparent Color--includes both the color due to substances in solution (true color) and the color due to suspended matter (turbidity).

Dissolved--filterable.

Filterable Residue--that portion of the total residue which passes through a filter (glass fiber filter discs, without organic binder, Reeve Angle Type 934-A 984-H, Gelman Type A, or equivalent).

Fixed Residue--nonvolatile residue.

Jackson Candle Turbidity--an empirical measure of turbidity in special apparatus. Based on the measurement of the depth of a column of water sample that is just sufficient to extinguish the image of a burning standard candle observed vertically through the sample.

Nonfilterable Residue--that portion of the total residue retained by a filter.

Nephelometric Turbidity--an empirical measure of turbidity based on a measurement of the light-scattering characteristics (Tyndall effect) of the particulate matter in the sample.

Nonsettleable Residue--that part of the total residue which will not settle (floating or dissolved material).

Nonvolatile Residue--that part of the total residues remaining after ignition for 1 hour at 550°C.

Particulate Matter--that matter, exclusive of gasses, existing in the nonliquid state which is dispersed in water to give a heterogeneous mixture.

Settleable Residue--that part of the total residue which will after sitting (or centrifuging to speed the process) settle to the bottom of the sample containers measured volumetrically.

Suspended--nonfilterable.

Total Residue--the sum of the homogeneous suspended and dissolved materials in a sample; evaporated and dried at 103°C to 105°C.

True Color--the color of water after the turbidity has been removed. The recommended method for the removal of turbidity is centrifugation.

Turbidity--a qualitative descriptor of water clarity.

Volatile Residue--that part of the total residues lost after ignition for one hour at 550°C.

METHODS OF MEASUREMENT

It is important to note that there are certain initial constraints on how suspended sediment is to be measured. The U.S. EPA issued permits for turbid discharges in natural waterways. To achieve maximum compatibility with existing guidelines, it would be desirable if remote monitoring could measure the same parameters specified in existing permits. Thus frequency of usage within the scientific/legal community dealing with water quality is felt to be an important criterion in deciding how sediment concentrations should be measured for this project.

A partial tabulation of the parameters specified in existing permits has been compiled by the Environmental Monitoring Systems Laboratory--Las Vegas (USEPA, undated memorandum). This tabulation listed 165 water quality parameters, of which 11 were thought to be closely related either directly or indirectly to water turbidity. An example of an indirect relationship would be that of certain dissolved solids which in themselves are colorless and cause no turbidity, but which are nutrients stimulating algae growth which results in water turbidity. Table 1 lists these turbidity-related parameters in order of decreasing frequency of occurrence in existing permits.

TABLE 1. TURBIDITY-RELATED PARAMETERS USED IN EPA PERMITS

Parameter	Number EPA Permits
Nonfilterable Residue (105°C)	3954
Settleable Residue (volumetric)	675
Nonsettleable Residue	404
Nonfilterable Residue (180°C)	334
Filterable Residue (180°C)	278
Nephelometric Turbidity (NTU)	235
Total Residue (105°C)	56
Filterable Residue (105°C)	51
Color (Pt-Co Units)	25
Fixed Residue (550°C)	9
Nonfilterable, Volatile Residue	6

Notice that in Table 1 a drying temperature is often specified. The three drying temperatures most commonly used give the following results:

105°C--the sample retains mechanically occluded water and water of crystallization. Organic loss is very slight if at all.

180°C--mechanically occluded water is almost all gone, some water of crystallization remains. Organic matter is reduced but not completely destroyed.

550°C--mechanically occluded water, water of crystallization, and organic matter are all gone.

The frequency-of-usage criterion clearly dictates the nonfilterable residue dried at 105°C as the best parameter to relate to spectral reflectance signatures. However, this parameter seems to be oriented toward point source wastewater discharges because it includes both organic and inorganic particulate matter. The nonpoint source water pollution, for which the remote techniques are especially useful, would consist primarily of inorganics such as silt, sand, and clay particles. This type of particulate matter would probably best be represented by nonfilterable, fixed residue. The fixed residue measurement, however, is virtually unused at this time. Furthermore, the elevated drying temperature (550°C) results in decreased accuracy in the laboratory measurement of this parameter. Thus, the choice between nonfilterable residue (105°C) and nonfilterable, fixed residue (550°C) is not obvious.

Fortunately, the water samples collected from Lake Mead contained negligible amounts of organic particulate matter and the two measurements were essentially equivalent. Thus, nonfilterable residue (105°C) has been selected as the primary water parameter of interest for this initial phase of study.

Nine of the 11 parameters listed in Table 1 (settleable and nonsettleable residues were omitted) were measured on the water samples collected at Lake Mead. In the course of the spectral data analysis it was found that nephelometric turbidity was a significant parameter. Nephelometric turbidity and nonfilterable residue (105°C) are then the two water quality parameters that have been used in the statistical analysis reported here. The other seven are not included in the analysis but are available if needed for more detailed analysis in the future.

The analysis of water samples was performed in the laboratories of the Methods Development and Analytical Support Branch at the EPA's Environmental Monitoring Systems Laboratory--Las Vegas (EMSL-LV). Measurements were conducted according to standard methods as defined by the American Public Health Association (1971). The reader is referred to this source for a detailed discussion of laboratory methods.

SECTION IV

PERIPHERAL EFFECTS

GENERAL DISCUSSION

The color of a water body, as observed from the air, is dependent upon phenomena that can be classified into four categories: illumination source, atmosphere, surface reflection, volume reflection. Only volume effects are indicative of water turbidity. Thus the volume spectral reflectance of the water, $\rho_w(\lambda)$, is the parameter which should be correlated with suspended sediment concentration (nonfilterable residue). Source, atmospheric, and surface effects are called peripheral effects because they mask the water color resulting from volume reflectance.

Peripheral effects have been ignored by most previous investigators who have usually worked with the surface albedo which is defined as the ratio of the energy leaving the water to that falling on it (Jerlov 1968). The albedo, therefore, contains the sum of the surface reflection plus the light backscattered from the water volume. If the albedo is measured from some altitude above the surface, the apparent albedo also contains light scattered into the sensor aperture by the intervening atmosphere. Using the surface albedo is a valid procedure for the typical "case study" approach where a statistical algorithm relating the albedo to some water quality parameter is derived from data collected the same day and under the same conditions as the data to which the algorithm will be applied. In this case peripheral effects have the same effect on all data and tend to cancel out in the statistical analysis. However, in developing a general algorithm for application to various data sets taken under differing conditions, peripheral effects must be removed, leaving the volume spectral reflectance which should be invariant under differing environmental conditions.

In developing a technique for removal of peripheral effects, the long-range objective of the project must be kept in mind. That objective is the development of techniques for remote turbidity measurement which are applicable to an airborne multispectral scanner. Therefore, any techniques must be easily transferable from boat data to airborne data. A technique similar to the Scene Color Standard (SCS) Technique (Piech and Walker 1971) was chosen as the best method of correcting the spectrometer data collected for this project, and also as being the most promising for use with airborne data.

The SCS technique originally had no provision for wind effects on the optical properties of the surface. Also, the lens effect (see page 20) of the surface was previously overlooked but has been added here. These changes should improve the accuracy of peripheral effects removal.

The following is a summary of some of the features which have been influential in the selection of this technique:

The technique can be used without ground truth if common materials of known reflectance can be found in the imagery.

If ground truth is required or desired to improve accuracy, only two spectral reflectance measurements are needed.

These measurements can usually be made days or weeks after overflight.

The above feature means that one can avoid the traditional shotgun approach to ground truth, i.e., gather as much data as possible in the hope that one will have the one or two numbers needed for data analysis. Data can be examined in detail first, and a team then sent out to get only the specific pieces of information that can be used.

Switching from boat to aircraft will require no change in the data quantification procedure.

The transition from spectrometer to scanner will also be no problem since many of the scan angle corrections have been included in the derivation, and those ignored can easily be added without impacting the basic analysis procedures.

Absolute calibration of the sensor is not required.

MATHEMATICAL DISCUSSION

The categorization of interfering color effects into illumination source, atmospheric, and surface reflection is convenient for conceptual purposes, because it facilitates an understanding of the physical processes involved in color masking. However, it is difficult to measure and remove these groups of effects from airborne data. The SCS technique is based on a grouping of peripheral effects into three parameters: α, α', and β. This grouping simplifies the mathematics, and most importantly, it makes the solution of the color masking problem practical.

The parameters α, α', and β are functions of wavelength and must, therefore, be evaluated for each spectral band sampled by the spectrometer. For a given wavelength band, the energy reaching the sensor can be written

$$E = \alpha\rho_w + \alpha'\rho_s + \beta \qquad (2)$$

The term $\alpha\rho_w$ is the energy resulting from reflection within the water with volume reflectance ρ_w. The energy coming from surface reflection of skylight is $\alpha'\rho_s$ where ρ_s is the reflectance of air-water interface. Correction for surface reflection of sunlight has not been included. Thus, ρ_w cannot be determined in the sun glitter portion of the imagery. Light that has never reached the scene, but is scattered into the sensor by the air column in the sensor field of view, is represented by the term β. Equation (2) gives a complete account of all of the factors influencing apparent water color, and it is from this equation that volume spectral reflectance must be obtained.

The parameter α is proportional to total irradiance, atmospheric transmittance, and water surface transmittance. It varies with weather conditions, sun angle, and many other factors which are individually unknown. The philosophy behind the SCS technique is that, although the variables cannot be measured individually, they can be lumped together as a single parameter, α, and the cumulative effects given a numerical value. Likewise, α', which is proportional to atmospheric transmittance and skylight irradiance, can be evaluated as a cumulative effect influencing surface reflection. Atmospheric scattering and total irradiance influences β, which can also be evaluated by the SCS technique.

Once numerical values have been assigned to α, α', and β, Equation (2) can be solved for ρ_w. This is done in each spectral band, and the result is the true volume spectral reflectance with color masking by peripheral effects removed.

Evaluation of Beta

Let us assume that the voltage output of the sensor is proportional to energy falling on the detector. This voltage is biased by some value, V_o, and thus,

$$V = k_\lambda E + V_o \qquad (3)$$

where k_λ is the calibration coefficient for wavelength λ. Within the scene imaged by the sensor we must find the shadow of some opaque object falling on a uniform reflecting surface as shown in Figure 1. We need not know ρ_c', the reflectance of the surface.

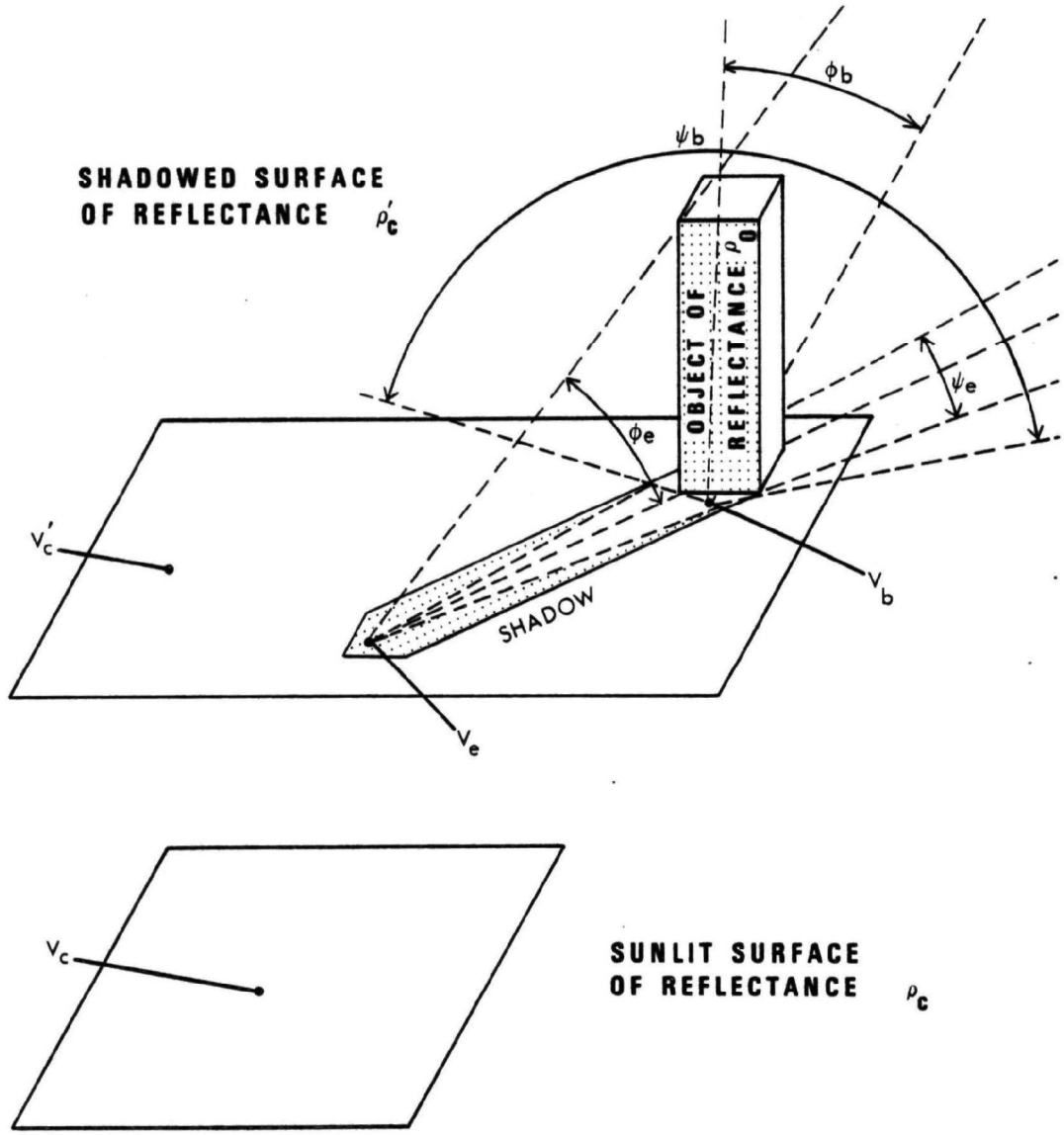

Figure 1. Geometry of measurement points and definition of variables used in removing peripheral effects.

The voltage out of the sensor as it looks at the outer edge of the shadow is

$$V_e = k_\lambda(k_e\alpha'\rho_c' + \beta) + V_o \tag{4}$$

and as the view is near the base of the object,

$$V_b = k_\lambda(k_b\alpha'\rho_c' + \beta) + V_o \tag{5}$$

Solving Equations 4 and 5 simultaneously gives

$$\beta = [k_eV_b - k_bV_e - V_o(k_e - k_b)]/k_\lambda(k_e - k_b) \tag{6}$$

The constants k_e and k_b are functions of object size, object reflectance, and sun angle. The object size and sun angle can be determined by photogrammetric techniques if stereo photo coverage is obtained from the sensor platform. The object reflectance, ρ_o, could be estimated for common materials, or an in situ reflectance measurement could be made to improve accuracy. Either k_e or k_b are approximated by the equation

$$k = 1 - \left[\frac{(\sin\phi)(1-\rho_o)\psi}{2\pi}\right] \tag{7}$$

where ψ is the horizontal angle in radians subtended by the object width

ϕ is the vertical angle subtended by the object height as viewed from the shadow edge or object base respectively.

Note from Equation 7 that if $\rho_o = 1$, then $k_e = 1$ and $k_b = 1$, and Equation 6 for β becomes undefined. Thus accuracy in β calculation is improved with smaller ρ_o values. Narrow objects also are preferable to wide ones since they maximize the quantity $(k_e - k_b)$ thus improving accuracy in β. In the optimum case where ρ_o would be nearly zero and the object very narrow, $k_e \simeq 1$ and $k_b \simeq \frac{1}{2}$. Beta in this idealized case would reduce to

$$\beta \simeq 2V_b - V_e - V_o)/k_\lambda \tag{8}$$

Approximation of Alpha

Alpha is approximated by finding in the scene, a sunlit surface of known reflectance, ρ_c. The reflectance of common surfaces may be estimated, or accuracy improved by measuring ρ_c. In either case, the voltage output as the sensor views the surface will be

$$V_c = k_\lambda(\alpha\rho_c + \beta) + V_o \tag{9}$$

Therefore,

$$\alpha_{approx} = (V_c - V_o - k_\lambda\beta)/k_\lambda\rho_c \tag{10}$$

This approximate α is used to calculate α', and then α' is used to convert the approximate α to the exact value.

Evaluation of Alpha Prime

The first step in the calculation of α' is to measure V_c', the output as the sensor views the sunlit portion of the shadowed surface of reflectance ρ_c'. This voltage is given by

$$V_c' = k_\lambda(\alpha\rho_c' + \beta) + V_o \tag{11}$$

which can be solved for ρ_c'.

$$\rho_c' = (V_c' - V_o - k_\lambda\beta)/k_\lambda\alpha \tag{12}$$

This value for ρ_c' is substituted into Equation 4 or 5 to give α'.

Using Equation 4, the solution for α' becomes

$$\alpha' = \alpha(V_e - V_o - k_\lambda\beta)/k_e(V_c' - V_o - k_\lambda\beta) \tag{13}$$

Correction of Approximate Alpha

The parameter α was determined from a solid surface of known reflectance. In this case, all incident energy is available for reflection and all reflected energy is propagated up into the atmosphere. However, in the volume reflectance of water, not all energy incident on the surface enters the water to be available for possible scattering. Likewise, not all back-scattered energy enters the atmosphere since some will be reflected back into the volume by the air-water interface. Transmittance of the water surface is a function of incidence angle and surface roughness.

The volume scattering problem is further complicated by the fact that the light entering the water undergoes a lens effect (Jerlov 1968) where light is refracted at the interface because of the discontinuity in the index of refraction. This refraction effect must be accounted for in relating the irradiance of reflectance panels in the air to the energy flux density in the water volume. The lens effect, like surface transmittance, is a function of surface roughness.

These factors differentiating water scattering from solid surface reflectance, which were ignored in the original SCS technique, have been accounted for here by making a correction to α_{approx}. The correction factor will include several surface transmittance and lens effect calculations as discussed in the following paragraphs.

Correction for Surface Transmittance of Sunlight

Since α is intended to be proportional to the incident energy density in the water volume, estimates of α made from observing the irradiance of a horizontal panel in the air must be reduced by reflection losses at the surface. Fresnel's Equation for the reflectance of unpolarized light from a plane air-water interface is

$$\rho_s(z) = \tfrac{1}{2}\left[\frac{\sin^2(z-j)}{\sin^2(z+j)} + \frac{\tan^2(z-j)}{\tan^2(z+j)}\right] \qquad (14)$$

where z is the sun zenith angle

$$j = \sin^{-1}(\sin z/1.33);$$

Thus, the first correction to α_{approx} is

$$\alpha = \alpha_{approx}\,(1 - \rho_s(z)) \qquad (15)$$

Correction for Lens Effect on Sunlight

Having corrected for surface transmittance, α is now correct if irradiance of an underwater horizontal panel were in question. However, α should be proportional to underwater energy density, not underwater surface irradiance. Underwater energy density would irradiate an underwater horizontal panel with efficiency equal to cos j. Thus, to determine energy density the α for underwater surface irradiance is modified further by removing the cos j factor. The total correction to α_{approx} for the direct sunlight case is then given by

$$\alpha = \alpha_{approx}(1 - \rho_s(z))/\cos j \qquad (16)$$

The name "lens effect" is used for the cos j term because j is a refraction related parameter and the magnitude of this correction is a function of the index of refraction.

The symbol τ will be used to represent the total correction factor for parallel rays of light incident on a flat water surface.

$$\tau = (1 - \rho_s(z))/\cos j \qquad (17)$$

Figure 2 is a plot of τ as a function of incidence angle. In this figure the difference between the Fresnel transmittance curve and τ is attributable to the lens effect. Piech and Walker (1971) included Fresnel reflection corrections in the SCS technique, but did not make any lens effect corrections which could introduce errors of as much as 20 percent at larger zenith angles. This error cannot be tolerated if volume spectral reflectance is to be quantified with a variance of less than 0.05.

Correction for Wind Roughening of Water Surface

When the surface of a water body is roughened by wind, the sloped wave faces alter the angle of incidence of sunlight. Also, sloped and curved surfaces will influence the magnitude of the lens effect. This problem has been handled by considering the rough surface to consist of a large number of small facets (plane surfaces). Equation 17 can be used to calculate the α correction factor for each facet, and these can be averaged to give a mean correction factor for the rough surface.

The distribution of facet slopes has been shown to be a function of a single variable, wind velocity (Cox and Munk 1956). Their experimental data was best fit with the Gram-Charlier Series of fourth order Hermite polynomials. This distribution can be approximated, with sufficient accuracy for

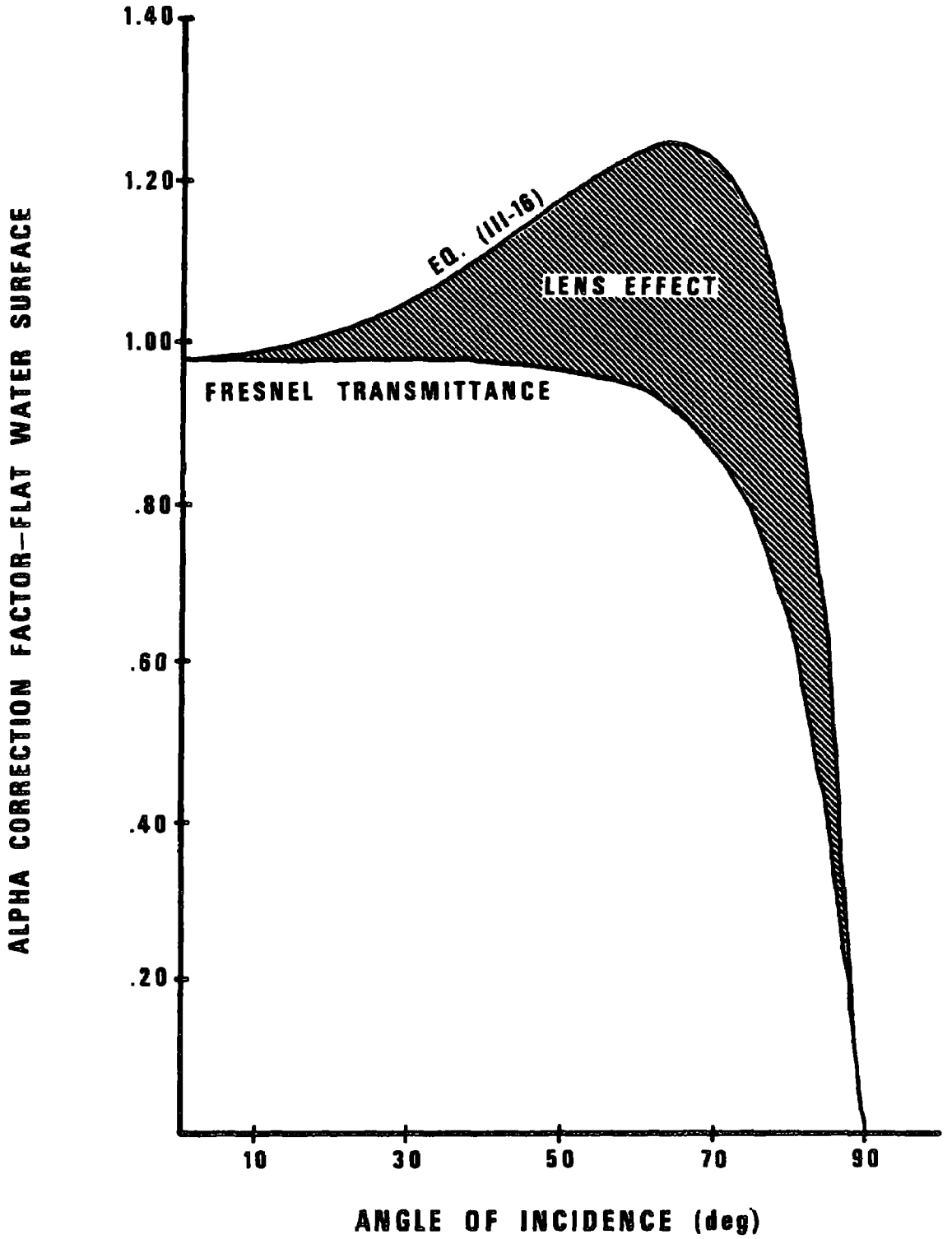

Figure 2. Correction factor to be applied to approximate alpha for sunlight on a flat water surface.

purposes of this project, by a Gaussian distribution function. In general, Cox and Munk found the distribution of upwind slope components to differ from crosswind slope component distributions. However, the spectrometer was mounted on the boat such that the field of view would normally include a superposition of direct waves and waves reflected from the side of the boat. In this mixture of waves traveling in different directions it has been assumed that any asymmetry with respect to wind direction has been lost. The standard deviations of the distributions of both upwind and crosswind slope components are given by

$$\sigma_u = \sigma_c = \left[\tfrac{1}{2}(0.003 + 0.00512W)\right]^{\frac{1}{2}} \tag{18}$$

where W is the wind velocity in meters/second.

The probability of a facet having a slope with upwind and crosswind components of u and c is

$$P(u,c) = \frac{1}{2\pi\sigma_u\sigma_c} e^{-\frac{1}{2}(u^2/\sigma_u^2 + c^2/\sigma_c^2)} \tag{19}$$

This is a two-dimensional distribution function, but since it is symmetrical, it can be represented by one-half a cross-section in any direction. Figure 3 shows the cross-section of the slope probability function for several wind velocities.

If the α correction factor for each facet and the probability of occurrence of any facet slope are known, it is possible to calculate the mean correction factor for the entire roughened surface. This becomes a numerical integration problem which is accomplished by stepping in small increments through all possible facet slopes and summing each τ weighted by P_i the normalized probability of slope angle γ_i. Let z be the incidence angle of sunlight on the ith facet.

$$\tau = \frac{1}{\cos z} \sum_{i=1}^{N} \frac{P_i[1 - \rho_s(z_i)] \cos z_i}{\cos j_i \cos \gamma_i} \tag{20}$$

The cos γ_i term in the above equation is a correction term resulting from the fact that a rough water surface has more area than a flat one.

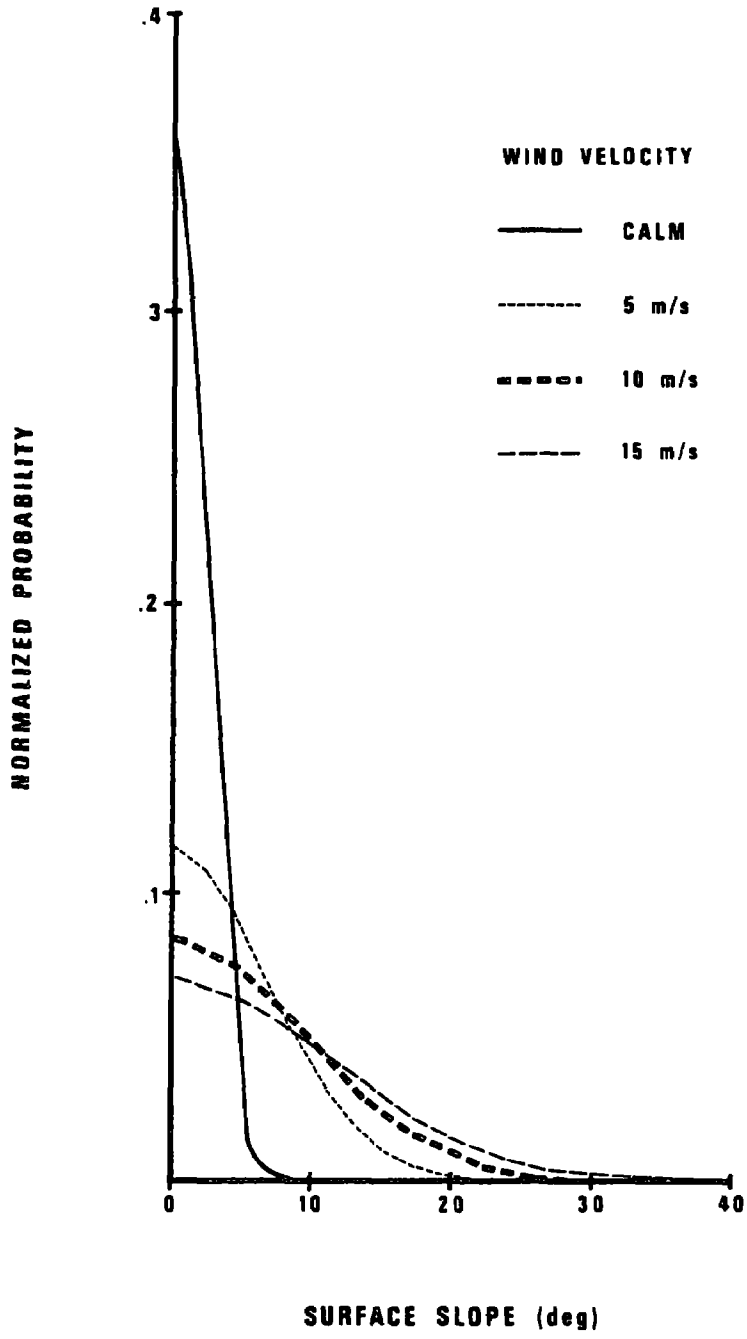

Figure 3. Surface slope distribution function for several wind velocities.

Figure 4 shows the mean α correction factor as a function of wind velocity for several sun zenith angles. Note that wind roughening does not have a drastic effect. For zenith angles less than 45° the correction factor increases with increasing wind, but for angles larger than 45° it decreases. At 45° the α correction is independent of the presence of waves.

Correction of Surface Transmittance and Lens Effect for Skylight on a Flat Water Surface

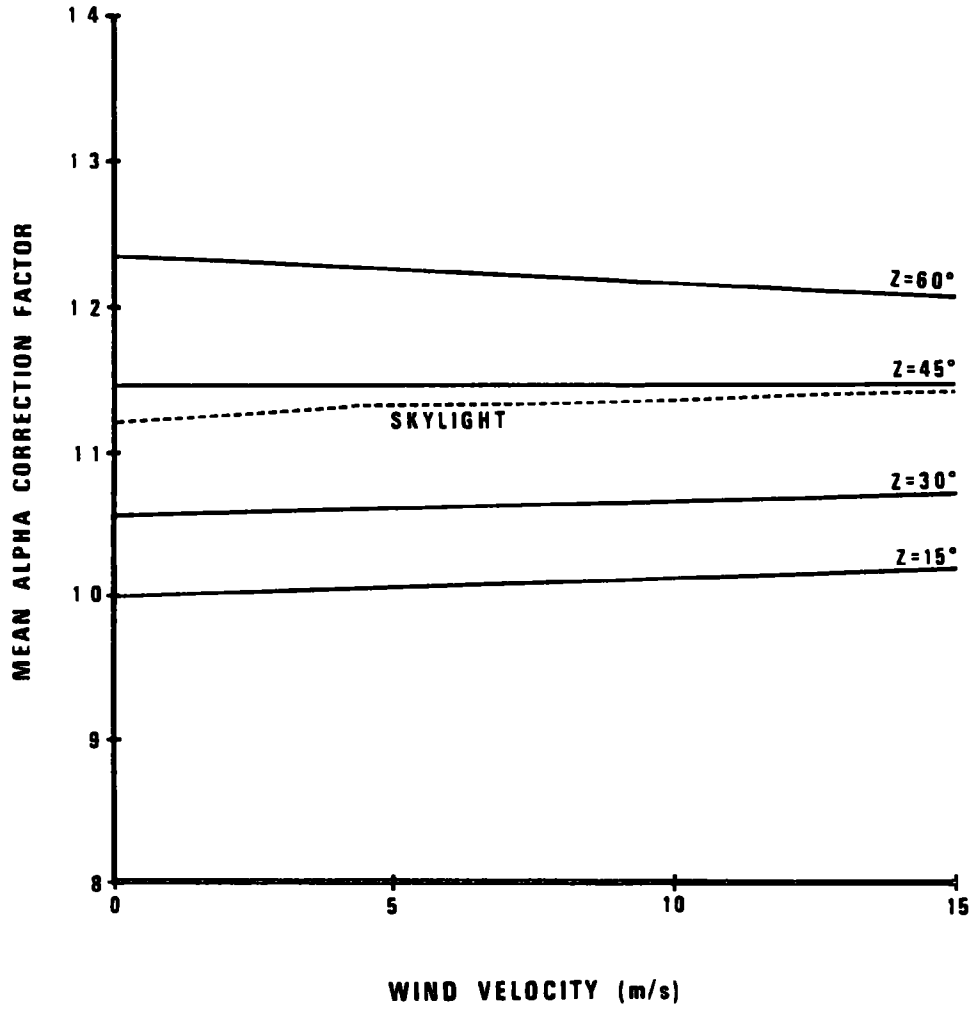

Figure 4. Mean α correction factors as a function of wind velocity for several sun zenith angles and for skylight.

In addition to direct sunlight, indirect sunlight scattered by the atmosphere illuminates the earth's surface. This scattered sunlight, called skylight, differs from direct sunlight in that it is incident upon the water surface from all directions rather than being in parallel rays with a single incidence angle. Alpha is proportional to the underwater energy density and, therefore, contains a contribution from skylight as well as sunlight. That portion of α_{approx} attributable to skylight must be corrected by a factor τ' which includes Fresnel transmittance and lens effects for skylight.

The skylight case can be evaluated numerically by considering a large number of point sources equally spaced about the sky. The contribution of the k source to the surface illumination is

$$I_k = I_0 \cos z_k \tag{21}$$

where I_0 is the illumination from a source directly overhead

z_k is the zenith angle of the k source.

The correction for irradiance from the k source is given by Equation 17. Summing the transmitted energy flux density from all k sources and dividing this by the sum of the surface irradiance from all sources gives τ'.

$$\tau' = \left[\sum_{k=1}^{K} [1 - \rho_s(z_k)]/\cos j_k \cos z_k \right] / \sum_{k=1}^{K} \cos z_k \tag{22}$$

This expression would be correct if skylight were unpolarized and the sky were of equal radiance at every point.

Unlike sunlight, which is unpolarized, light from a clear sky is partly polarized. The degree of polarization is dependent on the part of the sky under observation, the solar elevation, and the air turbidity (Sekera 1957). Polarization can range from zero to over 90 percent. Clouds have a strong depolarizing effect (Jerlov 1968). Therefore, the Fresnel reflectance used in Equation 22 is not necessarily applicable to the skylight case. However, we join with previous investigators, including the SCS technique developers, and ignore the polarization of skylight.

In developing the SCS technique, Piech and Walker (1971) also assumed that skylight was a uniform radiance distribution. Many other investigators have done likewise, and under this assumption the skylight correction factor calculated from Equation 22 is 1.115.

As the sky becomes overcast the radiance, L, can be represented as a function of incidence angle by a cardiodal distribution (Moon and Spencer 1942).

$$L(z) = L(\pi/2)\ (1 + 2\cos z) \tag{23}$$

Neither the uniform nor cardiodal distributions are really representative of a clear sky.

The clear sky radiance distribution (Jerlov 1968) shown in Figure 5 has a maximum near the sun and a minimum on the antisolar side. Weighting factors, W_k, for each of the k sources included in the calculation were taken from Figure 5. The transmittance is then given by

$$\tau' = \frac{\sum_{k=1}^{K} w_k [1 - \rho_s(z_k)]/\cos j_k \cos z_k}{\sum_{k=1}^{K} w_k \cos z_k} \tag{24}$$

This equation gives a correction factor of 1.122 which is not appreciably different from that calculated for uniform radiance. The distribution in Figure 5 was for a 40° sun elevation, and as the sun elevation changes, the skylight distribution also changes. For purposes of this project sun elevation has not been included as a variable affecting skylight α correction factors. The 40° sun elevation case is typical for our data and so the distribution given in Figure 5 was used in all cases.

Correction for Skylight on a Wind-Roughened Surface

As was the case with sunlight, the α correction factor for skylight will also be affected by the wind-induced roughening of the water surface. The correction factor for this case can be numerically evaluated as before by considering the rough surface to be made up of N facets. If the sky radiance is approximated by K sources, the correction factor for the k source is given by Equation 20. Summing the corrections of all k sources and normalizing by the total surface irradiance from all sources gives the skylight α correction factor for a wind-roughened surface.

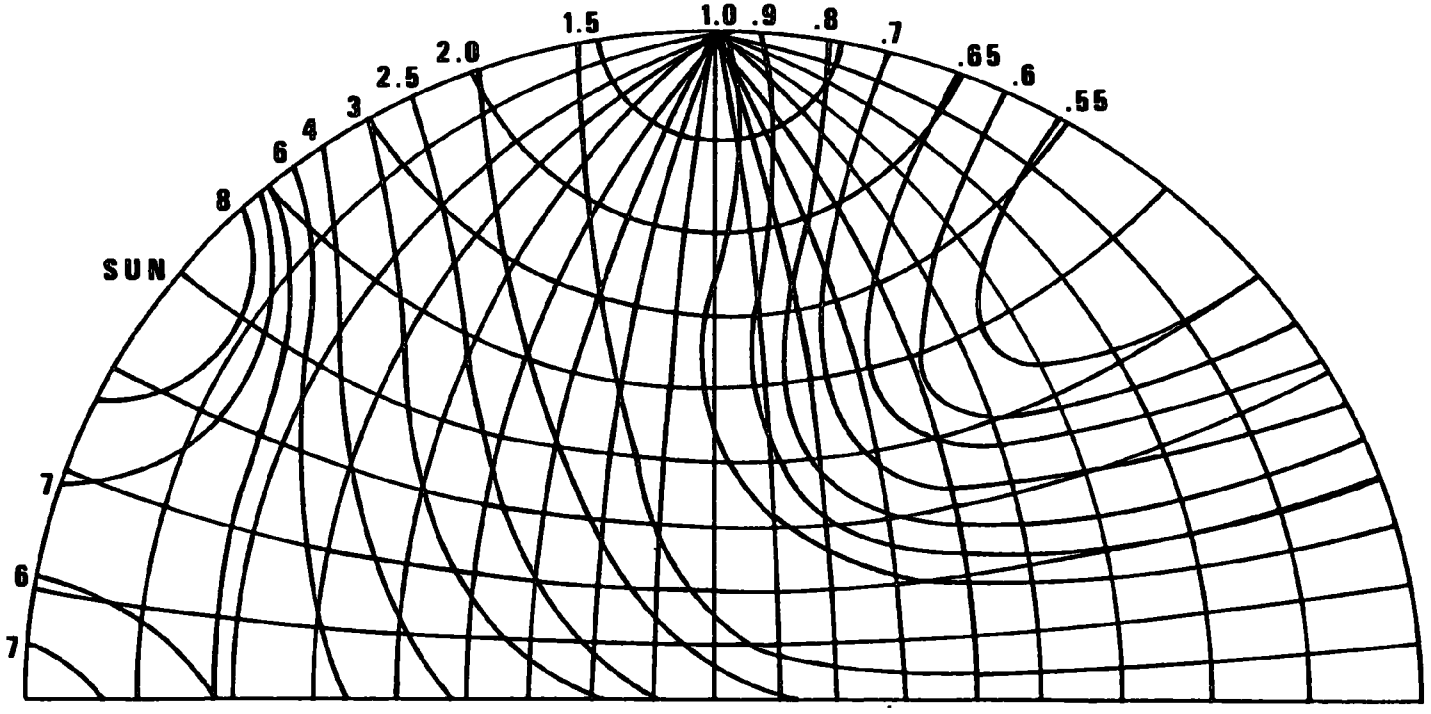

Figure 5. Radiance distribution for a clear sky (Jerlov, 1968).

$$\tau' = \frac{\sum_{k=1}^{K} w_k \cos z_k \sum_{i=1}^{N} P_i [1 - \rho_s(z_{ik})]/\cos j_{ik} \cos \gamma_i}{\sum_{k=1}^{K} w_k \cos z_k} \qquad (25)$$

This equation has been evaluated as a function of wind velocity using the radiance distribution shown in Figure 5. These results were included in Figure 4. The skylight α correction factor model Equation 25 was not evaluated for each data set because the calculations are very time consuming. The skylight factor was taken rather from the piecewise linear relationship shown in Figure 4.

$$\tau' = \begin{cases} 1.122 + 0.0022W & (W<5) \\ 1.133 + 0.0006(W - 5.0) & (W>5) \end{cases} \qquad (26)$$

By adding the lens effect and wind roughening the α correction factor for skylight is substantially different from that used in the SCS technique. For a typical case where W = 5 m/sec, a difference of 21 percent exists between our value of 1.133 and Piech and Walker's (1971) value of 0.934. This difference does not introduce a significant error into volume reflectance on clear days where less than 10 percent of the total irradiance is from skylight. However, on overcast days skylight accounts for nearly half of the total irradiance and this inaccuracy in the SCS technique is significant.

Surface Transmittance for Upwelling Light

As upwelling light reflected from within the water volume encounters the air-water interface another transmittance factor must be considered. The surface reduces the amount of upwelling energy entering the atmosphere and increases the irradiance of the water volume because of internal reflection.

With upwelling energy leaving the surface at angle θ, the observation angle is reduced by the Fresnel reflectance, $\rho_s(\theta)$; because of refraction, light leaving the surface at angle θ will be incident on the water surface from below an angle j where $j = \sin^{-1}(\sin\theta/1.33)$. If, as in the downwelling case, one considers the water surface to consist of numerous facets, the summation of transmittance over all facets yields the following expression for the effective transmittance, T, of upwelling light through the entire wind-roughened surface.

$$T = \frac{\sum_{i=1}^{N} P_i [(1 - \rho_s(\theta_i)] \cos j_i / \cos \gamma_1}{\sum_{i=1}^{N} P_i \cos \theta_i / \cos \gamma_i} \quad (27)$$

Light incident upon the water surface from below at angles greater than 48.6° is totally reflected back into the water volume. The upwelling scattered light can be considered diffuse to the first approximation, which means that a considerable amount of upwelling energy is incident on the surface at angles greater than 48.6°. Jerlov (1968) has evaluated the internal reflectance of water for upwelling diffuse light to be 48 percent. This internal reflection in effect adds to the irradiance of the water volume. For typical cases where $\rho_w \simeq 0.1$ and the slanting paths of internally reflected light are quite long, errors caused by ignoring internal reflection are on the order of 2 percent. Internal reflection was ignored in the data reduction procedures used here. It should be noted, however, that for high particulate concentrations (> 250 mg/l) where $\rho_w \simeq 0.2$ and mean free path lengths are small, ignoring internal reflection could cause errors on the order of 10 percent.

Summary of Approximate Alpha Correction

Equation 2 is the basic defining equation for removal of peripheral effects. In that equation, α represents the light available for scattering in the water volume just below the surface. Alpha was approximated by looking at a standard calibration panel exposed to both sun and sky irradiance. The direct sunlight component of α_{approx} is then

$$\alpha_{sun} = \alpha_{approx} - \alpha' \quad (28)$$

There are basic differences between reflectance of a panel above the water and scattering in an underwater volume. Thus the α_{approx} calculated from the reflectance panels in Equation 10 is not exactly correct for representing energy available for scattering. The transmittance, reflectance, and lens effect factors just discussed are employed to correct α_{approx} to a value truly representative of the water case. The sun component of α_{approx} is multiplied by the correction factor for sunlight (Equation 20) and the correction factor for upwelling light (Equation 27). Alpha prime is multiplied by the correction factor for skylight (Equation 25) and the correction factor for upwelling light (Equation 27). The corrected α is then given by

$$\alpha = \tau T \alpha_{approx} + T(\tau' - \tau)\alpha' \quad (29)$$

Evaluation of Skylight Reflectance

Reflected sunlight has been eliminated by avoiding observation angles where this effect occurs. However, surface reflected skylight will be present in any observation of a water body. The second term in Equation 2 represents reflected skylight. For a flat water surface the skylight reflectance, $\rho_s(\theta)$, is the Fresnel reflectance (Equation 14) evaluated at the observation angle, θ.

If the surface is roughened by wind, the surface reflectance can be computed by averaging the individual reflectances of a large number of facets as was done in the α correction factor calculation.

$$\rho_s(\theta) = \frac{\sum_{i=1}^{N} P_i \rho_s(\theta_i) \cos \theta_i / \cos \gamma_i}{\sum_{i=1}^{N} P_i \cos \theta_i / \cos \gamma_i} \tag{30}$$

Since only vertical observation data are included in the present analysis and because the surface slope distributions (Figure 3) show no slopes greater than 30°, any reflected skylight reaching the spectrometer was reflected at an incidence angle of 30° or less. Fresnel reflectance is nearly constant 0.02 over the 0° to 30° range, thus, this value was used and the individual reflectance of facets were not averaged. In dealing with other than vertical observation angles in the future, Equation 30 will have to be evaluated.

Calculating Volume Spectral Reflectance

Combining Equations 1 and 2 gives an expression for voltage output by the sensor when viewing water.

$$V_w = k_\lambda \alpha \rho_w + k_\lambda \alpha' \rho_s(\theta) + k_\lambda \beta + V_0 \tag{31}$$

Solving this equation for water reflectance results in the water volume reflectance with peripheral effects removed.

$$\rho_w = (V_w - k_\lambda \alpha' \rho_s(\theta) - V_0)/\alpha k_\lambda \tag{32}$$

For data taken from a boat, air-light is not a factor so the $k_\lambda \beta$ term has been dropped. The constants α, α', and V_0 are, in general, functions of wavelength. The volume spectral reflectance, $\rho_w(\lambda)$, is obtained when each

wavelength sampled by the spectrometer is evaluated in terms of these constants and solved in Equation 31.

The parameter k_λ, the spectrometer sensitivity, cancels out when the derived expressions for α, α', and β are substituted into Equation 32. This means that an absolute calibration of the spectrometer is not required. The only requirement is that the calibration be constant over the duration of a measurement sequence.

MAGNITUDE OF PERIPHERAL EFFECTS

Peripheral effects which mask the volume spectral reflectance of a water body obviously exist, but the question arises as to the magnitude and significance of these effects. What error could be expected if removal of peripheral effects were ignored and multispectral turbidity estimates were based on the albedo rather than volume reflectance? Is the accuracy of remote turbidity measurements increased significantly over the SCS technique? Two sample cases are presented here to indicate the typical magnitude of peripheral effects, and to provide a comparison between the two correction methods.

The sample chosen to represent a typical clear sky case was sample 24775-7 taken on 9/4/75 at the mouth of the Colorado River. The sun elevation for this observation was 50.2° and there was no wind. A Muddy River sample, 32375-5, was chosen to represent a typical case with a thinly overcast sky. Sun elevation in this case was 25.6° and a 1 m/s (3 mph) breeze was blowing when this sample was collected on 11/19/75. Figure 6 shows α'/α which represents the percentage of total underwater illumination which originates as skylight for these two cases. As would be expected intuitively the amount of skylight relative to direct sunlight is increased by the overcast which was quite thin in this case. For a heavy cloud cover, skylight would probably account for about 50 percent of the underwater energy density across the entire spectrum.

Since surface reflected skylight is one of the peripheral effects in question, it would be expected that the difference between the albedo and the volume reflectance would be larger on overcast days. Figures 7 and 8 show the albedo, SCS technique volume reflectance, and Equation 32 volume reflectance for the overcast and clear skies respectively. As expected the peripheral effects and the variation between methods is greater for the overcast sky than for the clear sky. The difference between the albedo and Equation 32 ranges from 20 percent to 30 percent in the visible part of the spectrum for the overcast case and from 10 percent to 15 percent for the clear case. In most places the SCS technique makes up less than one-half of this difference. Thus, the difference between Equation 31 and the SCS technique is definitely significant.

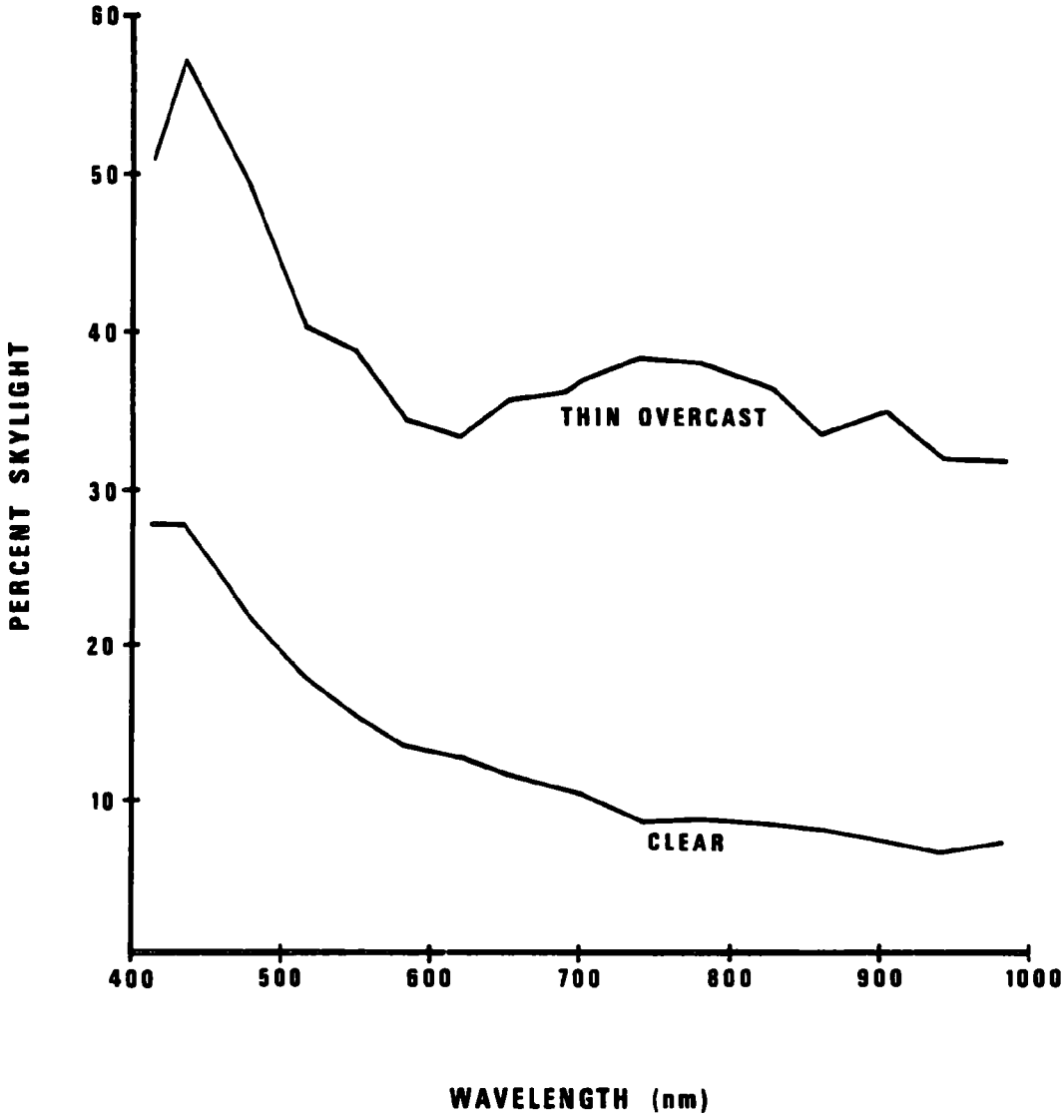

Figure 6. Percent of total underwater energy density attributable to skylight.

Based on these two samples it appears that the magnitude of typical peripheral effects can range from 10 percent to 30 percent of the volume spectral reflectance depending on weather conditions. Peripheral effects are definitely too large and too variable to be ignored if remote turbidity measurement is to be accomplished with EPA's desired accuracy.

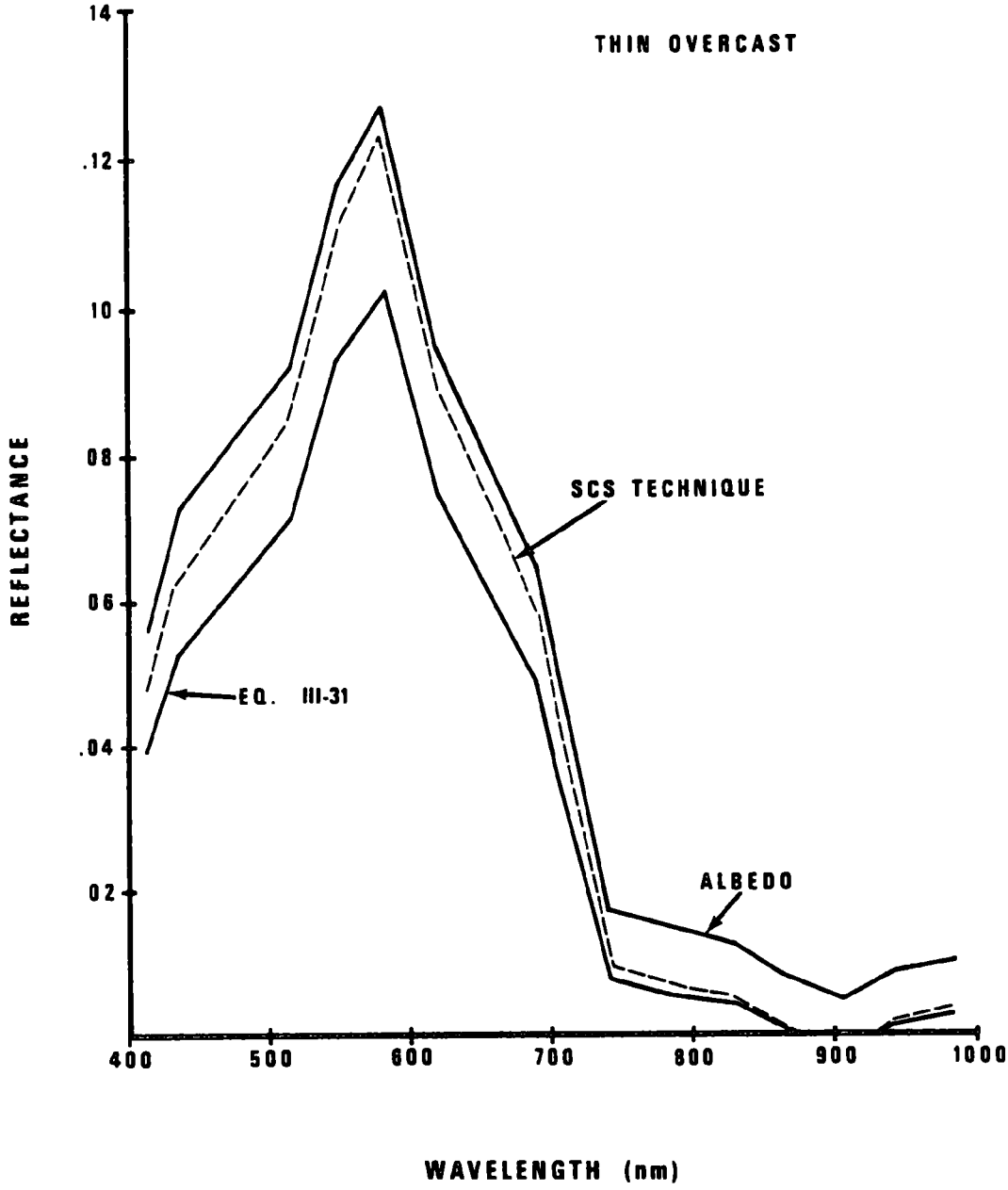

Figure 7. Comparison of surface albedo and calculated water volume reflectances for a typical overcast sky.

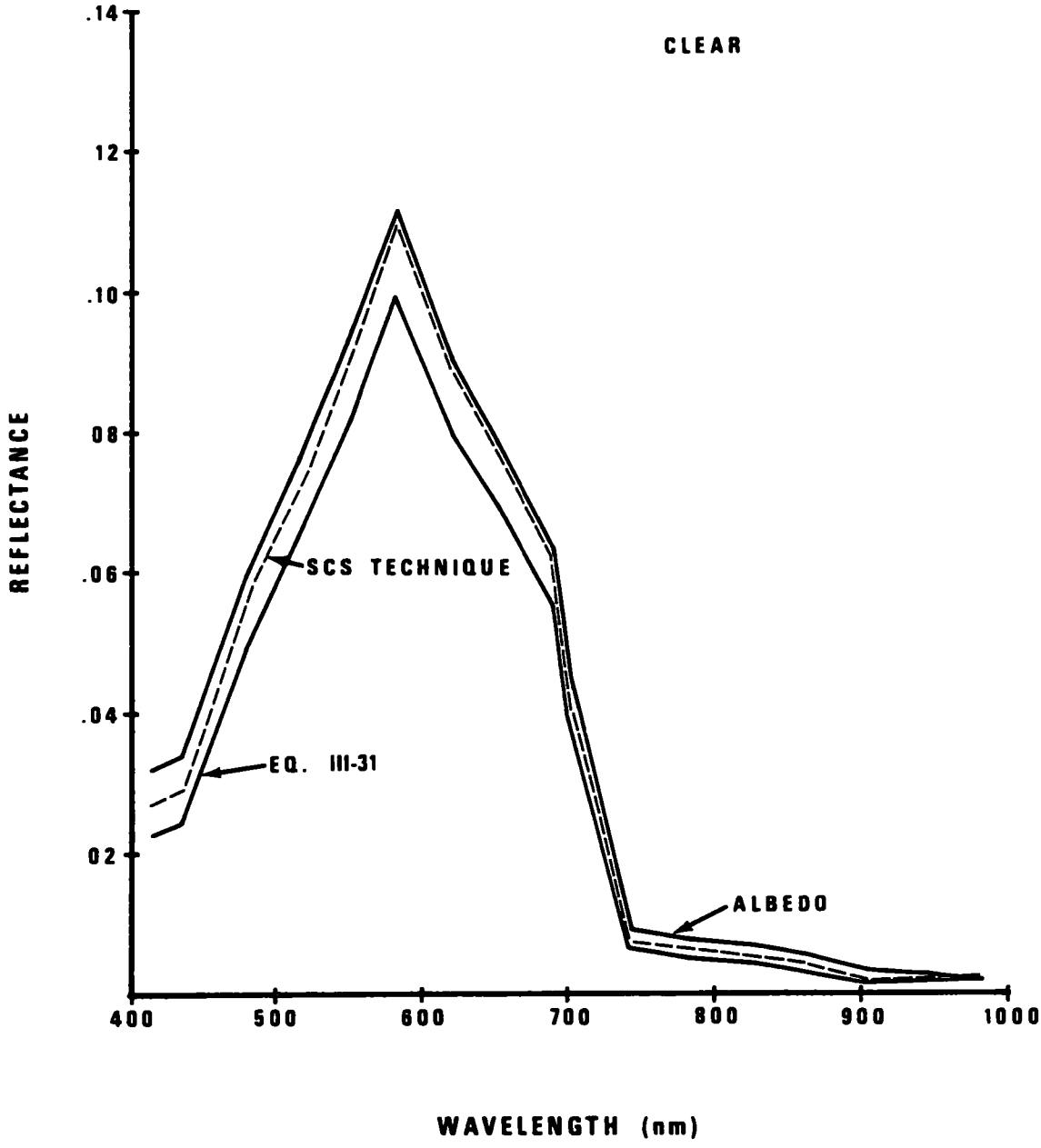

Figure 8. Comparison of surface albedo and calculated water volume reflectances for a typical clear sky.

SECTION V

INSTRUMENTATION

SPECTROMETER

Field measurements of water spectral radiance were made with a filter wheel spectroradiometer which was constructed for this project at the EPA's Environmental Monitoring Systems Laboratory, Las Vegas, Nevada. Detailed documentation of the engineering design of this instrument has already been written (Novotny 1975a, 1975b). Only a brief description of the major features of the spectrometer will be included here.

Filter Wheel

Spectral discrimination was accomplished with a circular filter wheel which is continuously variable from 343 to 690 nm and contained eight discrete filter elements in the 703- to 984-nm range. A stepping motor moved the filter wheel through the discrete filters and 12 positions on the continuously variable portion. The Jet Propulsion Laboratory (JPL) of the California Institute of Technology used a Cary 14 spectrophotometer equipped with an absorption slide wire to measure center wavelength and pass-band at each of the 20 filter positions. Table 2 contains the JPL measurement results.

Detector

The detector was a United Detector Technology, Inc., Model Pin 10DP. This is a planar diffused, silicon photovoltaic detector that was operated in the current mode. In this arrangement the detector can be considered a current source that is directly proportional to the incident radiation over 10 decades of light intensity.

Preamp

Signal amplification was achieved by a current mode operational amplifier. With Field Effect Transistor (FET) input and a 10-MΩ feedback resistor, the usable range of linearity was reduced to four or five decades. This configuration presents an intrinsic problem of drift due to lack of chopper stabilization. However, field procedures were developed with this in mind and drift was not thought to be a significant problem.

TABLE 2. JPL SUPPLIED FILTER DATA

Filter Position	Center Wavelength (nm)	Half-Power Pass-Band (nm)	Transmittance
1	343	18	0.36
2	377	19	0.29
3	385	14	0.28
4	415	12	0.30
5	436	13	0.29
6	480	15	0.28
7	517	15	0.26
8	550	14	0.27
9	583	13	0.25
10	620	16	0.26
11	652	15	0.27
12	690	16	0.29
13	703	18	0.68
14	742	21	0.53
15	782	21	0.58
16	829	24	0.36
17	862	20	0.40
18	905	19	0.47
19	942	21	0.48
20	984	21	0.34

Chart Recorder

The spectrometer data were recorded on an Astro-Med strip chart recorder that had two analog data channels and an event marker. One analog channel recorded the signal from the detector and the other a 10 pulse/revolution wavelength marker signal. The event marker recorded the begin-of-scan point.

Power Supply

Initial field work was performed with the electronics powered by Ni-Cd or lead-acid batteries. Battery failure was a frequent problem which was solved by installing a a.c. to d.c. inverter to obtain 110 Va.c. from the 12 Vd.c. boat battery. The 110 Va.c. drove a regulated power supply which supplied the 28 Vd.c. required by the spectrometer electronics.

SPECTROMETER MOUNTING

The spectrometer was mounted above the cabin roof of a 22-foot cabin cruiser as shown in Figure 9. The spectrometer head was affixed to a periscope tube with a 45° mirror which folded the field-of-view by 90° permitting vertical viewing of the water from a height of about 2.5 m. The mounting platform could be rotated for the spectrometer to view the water at angles up to 45° either side of the vertical. Laboratory experiments showed the field-of-view to be 7 cm in diameter at the periscope aperture. A half-angle divergence of 2.5° gave a field-of-view of about 25 cm at water level.

The flat black panel on the side of the boat served a twofold purpose. The first was to reduce the reflectance of sunlight from the side of the boat into the water volume viewed by the spectrometer. The second function is illustrated in Figure 10 which shows the lower portion of the panel folded down into a horizontal position to hold standard reflectance panels. This arrangement held the panels just a few centimeters above the water surface so that they would receive the same amount of sunlight and skylight irradiance as was incident on the water surface.

CALIBRATED REFLECTANCE STANDARDS

Since drift in the spectrometer electronics was thought probable, absolute calibration of the spectrometer was not attempted. The alternative to absolute calibration was to make relative measurements where backscattered light from the water is compared to radiance of a surface of known reflectance. Reflectance standards were, therefore, prepared for field use. The construction and calibration of the field reflectance panels is discussed below.

Construction

Two panels, one gray and one white, were used as reflectance standards. These were constructed by spray painting two 0.6-m by 0.9 m pieces of aluminum sheet metal. This gave fairly uniform reflectance surfaces and good durability when properly handled. The panels were repainted whenever they began to show wear which occurred seven times during the course of the project. Panels were recalibrated after each repainting.

The paint used was Krylon spray paint manufactured by Borden, Inc. The white panel was painted with Krylon Flat White Enamel, No. 1502, Federal Color Standard 595 No. 37875. This titanium dioxide-pigmented paint is believed to be of high quality and good diffuse reflectance since it has been considered in the past as a coating for optical integrating spheres (Grum and Luckey 1968).

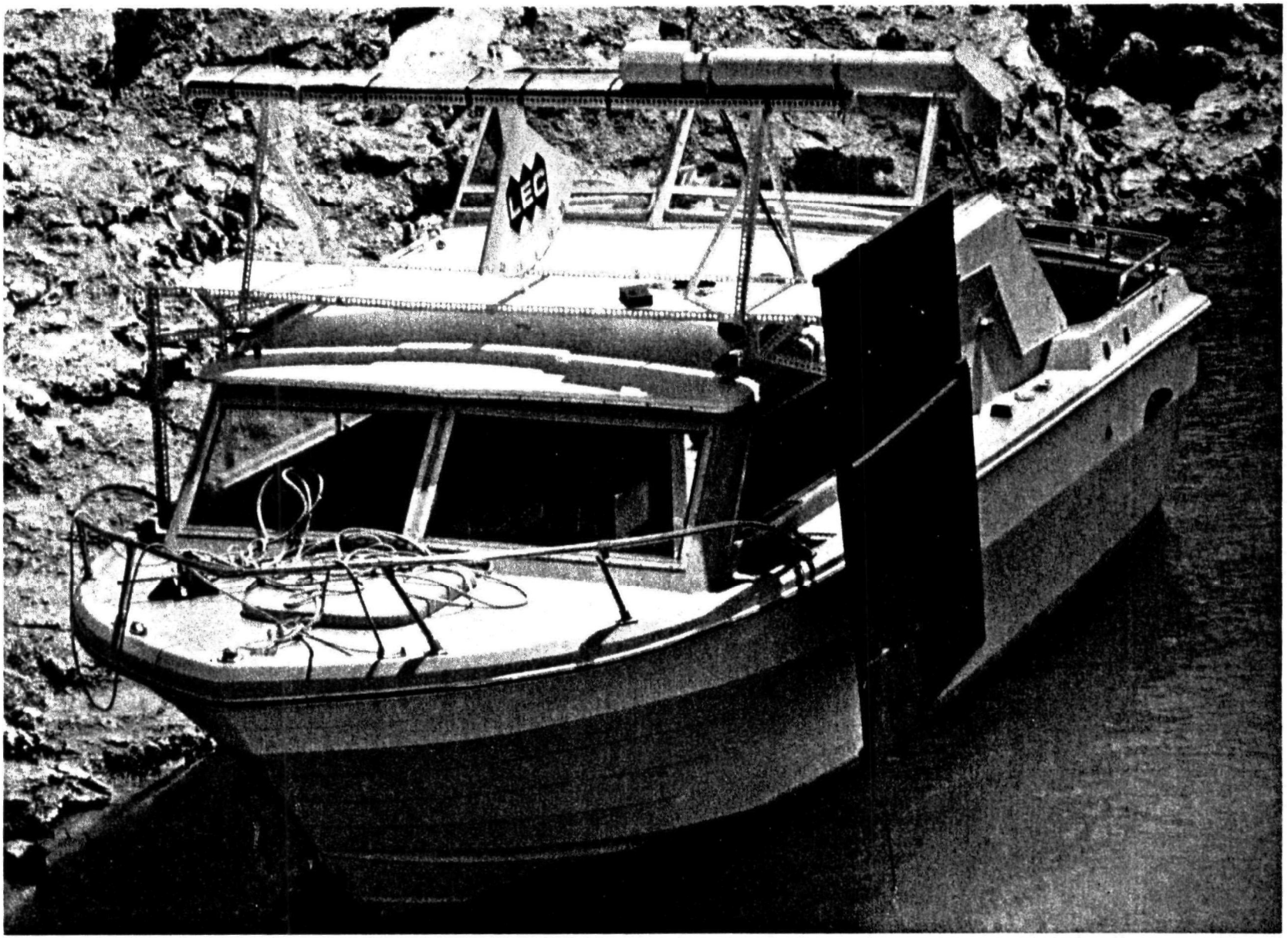

Figure 9. Spectrometer head, periscope, mounting platform, and reflectance panel holder installed on boat.

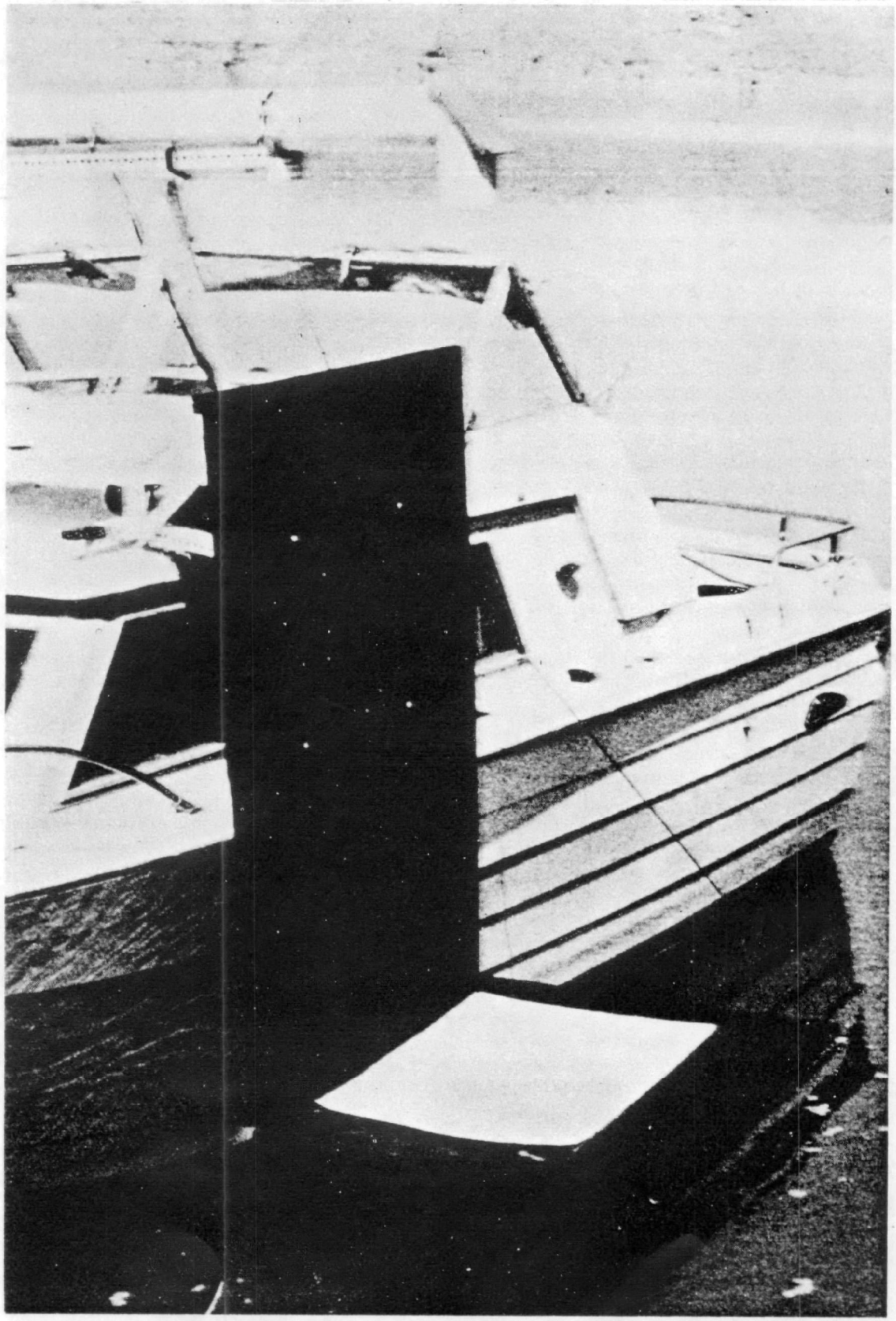

Figure 10. Reflectance panel holder in use.

The gray panel was painted with Krylon All-Purpose Gray, No. 1318. Like the white, the gray panels seemed to be fairly uniform and very diffuse. The nonuniformity of the panels has been measured and these results are presented in the error analysis section.

Calibration

The calibration of the field reflectance standards is traceable to freshly smoked magnesium oxide (MgO). Reflectance values for MgO were taken from two literature sources: Grum and Luckey (1968), and Encyclopedia of Industrial Chemical Analysis (1966). The NASA National Space Technology Laboratories at Bay St. Louis, Mississippi, used a Cary 17 Spectrophotometer and Reflectance Module to provide relative data for MgO compared to Kodak neutral test cards which had nominal reflectances of 18 percent and 90 percent. The reflectance values for MgO combined with the test cards/MgO relative data provided calibration of the neutral test cards. These cards were then the working standards for calibration of the painted panels.

The EPA spectrometer was brought into the laboratory to perform this calibration procedure. The neutral test cards and the painted panels were both viewed by the spectrometer under constant illumination conditions. The ratios of spectrometer outputs for two cases combined with the previously determined reflectance of the test cards resulted in assignment of values for the spectral reflectance of the field standards. Figure 11 shows the reflectance values for MgO and for typical test cards and painted panels.

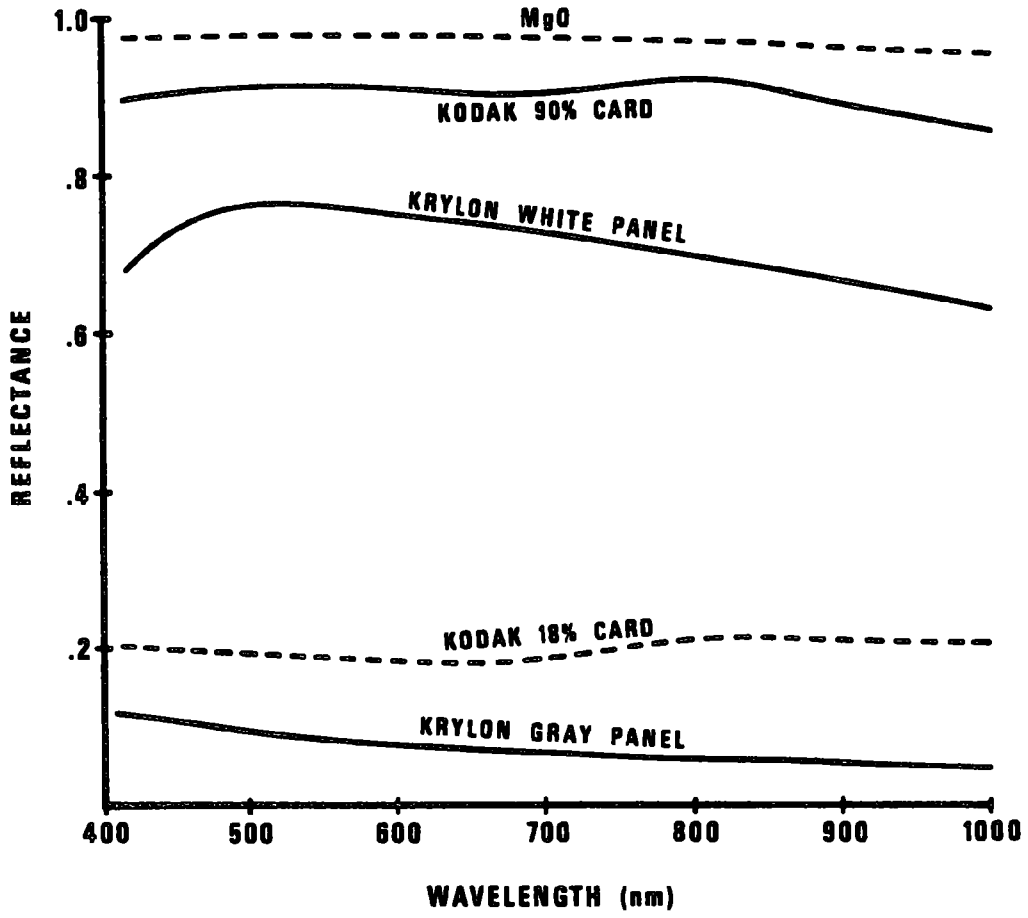

Figure 11. Typical reflectance values for MgO, Kodak neutral test cards, and painted calibration panels.

SECTION VI

ERROR ANALYSIS

INSTRUMENTAL UNCERTAINTIES

Uncertainties in Reflectance Measurement

Many variables affect the water volume reflectance calculated from data recorded by the spectrometer. Each of these variables has a degree of uncertainty associated with it, and the uncertainties in each variable contribute to an overall uncertainty in the calculated reflectance value. An error analysis has been performed to estimate the uncertainties in volume spectral reflectance which are attributable to instrumental sources.

Laboratory instruments for reflectance measurement generally consist of a light source, detector, and reflectance standard for comparison with the sample. Thus, the term instrument, as applied to field work, includes the illumination source (the sun) and the painted calibration panels in addition to the spectrometer which detects and records the reflected radiance.

The three types of data shown in Figure 12 are required to make a reflectance measurement. The spectrometer output recorded while viewing the calibration panel can be written as

$$V_A = k_\lambda L + C \tag{33}$$

where L is the radiance of the panel which has reflectance ρ_C

k_λ is the spectrometer sensitivity factor converting radiance to strip chart deflection

C is the spectrometer offset in units of chart deflection.

If the water of reflectance ρ_W is the target rather than the calibration panel, then the spectrometer output would be

$$F_B = (k_\lambda \rho_W L/\rho_C) + C \tag{34}$$

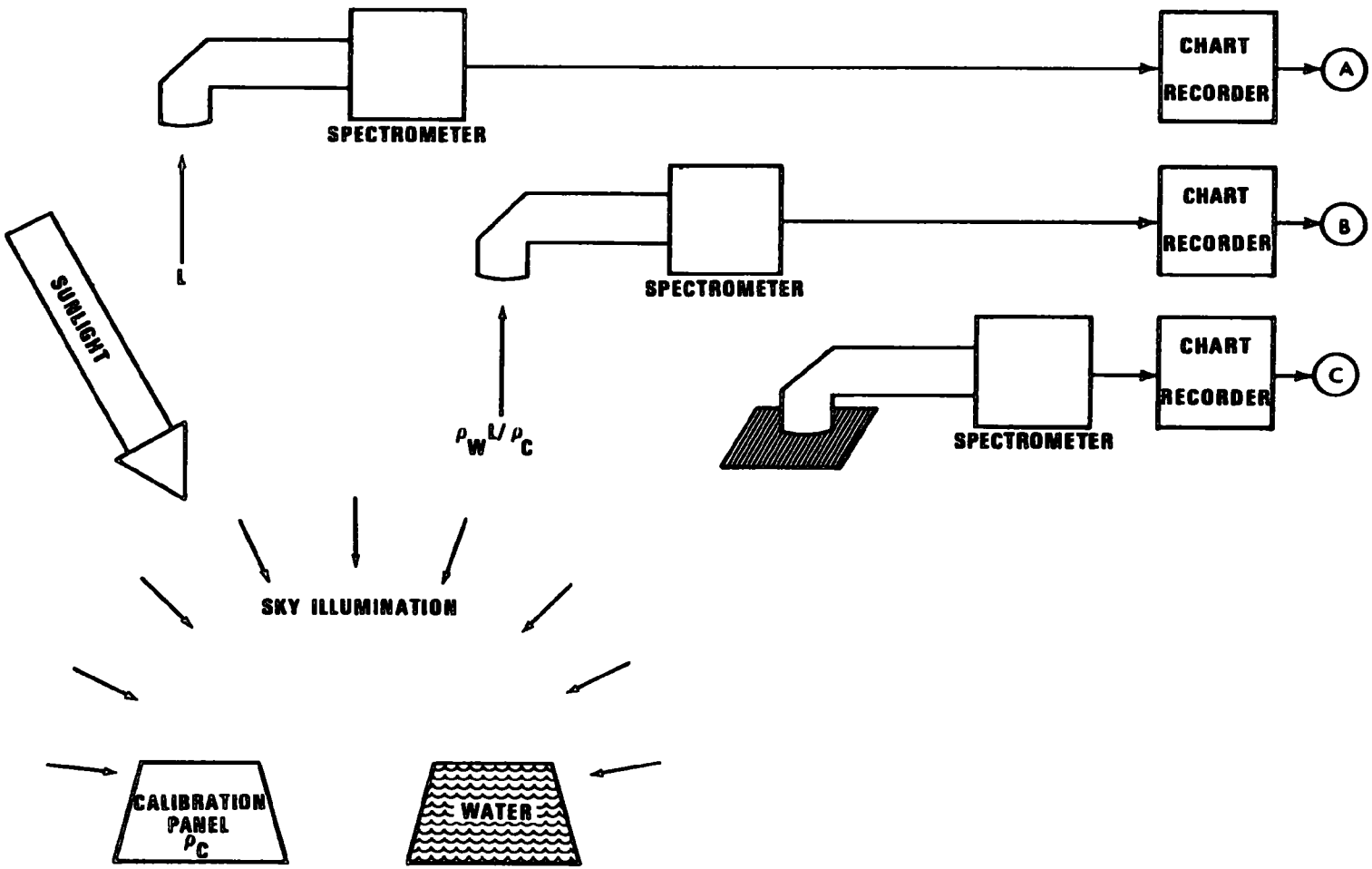

Figure 12. Experimental setup for measuring water reflectance.

Covering the spectrometer aperture prevents all light from entering and gives the output for the L = 0 case.

$$V_C = C \tag{35}$$

Solving Equation 33 for ρ_W and substituting terms from Equation 31 and Equation 34 allows us to write an equation for ρ_W in terms of V_A, V_B, and V_C.

$$\rho_W = \rho_C \frac{(V_B - V_C)}{(V_A - V_C)} \tag{36}$$

The spectrometer outputs used in calculating ρ_W are influenced by four variables; k_λ, ρ_C, L, and C. These variables have uncertainties associated with them as indicated by their standard deviations σ_{k_λ}, σ_{ρ_C}, σ_L, and σ_C. Some possible causes of these uncertainties are suggested below.

σ_{k_λ} - Fluctuations can occur in the gain of the spectrometer or recorder electronics.

σ_{ρ_C} - Nonuniformity of the painted calibration panel would result in varying reflectance as different spots are viewed.

Errors also exist in the measurements originally made to calibrate the panel.

σ_L - The targets are illuminated by light reflected from the side of the boat as well as direct light. Boat motion with respect to the sun results in a variable amount of indirect illumination and hence a variation in target irradiance.

σ_C - Electronic noise or drift in the bias circuitry of the spectrometer or recorder results in uncertainty in offsets. The accuracy with which signals can be read from the strip chart also has an effect on the uncertainty in offset values.

The problem is to relate these uncertainties in the individual variables to $\sigma^2_{\rho_W}$, the uncertainty in the measured water reflectance. Note that the variables k_λ and L always appear as a product. These variables cannot be measured separately and, therefore, σ_{k_λ} and σ_L cannot be separated either. Thus, the uncertainties resulting from these variables are combined into $\sigma^2_{k_\lambda L}$,

$$\sigma^2_{k_\lambda} = L^2\sigma^2_{k_\lambda} + k^2_\lambda\sigma^2_L \tag{37}$$

A complete derivation of the equations required for the error analysis is too lengthy to include here, but the formulas given resulted from algebraic manipulation of variances using the following formulas (Bevington 1969).

$$\begin{aligned} x = au + bv: \quad & \sigma^2_x = a^2\sigma^2_u + b^2\sigma^2_v + 2ab\sigma^2_{uv} \\ x = \pm auv: \quad & \sigma^2_x/x^2 = \sigma^2_u/u^2 + \sigma^2_v/v^2 + 2\sigma^2_{uv}/uv \\ x = \pm au/v: \quad & \sigma^2_x/x^2 = \sigma^2_u/u^2 + \sigma^2_v/v^2 - 2\sigma^2_{uv}/uv \end{aligned} \tag{38}$$

The variance in water reflectance normalized by the reflectance value can be shown to be

$$\frac{\sigma^2_{\rho_w}}{\rho^2_w} = \frac{\sigma^2_{\rho_c}}{\rho^2_c} + \frac{2}{k^2_\lambda L^2}\left[\sigma^2_{k_\lambda L} + \left(\frac{\rho^2_c}{G^2\rho^2_w} + 1\right)\sigma^2_c\right] \tag{39}$$

where G = 1 if water is recorded on low gain

G = 2.64 if water is recorded on high gain.

Notice the ρ_w on the right hand side of Equation 39 indicates that variance in water reflectance is a function of the reflectance value. Accuracy values must, therefore, be calculated at some specified turbidity/reflectance level.

The normalized variance in the calibration panel, $\sigma^2_{\rho_c}/\rho^2_c$, can be determined directly by making reflectance measurements on various spots on the different panels used throughout the project. Six panels painted with Krylon Gray Primer were used, and their reflectances were measured to give the mean spectral reflectance and standard deviations shown in Figure 13.

The uncertainties $\sigma^2_{k_\lambda L}$ and σ^2_c are not as easily determined but the routine field procedures did result in data suitable for making that measurement. The spectrometer was equipped with a gain switch which added an extra stage of amplification. Normally some of the data at each station were taken on high gain and some on low gain. Since it wasn't known if the gain of the additional stage was constant, the gain was measured at each station so that gain changes could be accurately removed in the data reduction process. The procedure for gain measurement is shown diagrammatically in Figure 14. The signal at point A is the same as Equation 33 and the signal at point B is

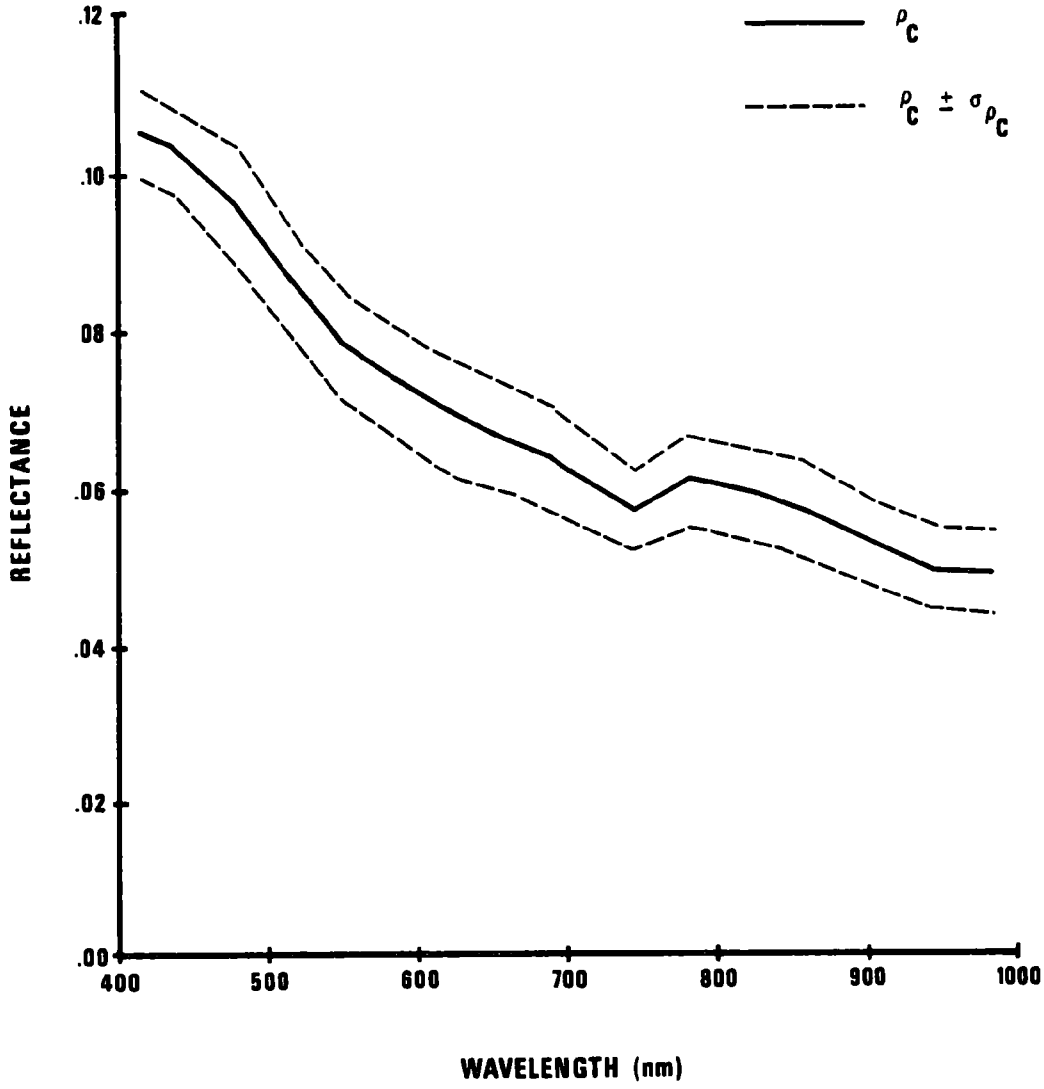

Figure 13. Spectral reflectance data for Krylon Gray Primer calibration panels.

$$V_D = Gk_\lambda L + C \tag{40}$$

Gain is therefore calculated by

$$G = (V_D - V_C)/(V_\lambda - V_C) \tag{41}$$

The uncertainty in the gain measurement can be expressed as a function of the variances of the individual variables.

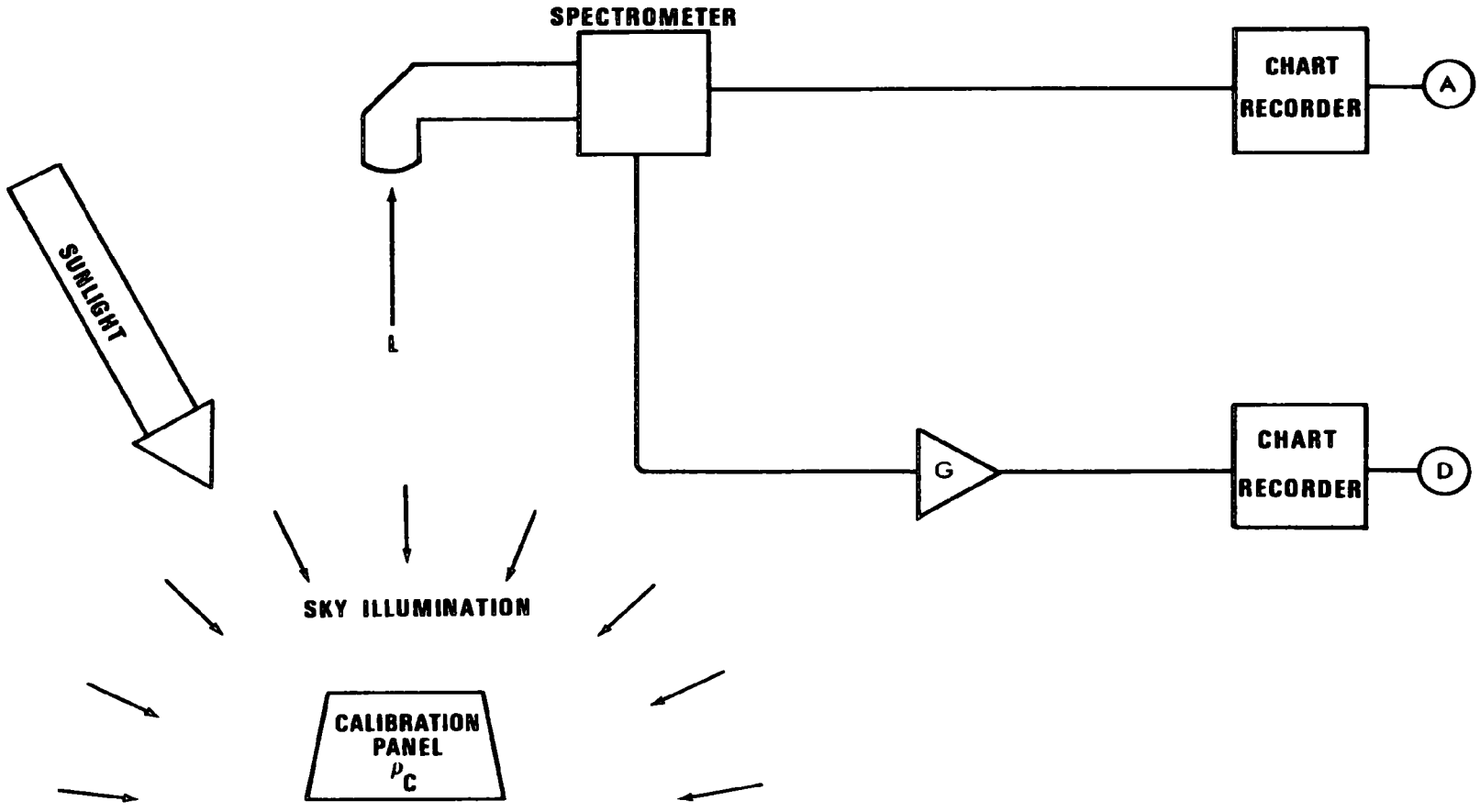

Figure 14. Experimental setup for measuring gain of last amplification stage of spectrometer electronics.

$$\sigma_G^2 = \frac{2}{k_\lambda L^2} \left[G^2 \sigma_{k_\lambda L}^2 + (G^2 + 1)\sigma_C^2 \right] \quad (42)$$

The variance in the gain values calculated from the field data should therefore give an indication of the cumulative effects of $\sigma_{k_\lambda L}^2$ and σ_C^2.

Data from 12 days was used to calculate gains at as many wavelengths as possible (high gain signals frequently went off scale at some wavelengths making gain calculation impossible). The mean value of the 145 calculations of G was 2.64 and σ_G^2 was determined to be 0.00899. The variance in the gain for the same wavelength on different days was not appreciably larger than the variance for different wavelengths on the same day. It is, therefore, concluded that the gain was constant throughout the project and the overall σ_G^2 value was all attributable to $\sigma_{k_\lambda L}^2$ and σ_C^2.

Equation 42 can be rewritten substituting 2.64 for G.

$$\sigma_G^2 = (k_\lambda L)^{-2} \left[13.94\ \sigma_{k_\lambda L}^2 + 15.94\ \sigma_C^2 \right] \quad (43)$$

The variance in the gain was observed to be different at different wavelengths. Figure 15 shows σ_G^2 as a function of wavelength. The product $k_\lambda L$ in Equation 43 is the strip chart deflection in centimeters when looking at the gray calibration panel (low gain setting) under typical field conditions. The average value of $k_\lambda L$ calculated from the same data used in determining σ_G^2 is shown in Figure 16.

The values for σ_G^2 and $k_\lambda L$ contained in these figures can be used in Equation 43 to obtain a value for the weighted sum of $\sigma_{k_\lambda L}^2$ and σ_C^2. However, we need to enter the values of these variables individually into Equation 39 to compute the variance of the reflectance measurement. The separation can be accomplished by realizing that σ_C^2 is the uncertainty in strip chart offset, and as such, it is independent of signal level and is not a function of wavelength. This offset uncertainty contains the inaccuracies in reading the strip chart as well as possible errors from other sources. Chart reading accuracies were estimated to be about ±0.02 cm. Therefore, σ_C^2 should be about 0.0004 cm^2 as a minimum, and possibly larger if other factors introduce significant errors into offsets. Figure 15 showed the smallest σ_G^2 value to be at 620 nm.

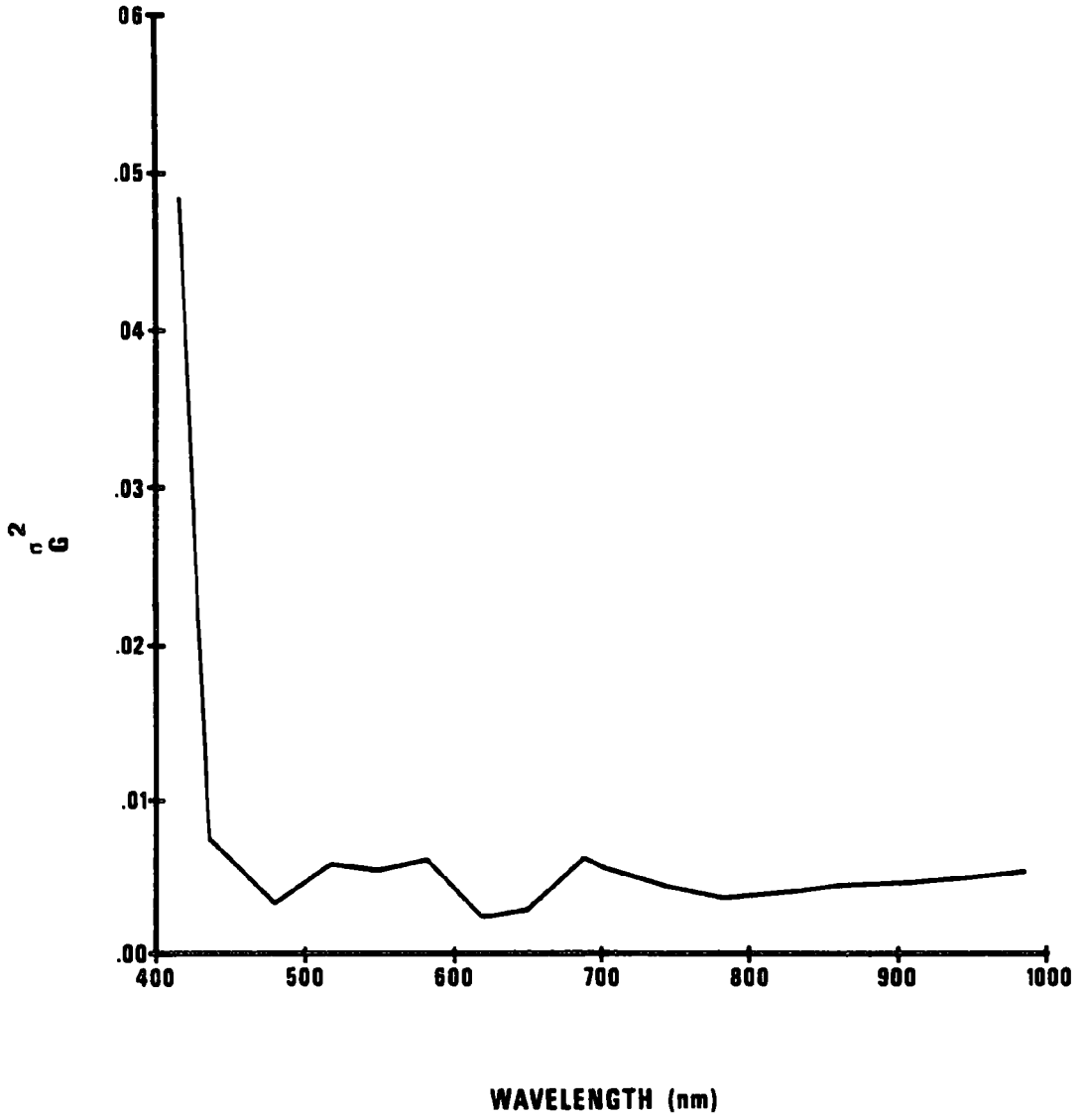

Figure 15. Variance in gain measurements as a function of wavelength.

Evaluating Equation 42 at this wavelength gives a - 0.00011 cm^2. A negative variance, which is mathematically impossible, apparently results from the fact that the 0.004 cm^2 estimate for σ^2_C was too large. If σ^2_C is reduced to 0.00031 cm^2 Equation 42 gives a $\sigma^2_{k_\lambda L}$ value of zero. This means that σ^2_C accounts for all the variability in measuring G, or in other words, the strip chart reading uncertainties are the only significant errors in determining offsets. A σ^2_C value of 0.00031 can, therefore, be assigned to all wavelengths allowing Equation 42 to be solved for $\sigma^2_{k_\lambda L}$. Figure 17 shows $\sigma^2_{k_\lambda L}$ as a function of wavelength.

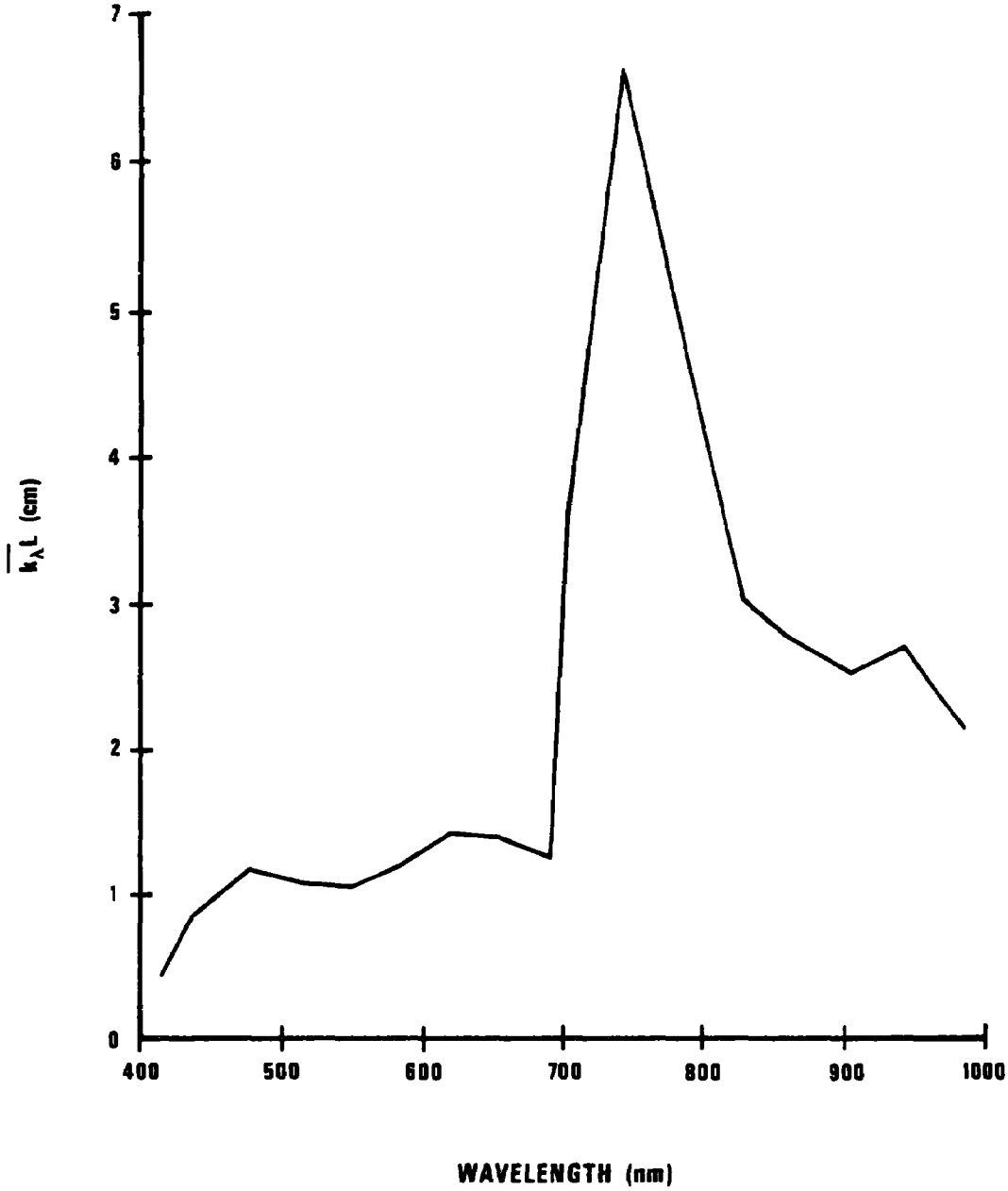

Figure 16. Average strip chart deflection as a function of wavelength for data used in calculating σ_G^2.

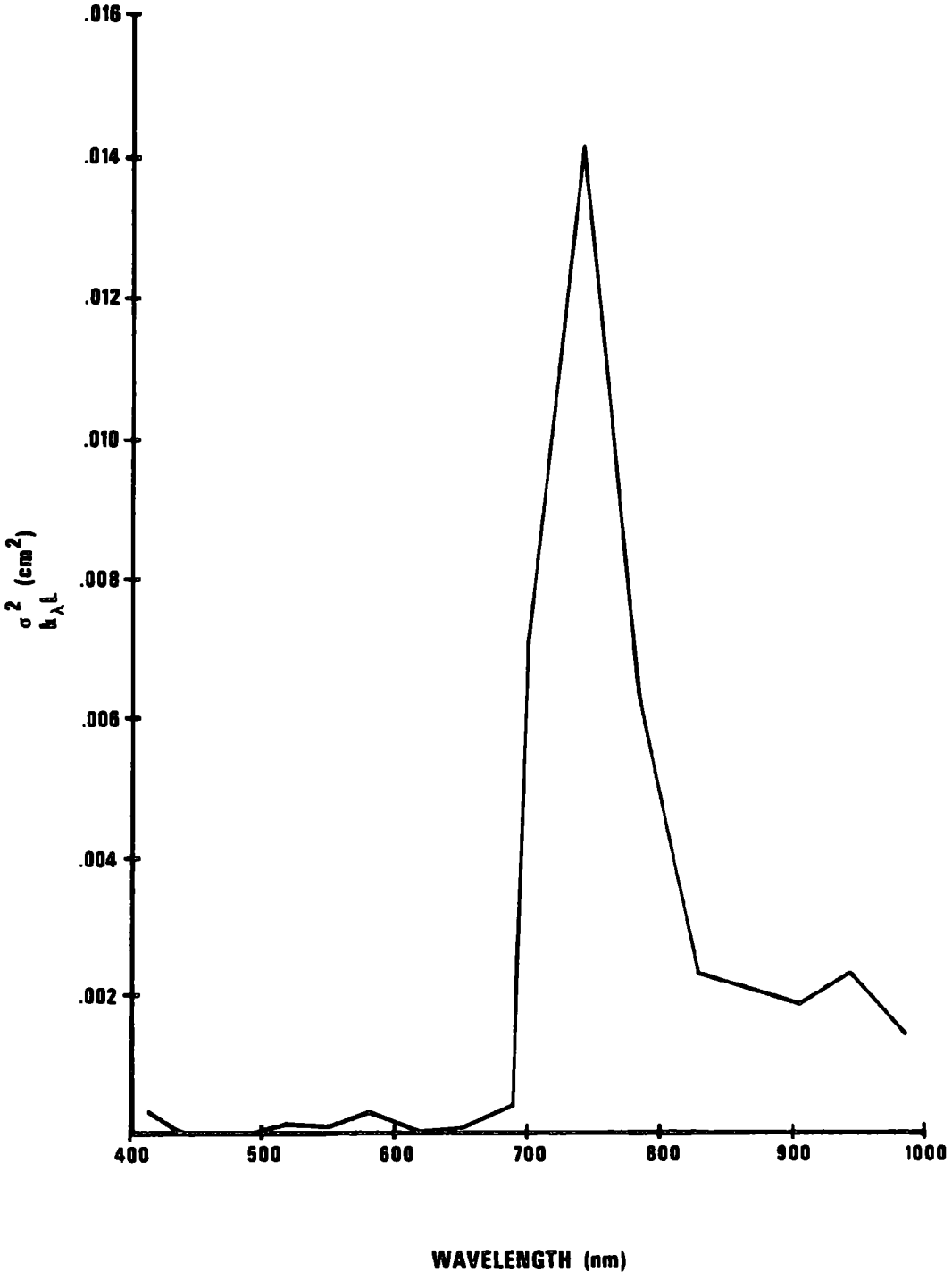

Figure 17. Variance in illumination and spectrometer electronics as a function of wavelength.

The last variable required for calculation of $\sigma^2_{\rho_W}$ is ρ_W, the volume reflectance of the water. In the analysis work described in Section IX unweighted second-order polynomials were fitted to the nonfilterable residue-volume reflectance relationships at each wavelength for silt and fine sand particles. These polynomials were used to calculate the typical volume spectral reflectance curves for sediment concentrations of 25 and 250 mg/l plotted in Figure 18.

All information is now at hand for using Equation 38 to calculate the total instrumental uncertainties in volume reflectance. This calculation was performed for 25 and 250 mg/l cases and the results are shown in Figure 19. At 250 mg/l the spectrometer would have been on low gain, and at 25 mg/l it would have been on high gain; so these gain settings were used in the calculation.

Figure 19 shows the normalized variance in water volume spectral reflectance to be less than 0.05 over the entire spectral range of the instrument for concentrations of 25 mg/l and above.

Uncertainties in Units of Suspended Sediment

If volume reflectance was linearly related to suspended sediment concentration and if zero sediment corresponded to zero reflectance, then the normalized variance in terms of suspended sediment would be equivalent to the normalized variance in reflectance measurements. However, neither of these conditions holds true so additional information and calculation is required to relate instrumental uncertainties in reflectance to uncertainties in units of nonfilterable residue (105°C).

Let reflectance sensitivity, $\Delta\rho_W$, be defined as the change in reflectance resulting from a 1 mg/l change in sediment concentration. In other words, sensitivity is the slope of the reflectance-nonfilteraable residue curve. The instrumental uncertainties in units of reflectance can be converted to milligrams per liter using $\Delta\rho_W$ as follows:

$$\sigma_{residue} = (\sigma^2_{\rho_W}/\rho_W)^{\frac{1}{2}} \rho_W \Delta\rho_W \qquad (44)$$

Figure 20 shows reflectance sensitivity as a function of wavelength for typical 25 and 250 mg/l cases for silt and fine sand particles. Sensitivities were calculated from polynomial fits to the Lake Mead data reported in Section IX.

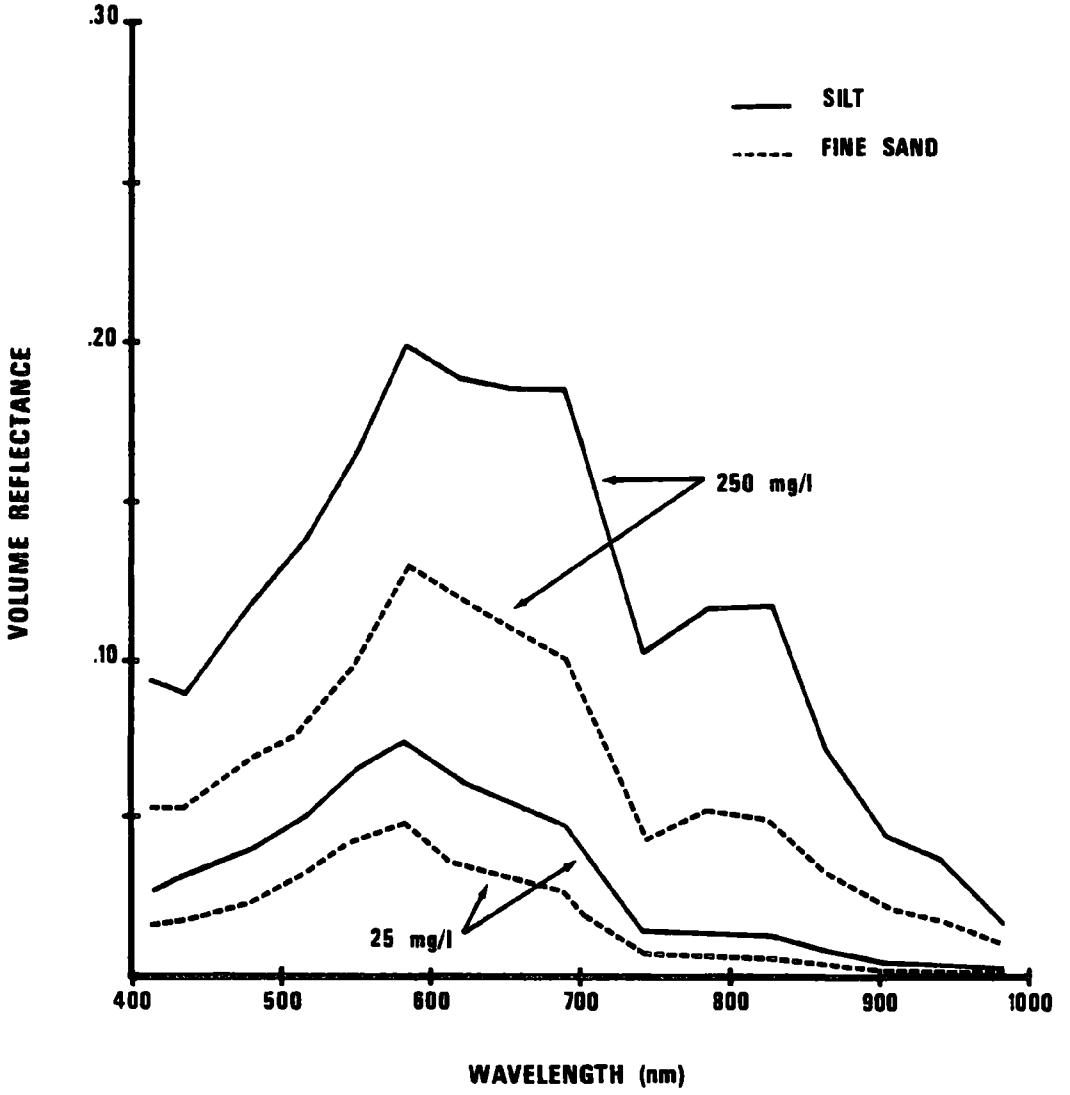

Figure 18. Typical volume spectral reflectance curves for water containing suspended sediment concentrations of 25 and 250 mg/l.

Data from Figure 20 were used with Equation 44 to calculate the instrumental uncertainties in units of mg/l of nonfilterable residue shown in Figures 21 and 22. These figures show the instrumental errors to be smallest at the near infrared (IR) wavelengths. It should be kept in mind that these results are unique to the instrument used here, and that for another sensor system the spectral distribution of instrumental uncertainties could be entirely different.

Comparison of Figure 21 with Figure 19 leads to a significant conclusion. Figure 19 shows that the spectrometer is capable of $\sigma^2 = 0.05$ accuracy in measuring the volume reflectance of typical water containing 25 mg/l of

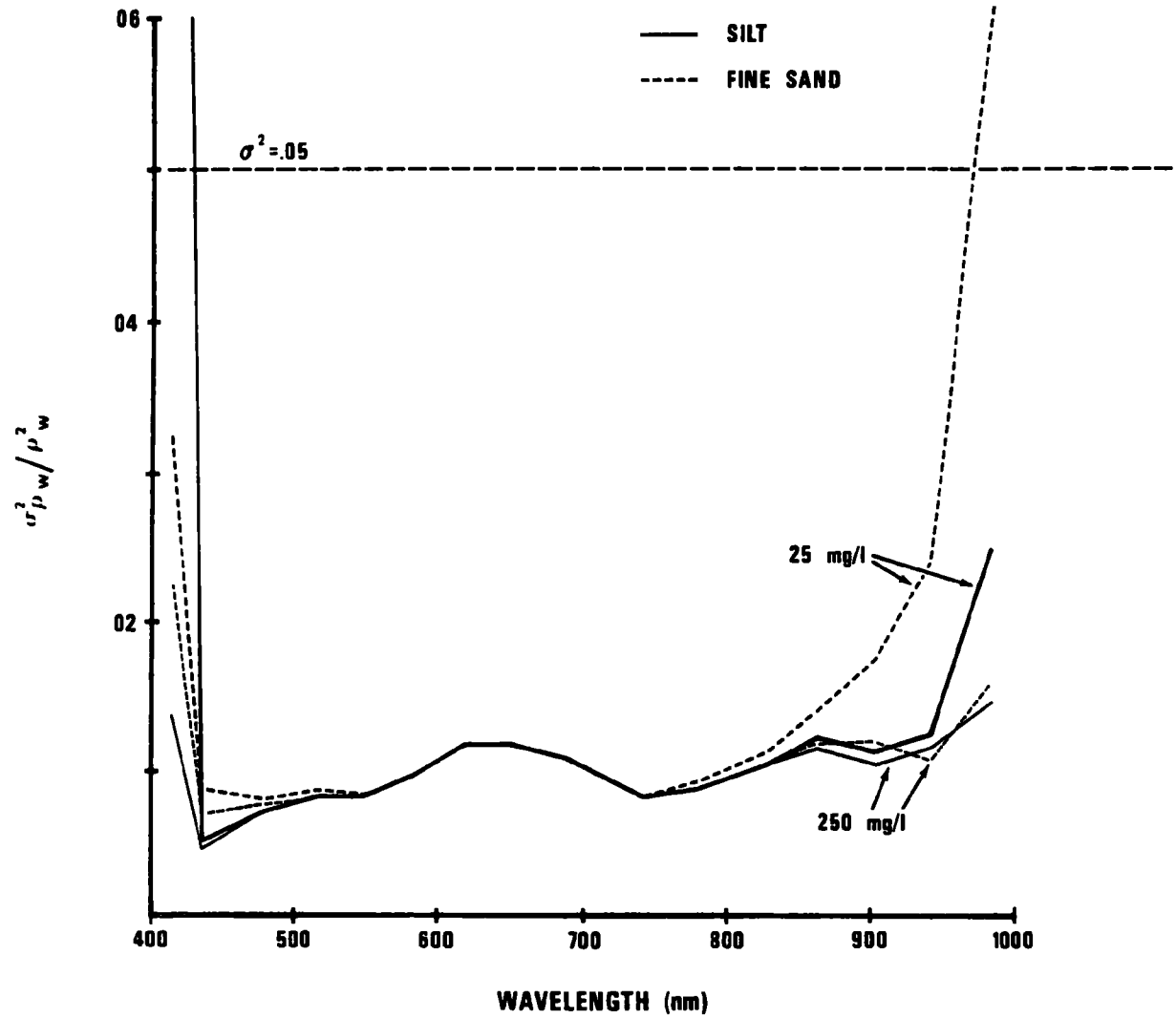

Figure 19. Normalized variance in volume spectral reflectance resulting from instrumental uncertainties.

suspended sediment. Yet when instrumental uncertainties are expressed in terms of uncertainty in residue values, Figure 21 shows that the instrument is not capable of the desired accuracy over most of the visible portion of the spectrum. Accuracy in reflectance measurement and accuracy in sediment measurement can be drastically different, thus a given accuracy in the measurement of some turbidity-related parameter will require an instrument of considerably better accuracy.

Uncertainties in Units of Nephelometric Turbidity

In the course of this study nephelometric turbidity emerged as an important parameter. Since this parameter became heavily used in the data

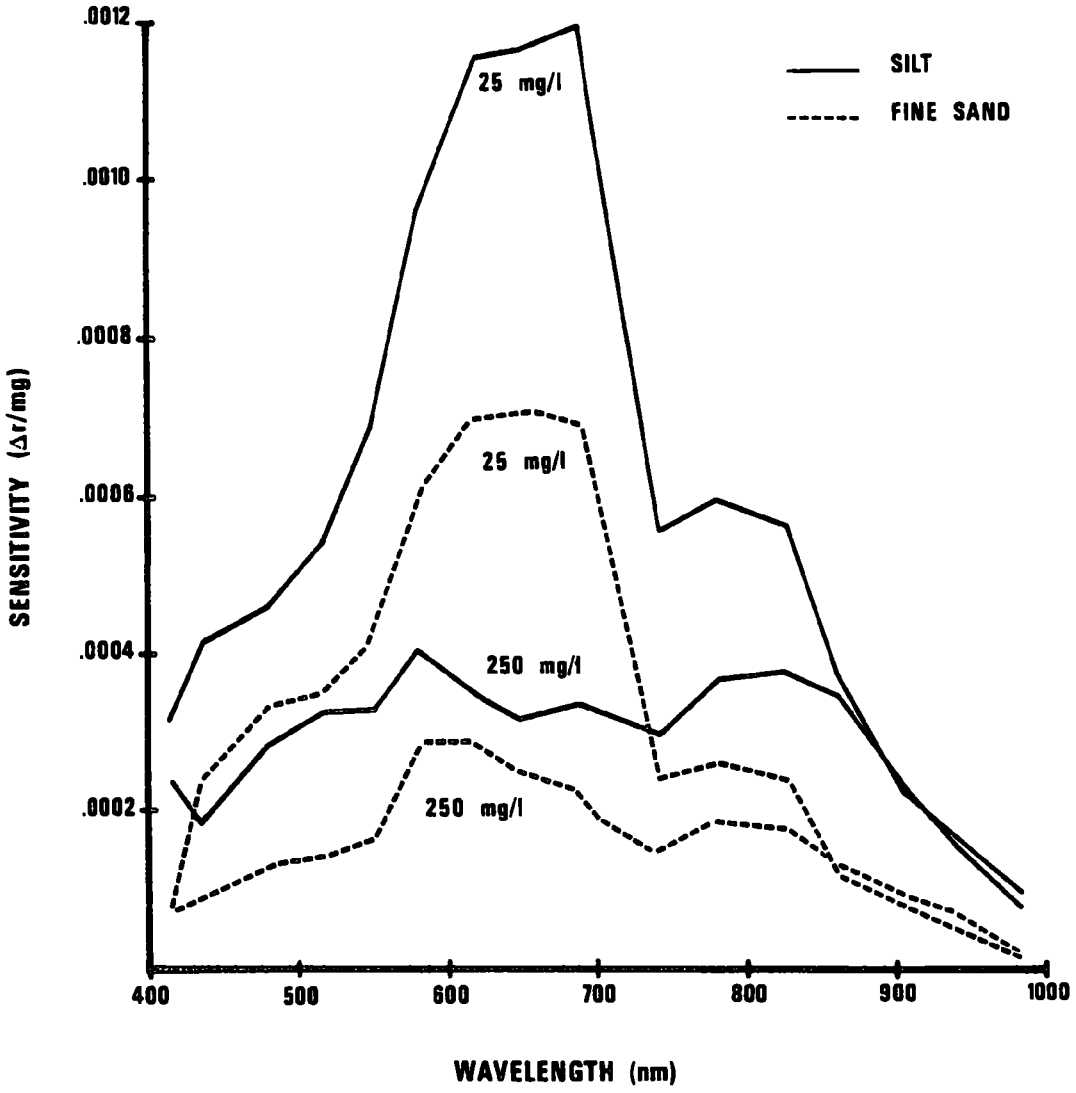

Figure 20. Sensitivity of reflectance to changes in sediment concentration as a function of wavelength.

analysis, it was thought useful to transform instrumental uncertainties into NTUs. The same procedure was used for this calculation as was used in converting to units of nonfilterable residue - 105°C. Calculations were performed for turbidities of 15 and 150 NTU with the results shown in Figure 23.

In terms of normalized variances the instrumental uncertainties in residue measurements at 25 mg/l are about the same as the uncertainties in turbidity measurement at 15 NTU. However, the 150 NTU curve shows somewnat larger uncertainties in the red portion of the spectrum than did the 250 mg/l residue curve.

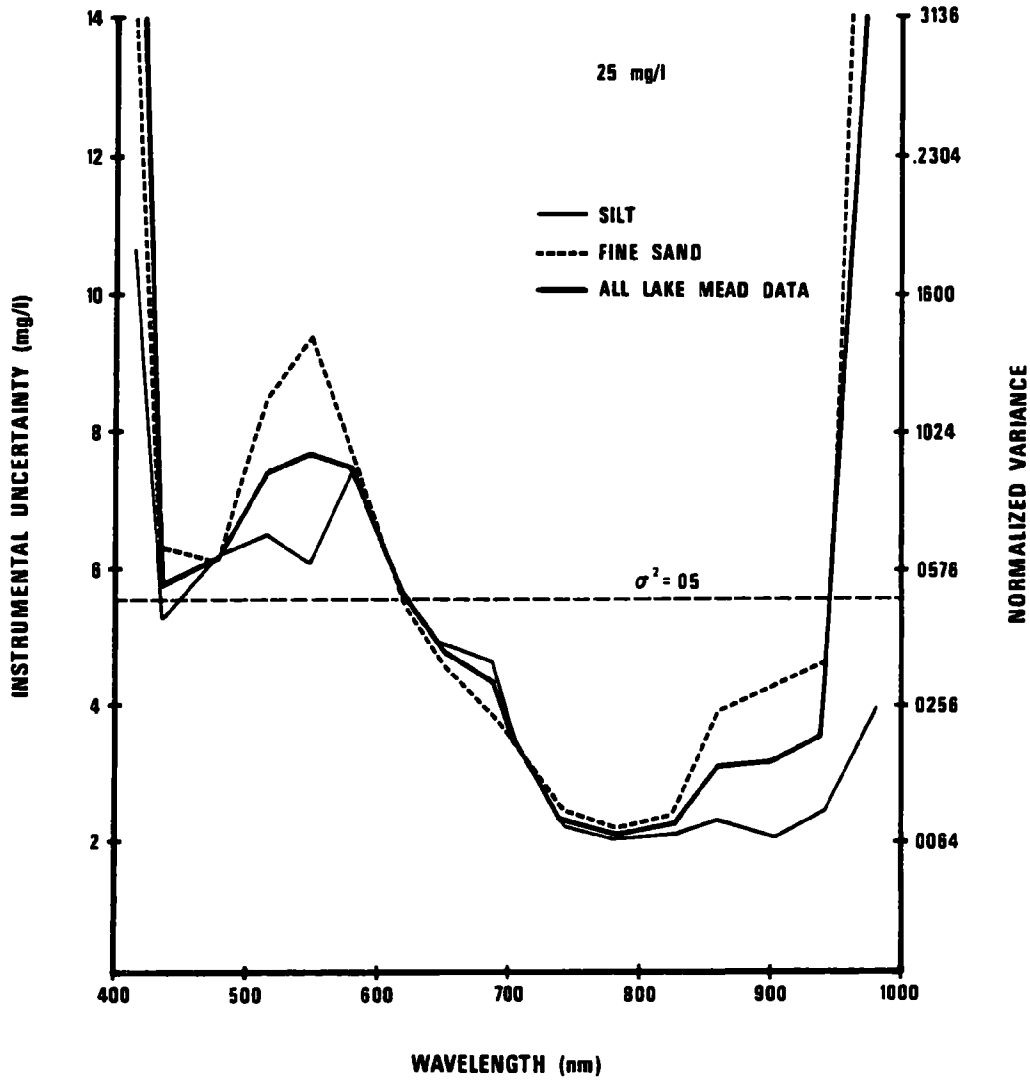

Figure 21. Instrumental uncertainties expressed in units of sediment concentration for 25 mg/l water.

CONCEPTUAL UNCERTAINTIES

Attention is now directed at a different class of errors which result from lack of precision in concepts as opposed to instrumental uncertainties which result from lack of precision in measuring instruments. For example, turbidity in a water body is generally expected to be a function of depth. This function was not measured in the field. The procedure was to sample both ends of the function (surface and Secchi depth) and average these values to give a single value. It is conceptually incorrect to represent an unknown function by the mean value of its end points unless the function is linear.

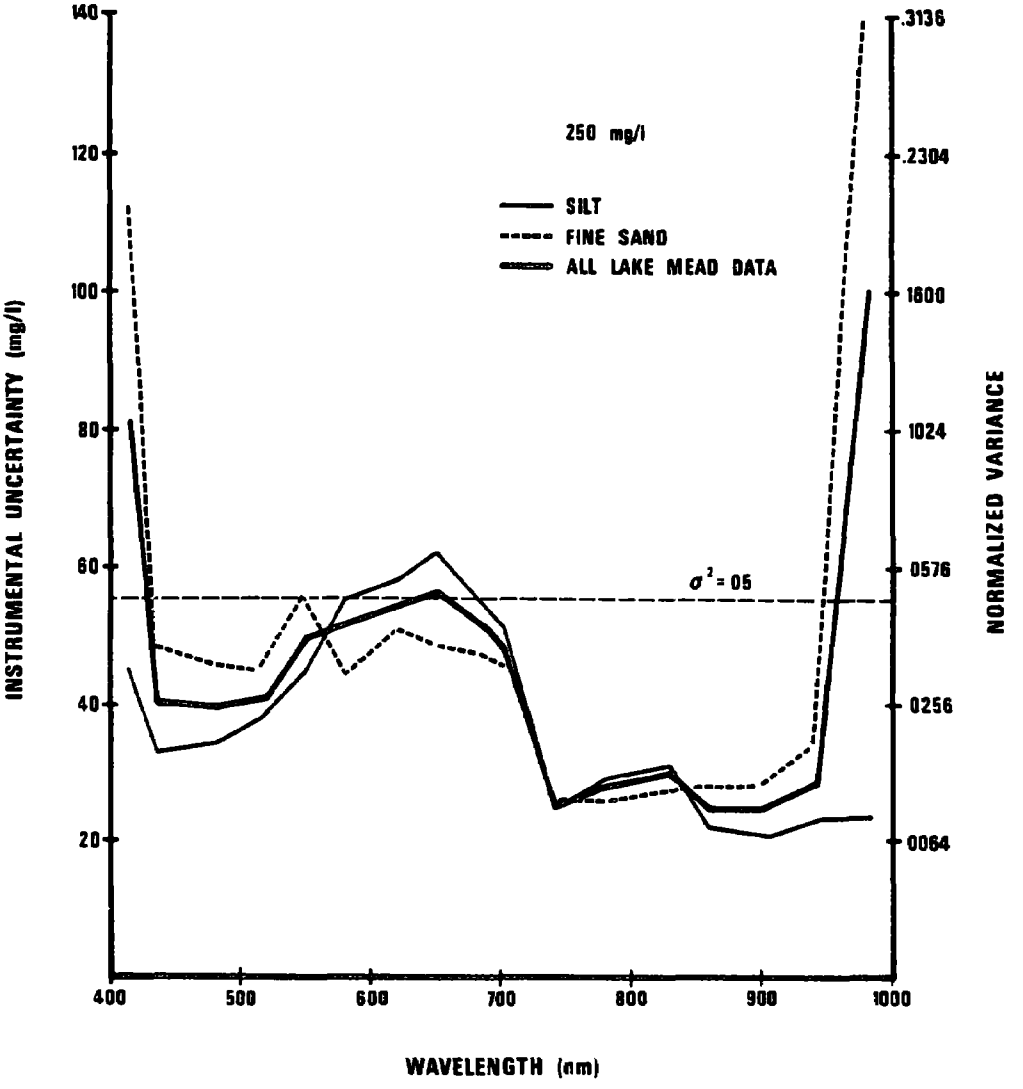

Figure 22. Instrumental uncertainties expressed in units of sediment concentration for 250 mg/l water.

Thus, the ground-truth values are subject to a certain amount of uncertainty because of this conceptual imprecision.

Another possible source of conceptual uncertainty in the ground-truth data results from the choice of a filter with a 0.00045-nm pore size for separating filterable from nonfilterable residues. This selection carries with it the tacit assumption that all sediment particles in the water sample are larger

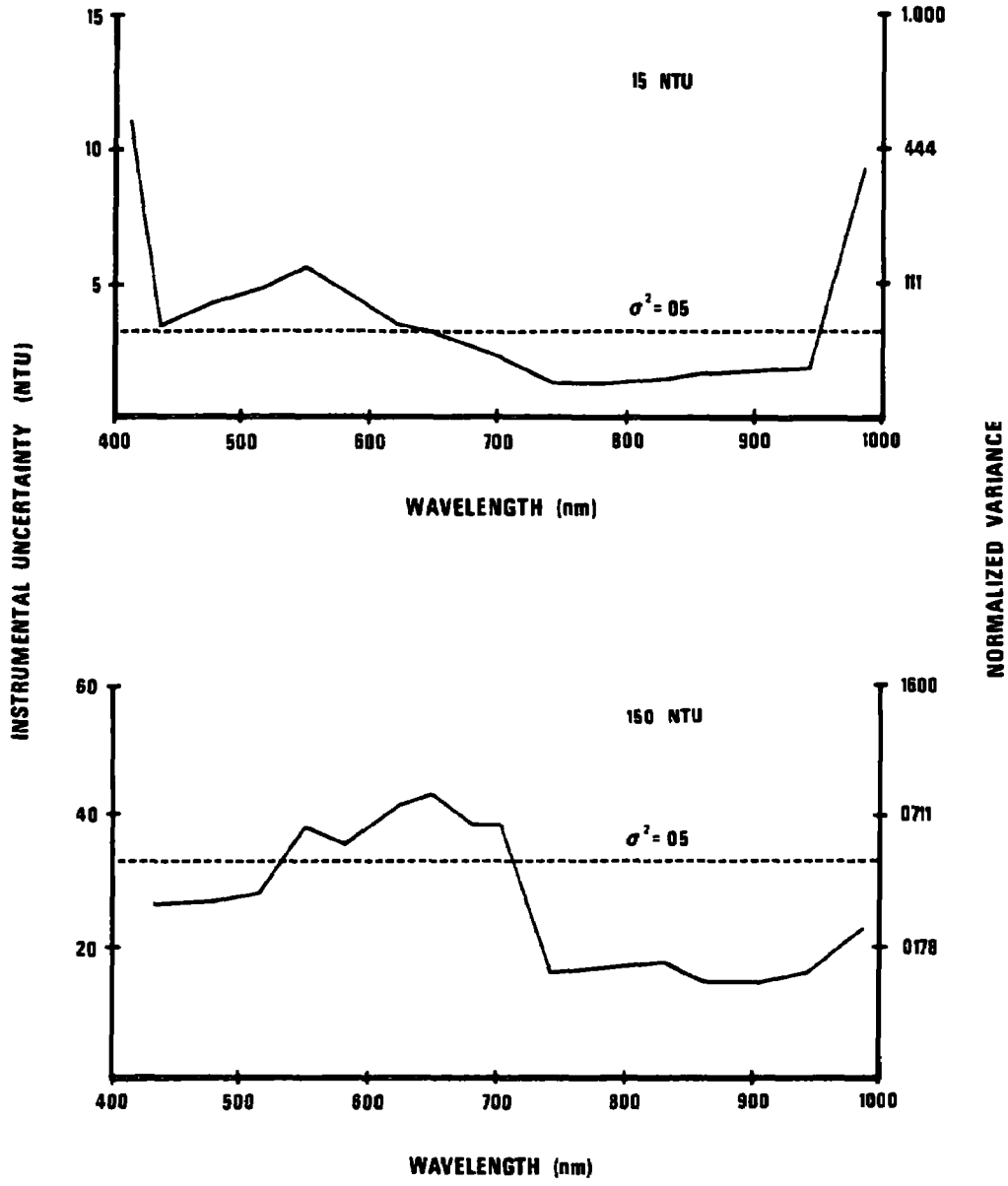

Figure 23. Instrumental uncertainties expressed in units of nephelometric turbidity for 15 and 150 NTU water.

than 0.00045 nm in diameter. Table 3 lists the diameters and settling times of various classes of particulates.

Part of the clay particle size range is smaller than the pore size of the filter used in the laboratory analysis of water samples. Thus, if two samples have the same amount of sediment but a different distribution of particle sizes, the laboratory analysis could detect a different percentage of the particles in each sample. The result would be a different nonfilterable residue value for each when, in fact, the sediment concentrations were identical.

TABLE 3. SIZE RANGES OF VARIOUS PARTICULATES

Diameter (mm)	Order of Size	Time to Settle 1 Ft.
>10	Gravel	0.3 sec.
10 - 0.15	Course sand	0.3 - 38 sec.
0.15 - 0.015	Fine sand	38 sec. - 33 min.
0.015 - 0.0015	Silt	33 min. - 55 hrs.
0.001	Bacteria	55 hrs.
0.002 - 0.0001	Clay particles	230 days
0.00001	Colloidal particles	63 years

Additional uncertainty results from procedures used for removal of peripheral effects. Certain assumptions and approximations are made in developing a method for removal of these effects (Section IV). These approximations are probably valid on the average, but for any given sample they may not be absolutely true.

The possible sources of conceptual uncertainty are numerous, but these three examples, plus one other, are probably the most significant. Estimates are given below for the typical magnitudes of these four sources of uncertainty in the Lake Mead data.

Depth Distribution of Turbidity

This error source actually involves more than just the assumption that turbidity, which is a function of depth, can be represented by the mean value of samples taken at the surface and at the Secchi depth. Because water attenuation is a function of wavelength, each wavelength of incident light can penetrate to a different depth. The Secchi depth is representative of maximum penetration for the visible wavelengths. However, penetration for the near-IR wavelengths may be only a few centimeters. This means that unless the turbidity is uniform with depth, each wavelength will be reflected from a volume

with a different effective sediment concentration. Figure 24 shows the estimated penetration depth as a function of wavelength assuming a typical particulate reflectance and a 2 percent return to the surface. Errors are, therefore, being introduced not only by representing functions with single values, but also by ignoring the fact that the best value for representing the function will change with wavelength.

To estimate the magnitude of this type of error, 70 surface-depth sample pairs were examined and nonfilterable residue values at 105°C ranged from 10 to 64 mg/l. The mean value for each pair was calculated and the standard deviation of the individual measurements about the means was found to be ±7.38 mg/l. A portion of this variability is due to instrumental uncertainty in the laboratory measurement of nonfilterable residues. To determine the contributions from laboratory instrumental uncertainties, 12 water samples with residues in the same 10 to 64 mg/l range were subjected to replicate sample analysis. Samples were divided and each half treated as a separate sample. The standard deviation between the values for each half and the mean values for both halves was found to be ±3.39 mg/l, which is attributable to only instrumental errors. Removing instrumental errors leaves a standard deviation of ±6.5 mg/l, which must be attributed to the variability of residue concentration with depth.

The mean residue value for the 70 surface-depth sample pairs was 25.3 mg/l. Thus, the conceptual uncertainty resulting from the depth variability of turbidity expressed as a normalized variance is 0.067. This is larger than the 0.05 variance requirement established by EPA.

It should be noted that the same problem arises with in situ instrumentation. If sediment concentration varies with depth, measurements taken with a sampling depth with the in situ sensor may not represent the sediment concentration in that water body. Since this type of error is characteristic of the turbidity measurement problem in general and not unique to the airborne multispectral method, it probably should not be included in the estimates of accuracy of the remote measurements. However, it must not be forgotten that this estimated variability of ±6.5 mg/l did exist within the upper 2 meters of the Lake Mead test sites, and anytime ground truth is used to verify a remote result this factor will enter in.

The same procedure was used to estimate the depth variability of nephelometric turbidity. The result in this case was ±2.8 NTU about a mean of 13.8 NTU for normalized variance of 0.041.

Pore Size of Filters for Extracting Nonfilterable Residues

In the laboratory analysis of water samples, a filtration process was used to extract nonfilterable residue which presumably is the sediment in the sample. The nonfilterable residue value will be an accurate measure of sediment concentration only if the filter catches nearly all of the sediment present. As previously mentioned, clay particles can be smaller than the 0.00045-mm pore size of the filters so that part of the sediment in the clay particle-size range would not be detected by the sample analysis.

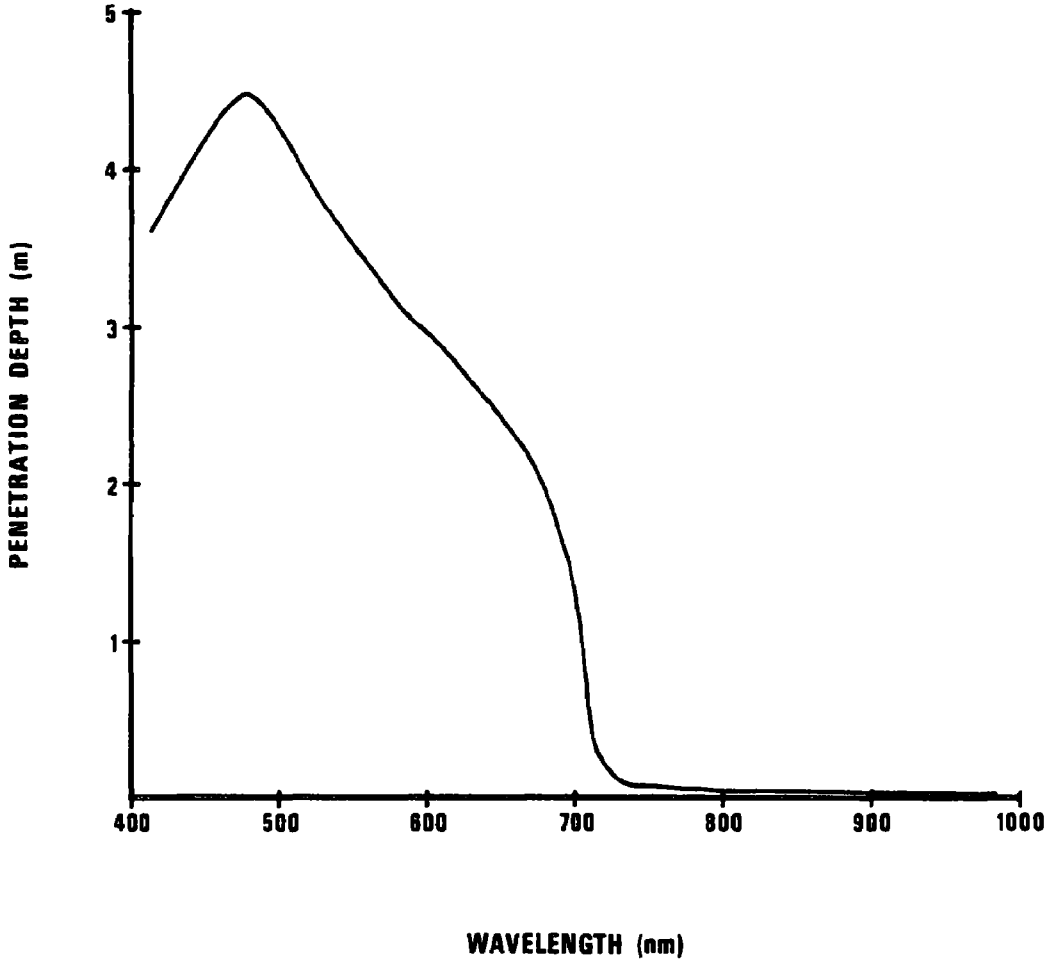

Figure 24. Maximum depth of water penetration by sunlight assuming reflectance from a panel with a typical sediment spectral reflectance and a two percent return to the surface.

Two reasons can be given in support of the fact that there was no significant amount of small clay particles in the Lake Mead samples. The first argument is based on the settling time given for clay particles in Table 3. It was observed in the field that stations which had sediment concentrations of several hundred milligrams/liter and Secchi depths of only a few centimeters on one day would be sediment free with Secchi depths of several meters the next day. If clay particles take 230 days to settle 1 foot, the sediment load on the first day could not have included significant amounts of clay particles or the water would not have cleared within 24 hours.

The second argument against the presence of significant amounts of clay particles comes from a statistical analysis of the laboratory data. If a portion of the suspended sediment in the samples is clay particles, it would

be expected that samples with higher sediment content would result in higher filterable residue values as a result of the small sediment particles passed by the filter. One would expect in this case to see statistical correlation between filterable and nonfilterable residues.

Before analyzing residue data for this type of correlation it must be noted that other factors could also cause correlation to exist. For example, if sediment-bearing water from a river is emptying into a lake and the river is of higher salinity than the lake, then dilution processes would cause both the sediment concentration and the salinity (filterable residue) to decrease with distance from the mouth of the river. One would then observe correlation between filterable and nonfilterable residues but this would result from dilution rather than filters passing a portion of the sediment. For this reason data from the Colorado River and Las Vegas Wash test sites must be excluded from the analysis since these sites contained inflows of water of lower and higher salinity content respectively. Figure 25 shows a least-squares linear fit to the filterable-nonfilterable residue relationships for the Colorado River and Las Vegas Wash data. The large and opposite slopes of these lines results from dilution of high and low salinity inflows with the Lake Mead water.

Dilution was not thought to be a factor at the other three test sites. The filterable-nonfilterable residue relationships in these cases should indicate the amount of sediment passed through the filter. Forty-four samples with nonfilterable residue values in the range 10 to 100 mg/l were available for analysis from the Muddy River, Virgin River, and Government Wash test sites. A least-square fit to these data is shown by the middle line in Figure 25. This shows a slight decrease in filterable residues with increasing nonfilterable residues. The negative slope to the line is not statistically significant. If the number of samples used and the scatter in the data are considered, the slope would have to exceed the dotted lines in Figure 25 to be statistically significant at the 90 percent confidence level. Thus, it can be concluded that within the accuracy limits of the Lake Mead data, there is no correlation between filterable and nonfilterable residues. This in turn leads to the conclusion that there was not a significant amount of clay particles being passed through the filters.

For the Lake Mead data there is apparently no conceptual uncertainty introduced by the choice of filter pore size. However, for other water bodies this may not be the case and it should be kept in mind in future studies that this type of uncertainty could be significant.

Removal of Peripheral Effects

A good test of the accuracy in removal of peripheral effects would be to look at water of known constant volume reflectance under varying solar, atmospheric, and surface conditions. Unfortunately, this is not easily done in the field since the time required for a change in weather conditions is usually sufficient to allow a possible change in water turbidity. In fact, the suspended sediment at many sampling stations resulted from resuspension of bottom deposits by wind and wave action. This observed correlation between

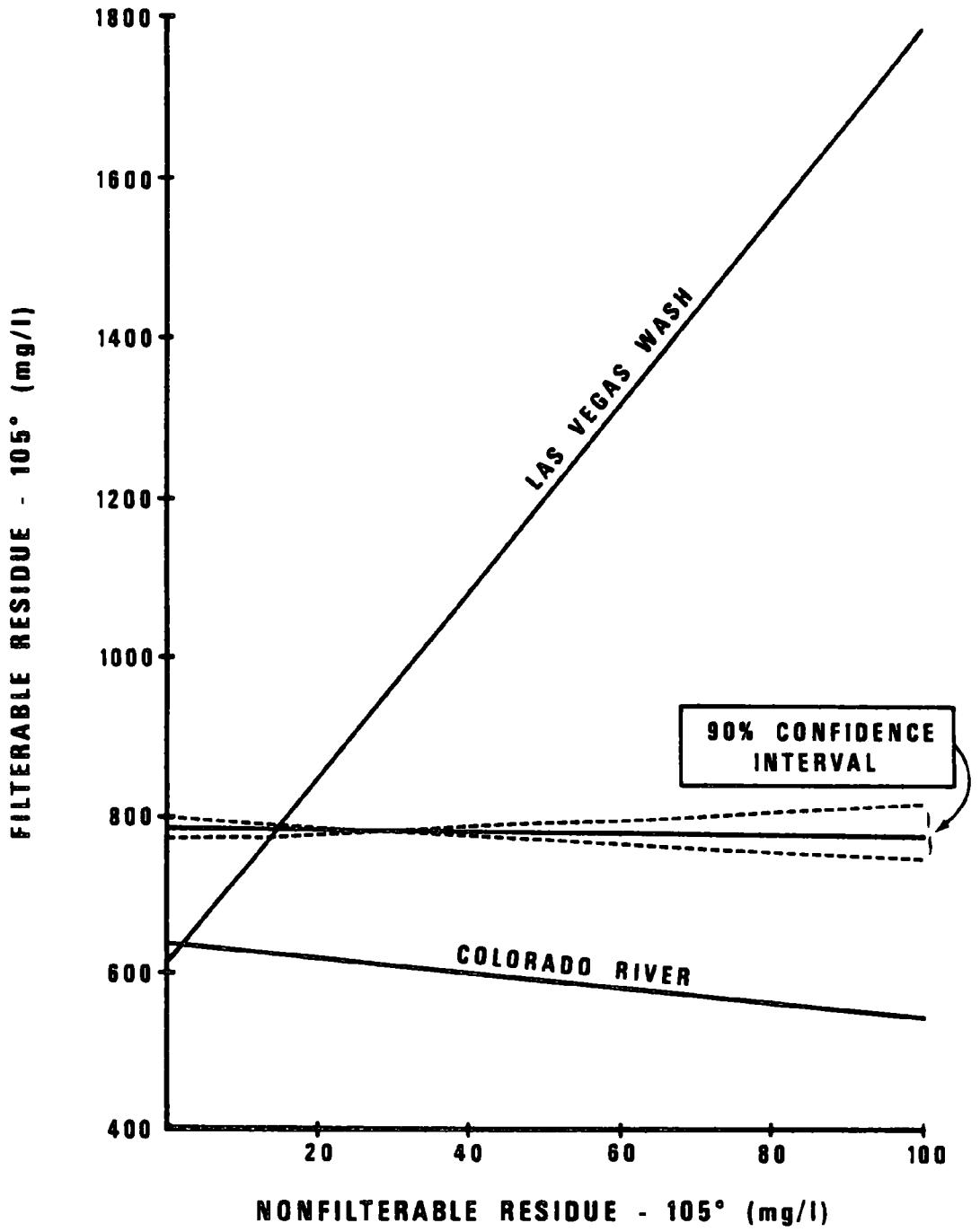

Figure 25. Least-squares linear fits to filterable and nonfilterable residue values from the analysis of the Lake Mead water samples.

weather and sediment concentration would preclude the general assumption that water volume spectral reflectance remains constant under changing weather conditions.

The assumption of uniform water would tend to be more valid in the open-water areas of the lake. One open-water station, MV1 (see Figure 31), was sampled under both clear and overcast sky conditions. Unfortunately, a few days prior to the collection of the overcast sky data on November 14, 1975, the lake apparently underwent an inversion. This changed the water color from its blue-green summertime appearance, which it had when the clear sky data were recorded on August 8, 1975, to a yellow-green color. The assumption of uniform volume reflectance is, therefore, questionable even for this open-water case. This is, however, the best test case we have, and although a shift of the reflectance peak from blue-green to yellow-green is expected, the magnitude of the reflectance might be expected to be about the same in both cases. Table 4 gives a comparison of sky and water conditions on these two days.

TABLE 4. SKY AND WATER CONDITION AT STATION MV1 ON 8/8/75 AND 11/14/75

Parameter	8/8/75	11/14/75
Cloud cover	Clear	Overcast
Percent illumination @ 652 nm resulting from skylight	6%	35%
Sun elevation	70 deg.	24 deg.
Wind velocity	1.0 m/sec.	Calm
Sea State	2 cm	--------
Secchi depth	5 m	2 m
Nonfilterable residue (105°C)	<5 mg/l	<5 mg/l
Turbidity	1.0 NTU	3.3 NTU

Data acquisition at station MV1 on November 14, 1975, was done under the heaviest cloud cover encountered during the entire project. These two examples probably represent the largest possible contrast in peripheral effects within the Lake Mead data.

Figure 26 shows a different albedo for the overcast and clear sky cases which were assumed to be of approximately equal water volume reflectance. The albedo can be divided into a volume reflectance component and a peripheral effects component according to the model developed in Section IV. Figure 26 shows the two components for each case. The peripheral effects component is much larger on the overcast day, and the volume reflectances are about equal. Both results are as expected, indicating that the procedure for removing peripheral effects was fairly accurate in this case if the assumption of equal reflectance was valid.

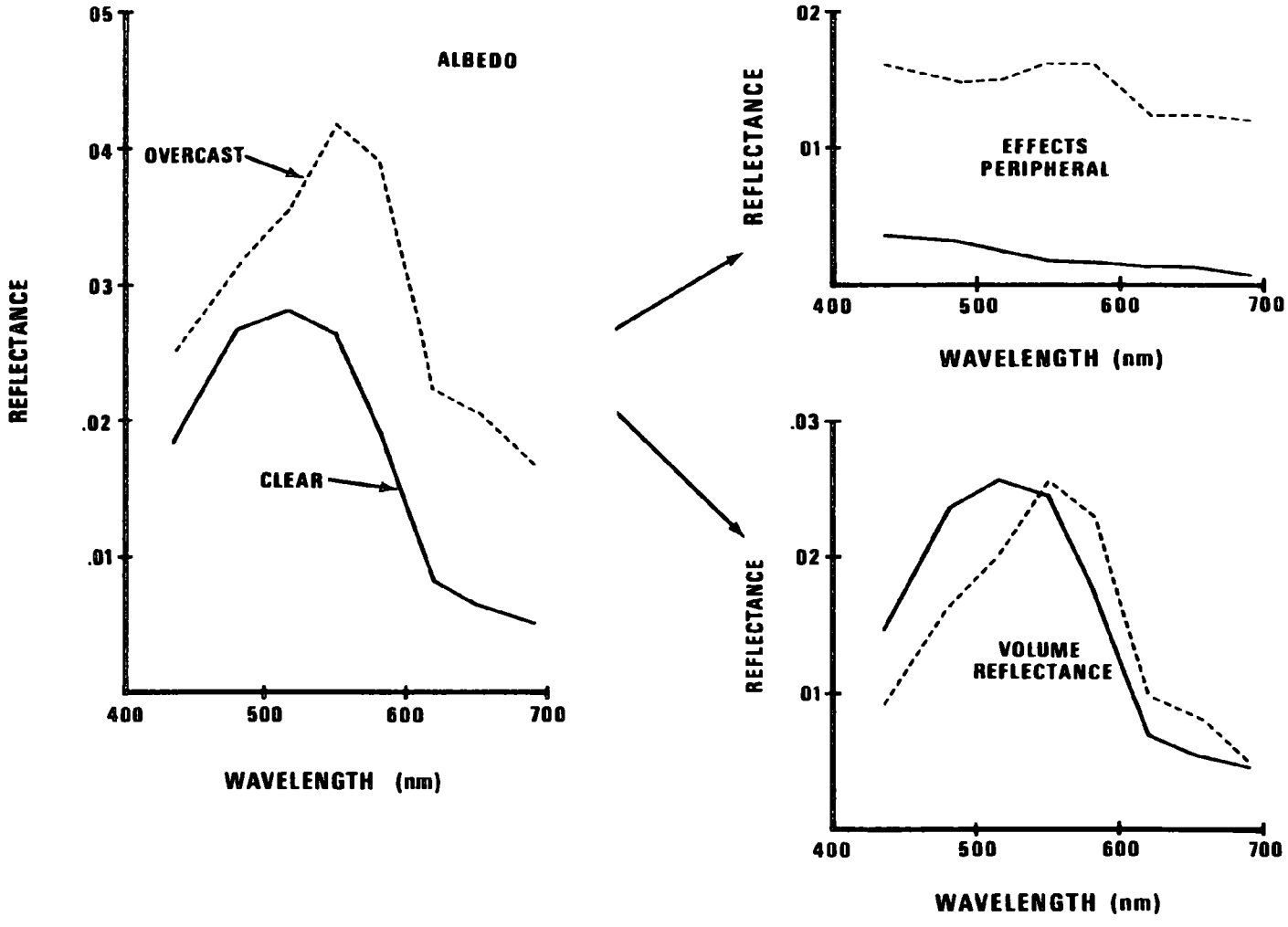

Figure 26. Albedos, peripheral effects, and volume reflectances of a clear and an overcast day at station MV1.

There is no sufficient data to assign a numerical value to the uncertainty in removing peripheral effects, nor can it be claimed on the basis of one sample that the uncertainty will always be relatively small. A quantitative analysis of the errors associated with the removal of peripheral effects is a subject which needs to be included in the next phase of the turbidity study.

Coincidence of Reflectance Data and Water Samples

The water viewed by the spectrometer is not the same water that is put into the sample bottle. Normally the water is homogeneous enough that this fact is of no consequence. However, in some cases where the water is non-uniform and moving, this problem can be significant.

Sampling stations L06 and C06 through C11 normally had currents with velocities up to 1.5 m/sec. Since the spectrometer required 30 seconds to sample its entire spectral range, the data were from a 45 m stretch of river rather than from a single point. Swirls and eddies associated with the water movement made the sediment concentration quite variable. Thus, each wavelength was in effect seeing a different sediment concentration and what went into the sample bottle was different yet.

Wherever this moving water was a problem, sediment concentrations were high and Secchi depths very small and both water samples were really surface samples. An examination of the variability in these replicate surface samples can give an estimate of the magnitude of the uncertainty associated with the lack of coincidence of reflectance and ground truth data. Thirty-one sample pairs from stations with currents were analyzed and found to have a standard deviation of ±33.8 mg/l about a mean value of 230 mg/l. Expressed as a normalized variance this uncertainty is 0.022.

The data coincidence uncertainty was also evaluated in units of nephelometric turbidity. The same 31 samples had a mean value of 129 NTU, a standard deviation of ±14.8 NTU, and a normalized variance of 0.013.

LABORATORY ACCURACY

The laboratory analysis of water samples collected coincident with spectral reflectance data provided the ground truth for derivation and evaluation of multispectral turbidity algorithms. The laboratory procedures for measuring the turbidity-related water parameters described in Section III are subject to a certain amount of error which contributes to the overall uncertainty in the statistical results obtained from the Lake Mead data.

Laboratory accuracies for the seven measurements were determined by replicate sample analysis of 21 selected samples. These samples were divided in half and each half treated as a separate sample. The difference between results for the halves of the same sample is an indication of the accuracy of the laboratory procedures. Color and turbidity measurements were not included

in the replicate sample analysis. Accuracies for these parameters are taken from method description (American Public Health Association, 1971). Table 5 gives the accuracies of the nine measured water parameters.

TABLE 5. UNCERTAINTIES IN LABORATORY ANALYSIS RESULTS

Parameter	Mean	Standard Deviation	Normalized Variance
Filterable Residue (105°C)	781 mg/l	±9.3 mg/l	0.0001
Filterable Residue (180°C)	747 mg/l	±13.3 mg/l	0.0003
Nonfilterable Residue (105°C)	27.1 mg/l	±4.3 mg/l	0.0252
Nonfilterable Residue (180°C)	24.4 mg/l	±5.7 mg/l	0.0546
Nonfilterable Residue (550°C)	20.4 mg/l	±8.2 mg/l	0.1616
Nonfilterable, Volatile Residue	4.4 mg/l	±10.0 mg/l	5.1653
Total Residue (105°C)	808 mg/l	±10.3 mg/l	0.0002
Color	20	±5	0.0625
Turbidity	5 NTU	±0.05 NTU	0.0001
	25 NTU	±0.5 NTU	0.0004
	70 NTU	±2.5 NTU	0.0013
	250 NTU	±5.0 NTU	0.0001

Note the large variances associated with the nonfilterable residues compared with the small variances associated with turbidity. This seems to indicate the superiority of optical techniques over gravimetric techniques for measuring the low sediment concentrations typical of natural water bodies. Since the remote method is optical, it is possible that the accuracy of remote techniques may exceed the accuracy of laboratory measurements made gravimetrically.

ERROR SUMMARY

Table 6 contains a summary of the error sources discussed in this section. Since instrumental errors are a function of wavelength, total uncertainty will vary slightly with wavelength. Table 6 contains data for the 652 nm (red) and 782 nm (near-IR) wavelengths only.

TABLE 6. SUMMARY OF UNCERTAINTIES IN THE LAKE MEAD DATA IN UNITS OF SUSPENDED SEDIMENT

		25 mg/l Water		250 mg/l Water	
Type	Source	652 nm	782 nm	652 nm	782 nm
Instrumental	Spectrometer	4.8	2.1	57.0	28.0
	Laboratory	3.4	3.4	12.5	12.5
Conceptual	Depth Distribution	6.5	6.5	----	----
	Peripheral Effects	----	----	----	----
	Filter Pore Size	0.0	0.0	0.0	0.0
	Sample Coincidence	----	----	36.7	36.7
Total		8.8 mg/l	7.6 mg/l	68.9 mg/l	47.8 mg/l

Table 7 is the error summary given in units of nephelometric turbidity.

TABLE 7. SUMMARY OF UNCERTAINTIES IN THE LAKE MEAD DATA IN UNITS OF NEPHELOMETRIC TURBIDITY

		15 NTU Water		150 NTU Water	
Type	Source	652 nm	782 nm	652 nm	782 nm
Instrumental	Spectrometer	3.1	1.3	43	16.5
	Laboratory	0.3	0.3	3.6	3.6
Conceptual	Depth Distribution	3.0	3.0	----	----
	Peripheral Effects	----	----	----	----
	Filter Pore Size	0.0	0.0	0.0	0.0
	Sample Coincidence	----	----	17.2	17.2
Total		4.3 NTU	3.3 NTU	46.6 NTU	24.1 NTU

If it is assumed that errors for sediment concentrations or turbidities other than those specifically evaluated are represented by a linear interpolation between the evaluated points, then expected accuracies as a function of ground truth value would be as shown in Figure 27. This figure would tend to lead to the following conclusions.

Algorithms based on IR wavelengths will be more accurate than those operating at visible wavelengths. This is a result of the spectral response of the spectrometer used here and is not an inherent property of water volume reflectance.

In the visible wavelength there is not a significant difference in accuracy between measurements of nonfilterable residues and nephelometric turbidities. However, in the near-IR wavelengths nephelometric turbidity can be measured more accurately.

Visible algorithms are not expected to meet EPA's desired accuracy of $\sigma^2 = 0.05$. IR algorithms should achieve this accuracy for high sediment concentrations. Nephelometric turbidity measurements at IR wavelengths may be capable of 0.05 variances down to the desired 25 mg/l ($\simeq$ 15 NTU) threshold.

Although the desired accuracy cannot be met in every case, we should not miss it by far. If the error analysis results are verified by the performance of actual algorithms, accuracy should be close enough to what was desired that remote multispectral techniques will prove to be feasible for EPA monitoring purposes.

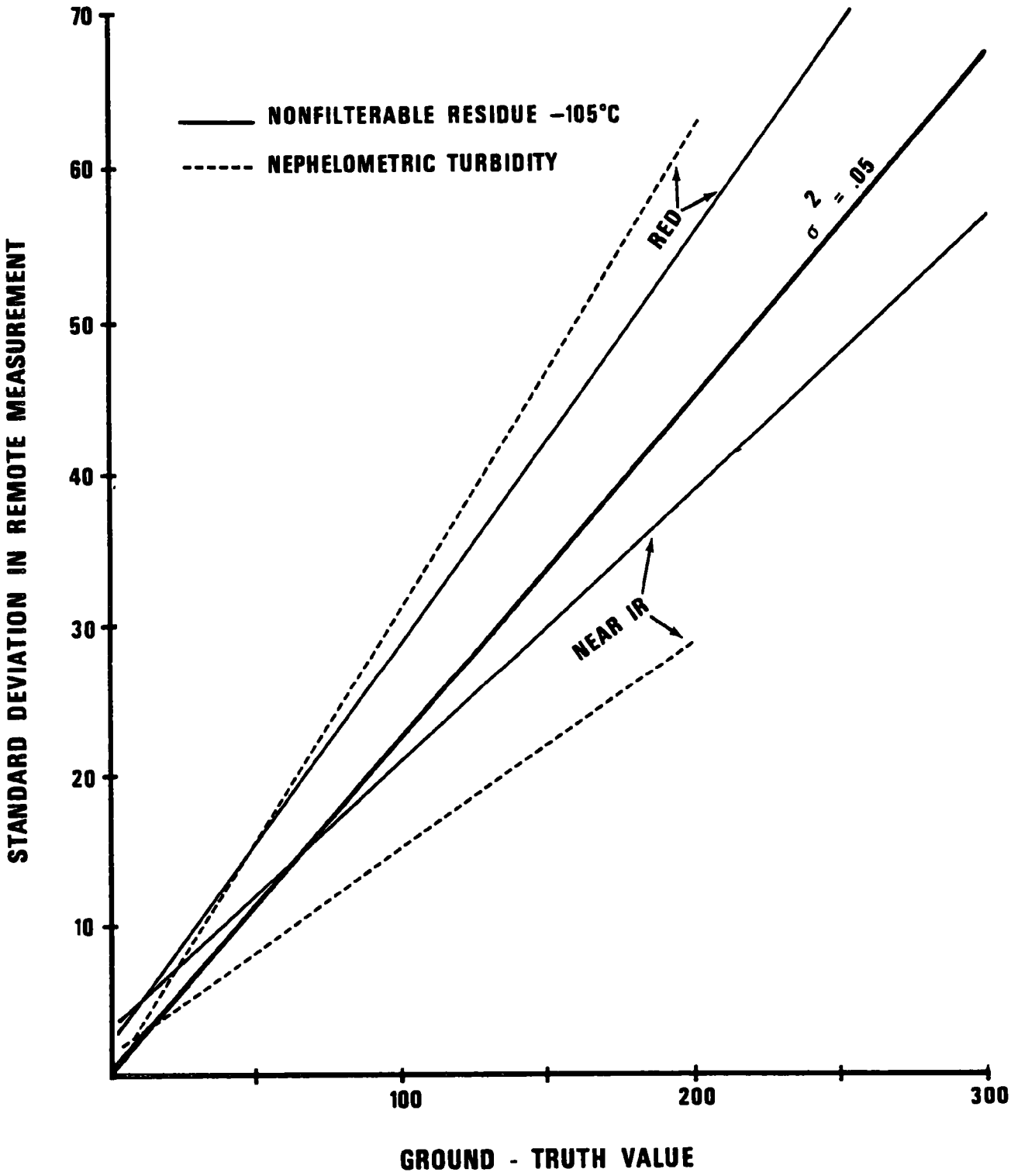

Figure 27. Uncertainties in the Lake Mead data as a function of residue and turbidity values.

SECTION VII

DATA ACQUISITION

LAKE MEAD TEST SITES

The data base for the analysis work undertaken to determine feasibility of remote techniques for monitoring suspended sediment was acquired through field operations as Lake Mead, Nevada-Arizona, from June 20, 1975, to January 8, 1976. Lake Mead is not a turbid water body and is, therefore, not an ideal test site for water turbidity studies. It was selected because of its proximity to the Las Vegas, Nevada, offices of project personnel. Although the lake was not ideal, it proved to be an adequate test site.

Since an investigation of the transferability of signatures is a prime objective of this study, five test sites within the lake were selected which we hoped would have different sediment types. These sites are shown in Figure 28. The physical characteristics of each site are described below.

Colorado River Inflow

The Colorado River, spanned by Hoover Dam to form Lake Mead, carries a considerable sediment load into the lake. The Glen Canyon Dam 483 kilometers (300 miles) upstream from Lake Mead forms Lake Powell which collects all sediment from the upper basin of the Colorado River watershed. Thus, the sediment entering Lake Mead originates from bed and beach degradation in the canyon areas below Glen Canyon Dam. The Grand Canyon gauging station 322 kilometers (200 miles) above Lake Mead measured an annual sediment load of 13.1 million metric tons in 1969, the last year for which data are available (Laursen and Silverston 1976).

Sampling extended up to Columbine Falls in an area known as the Lower Granite Gorge. At this point the river current was observed to be quite variable ranging up to 1.5 m/sec. At times of high current, suspended sediment concentration was greatly increased, probably because of resuspension of particles which had settled during times of slack current. Sampling at this site was conducted during the month of September and at this time the river water was 18°C compared to reported lake water temperatures of 27°C.

Government Wash

There is no natural inflow at this test site except from very infrequent flash-floods. Bottom sediments here were thought to consist of particles

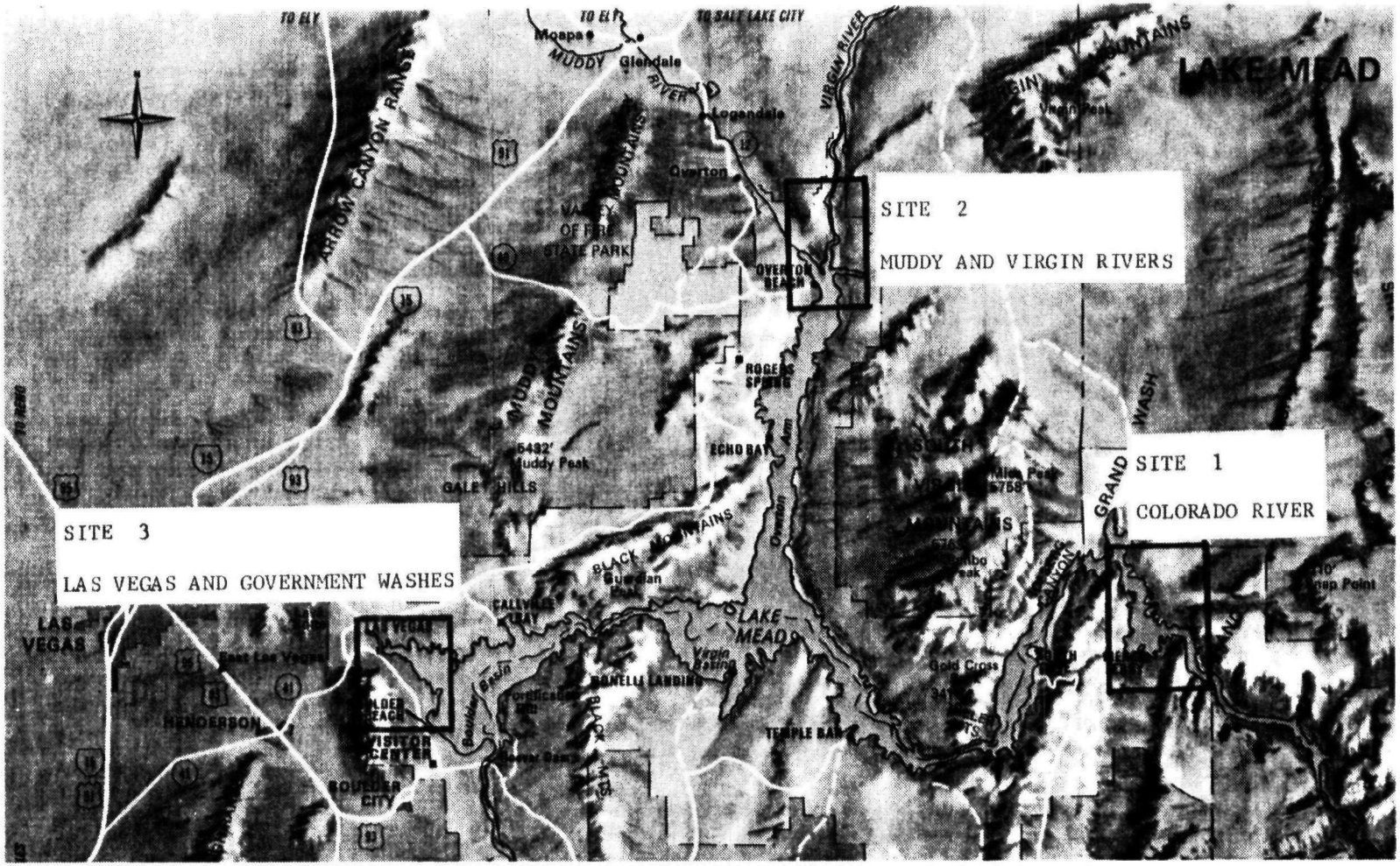

Figure 28. Lake Mead test sites.

resulting from bank erosion in the wash during flash-flood periods. Turbidity at this site was the result of resuspension of bottom sediments. During the summer months man-made agitation (swimming, water skiing, boating, etc.) provided the resuspension mechanism. During the winter months wind and wave action would occasionally generate considerable resuspension but generally the water was very clear. We were forced to resort to using the prop wash of the boat over shallow areas to artificially resuspend sediments in order to obtain high turbidity data in the wintertime.

Las Vegas Wash

This wash receives a continual flow of wastewater from the Clark County sewage treatment facilities. The inflow here is extremely turbid, presumably as the result of bank erosion in the sand bed of the wash. The sediment was observed to settle almost immediately upon entering the slack water of the lake.

Because of its origin this inflow was thought to be rich in dissolved matter, some of which would contribute to accelerated growth of algae and phytoplankton. This site was sampled for this reason, in hope that the question of chlorophyll interference could be investigated from data collected here.

Muddy River

The Muddy River is a constant running stream originating from warm springs about 40 kilometers (25 miles) above Lake Mead. Except in times of heavy rains and flash-flooding, it probably carries little sediment. Extensive agricultural activities are conducted over the entire length of this river valley, and sediment and wastes resulting from agriculture undoubtedly enter the river at times.

The mouth of the river was not accessible from the lake in a boat of the size being used and so no current-suspended sediment was observed here. Turbidity was quite variable from day to day, but no correlation was observed between turbidity and any specific factor such as river inflow or wind velocity.

Virgin River

Water flow in this river is seasonal. Snowmelt runoff from southwestern Utah results in large flow-rates and substantial sediment loads in the springtime. The July through November sampling period at this site corresponded to periods of no significant inflow.

Although river flow did not bring suspended sediment to this site, wave action over submerged mud flats near the mouth of the river did generate good sediment concentrations when the conditions were right.

The Virgin River, like the Muddy River, supports agriculture alony its banks for many miles above Lake Mead. Pollutants associated with agricultural activities undoubtedly enter the lake from this river, but since flow had ceased during our data acquisition, this is not thought to be a factor in this study.

SAMPLING STATIONS

Specific sampling stations were selected at each site. These locations are shown in Figures 29 through 31. No attempt was made to obtain equal numbers of samples from each station. Stations with higher turbidity were generally sampled more frequently than others. Forty samples were acquired from each of the five sites for a total of 200 samples.

FIELD PROCEDURES

Each station sampling consisted of the recording of spectrometer data, the collection of water samples, and atmospheric or sun conditions. Widely varying conditions were encountered which required occasional adjustments in field procedures. However, for the majority of samples the field procedures were as described below.

Spectrometer Data

Once the boat was positioned and anchored with the spectrometer side toward the sun, the acquisition of spectrometer data proceeded as follows.

The holder for the calibration panels was lowered into the horizontal position and the gray panel was put in place. With the spectrometer on the low gain setting, the sunlit gray panel was used to adjust the strip chart gain so that maximum chart deflection would be about 80 percent of full scale. The chart recorder gain was not changed again at this station.

Two complete spectral scans of gray panel data were recorded: one at the spectrometer high gain position and one at the low gain position.

The gray calibration panel was replaced with the white one. With the spectrometer on low gain and a shadow cast on the white panel, one spectral scan is recorded. The shadow was created by a hand-held device as shown in Figure 32.

After covering the aperture of the spectrometer to block all light from entering, one scan was recorded at both the high gain and low gain position.

Calibration panels were removed and panel holder raised to permit viewing of the water. Either the high or low

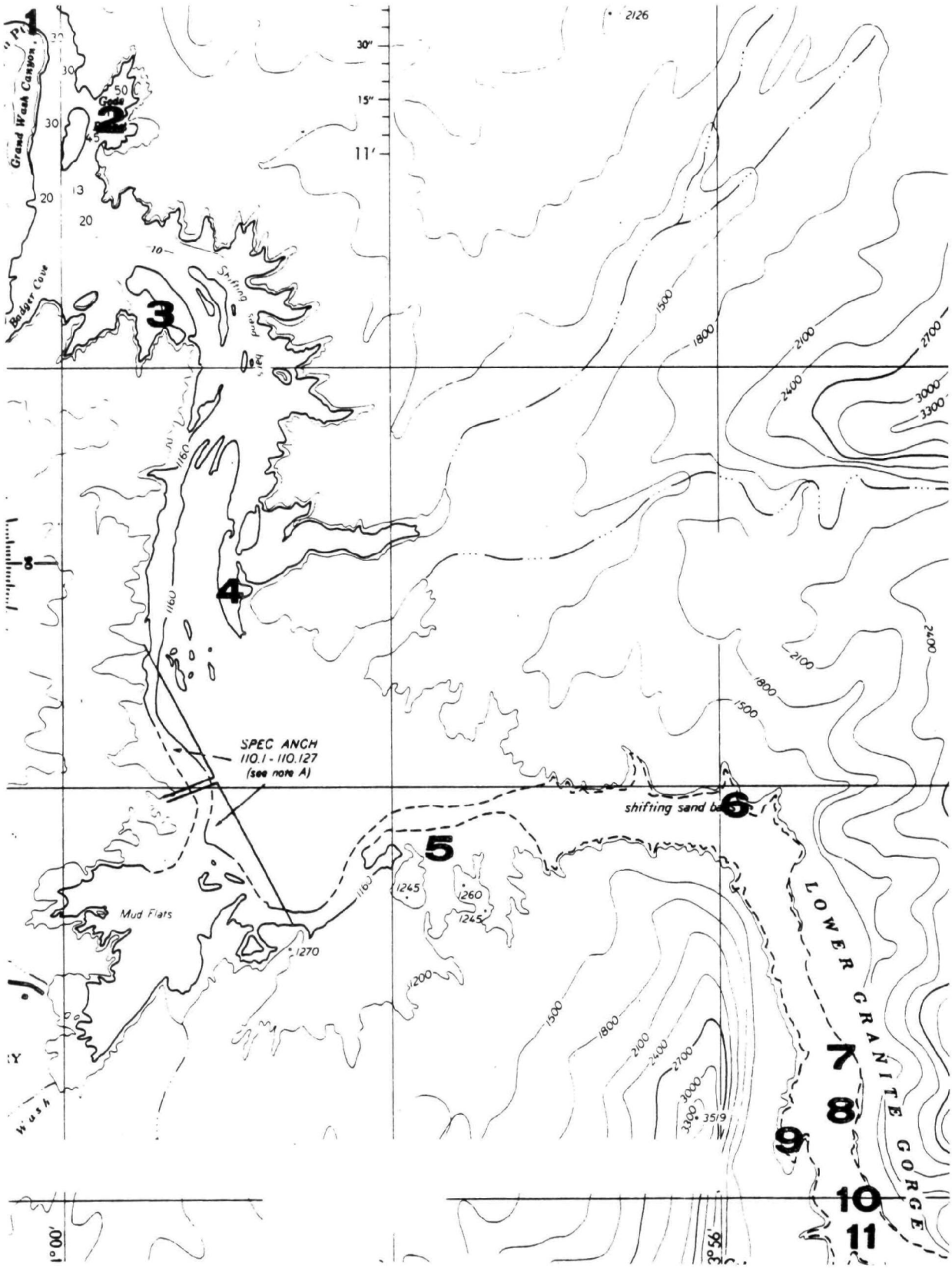

Figure 29. Sampling stations at the Colorado River site.

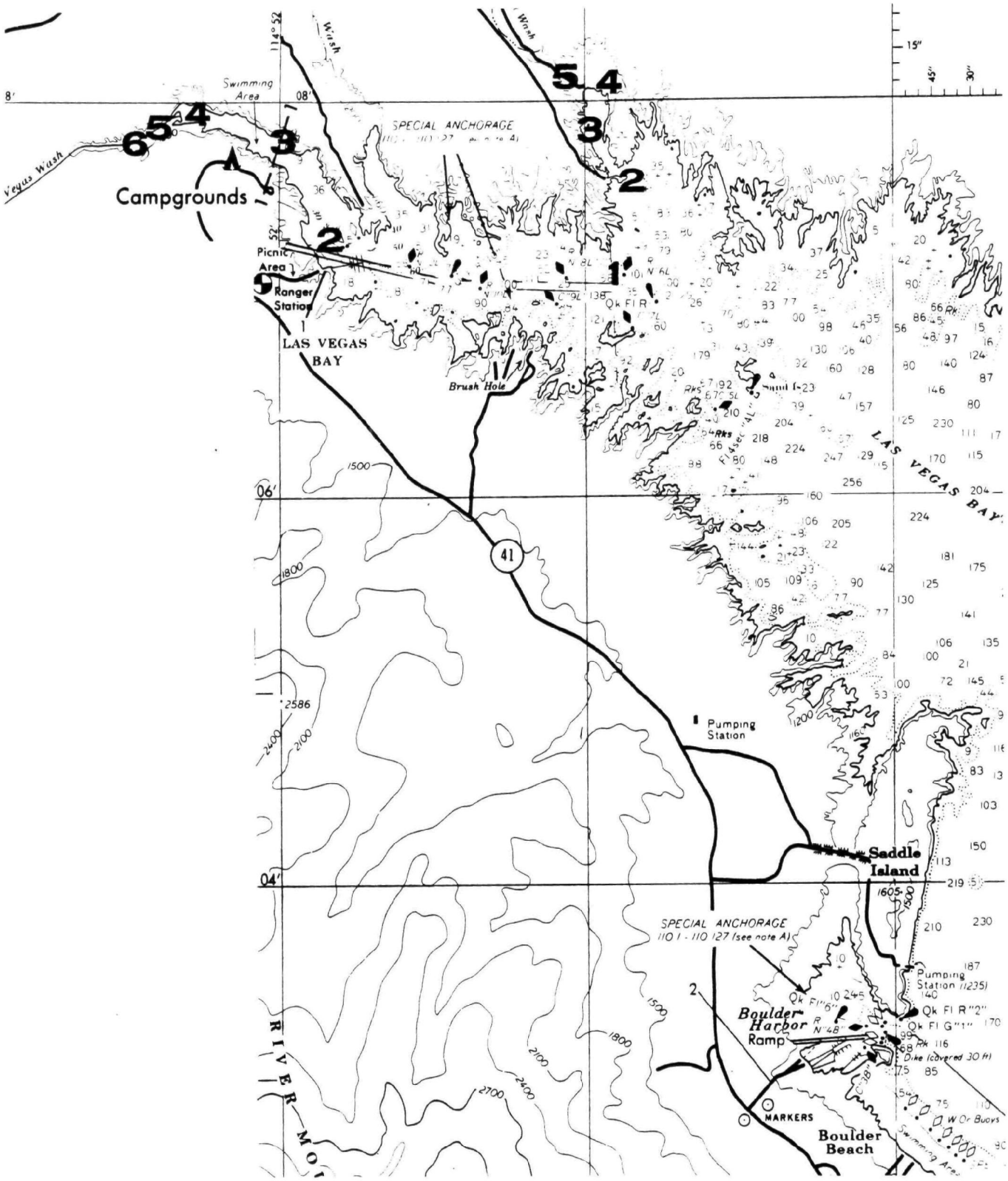

Figure 30. Sampling stations at the Las Vegas Wash and Government Wash sites.

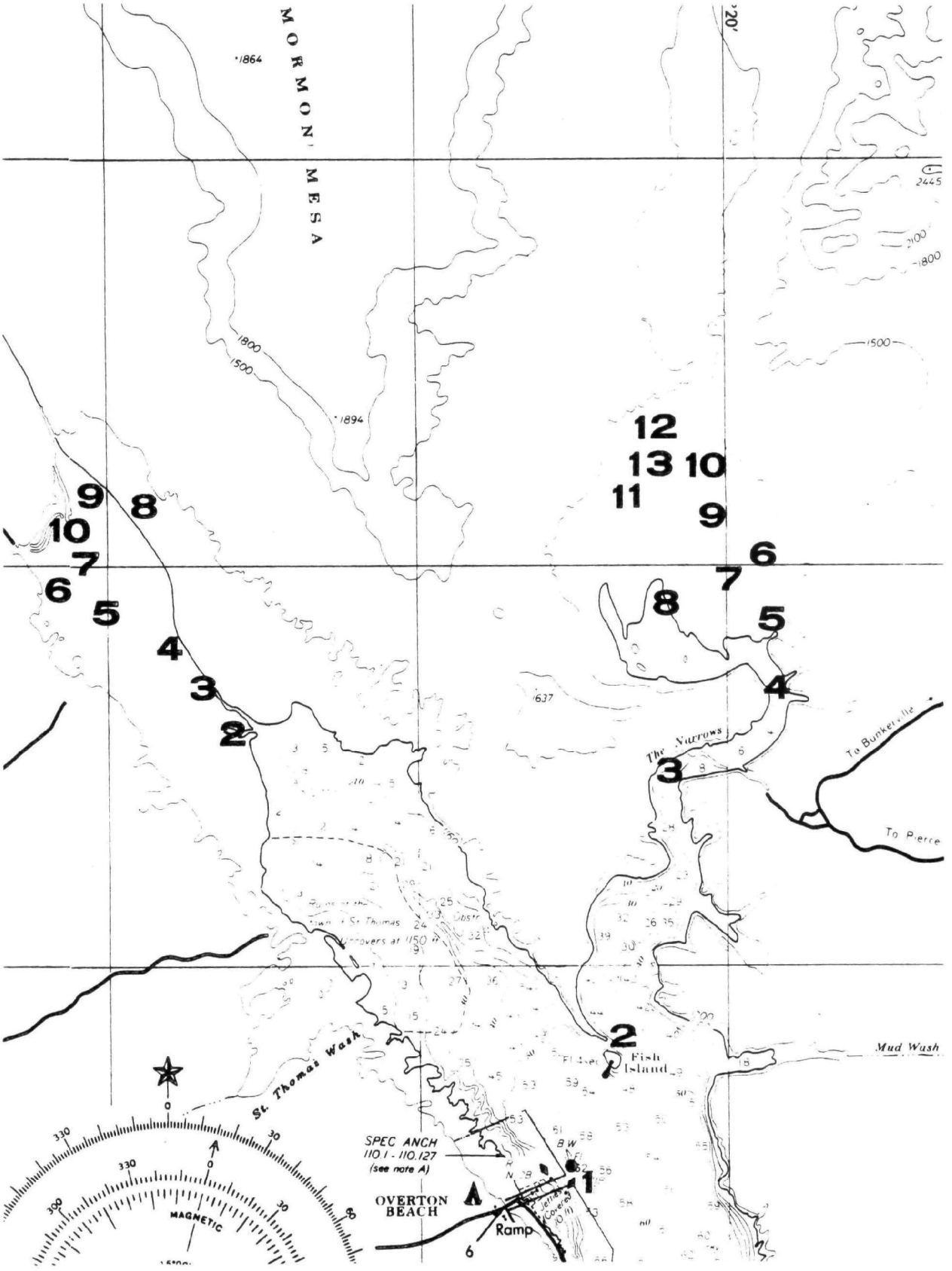

Figure 31. Sampling stations at the Virgin River and Muddy River sites.

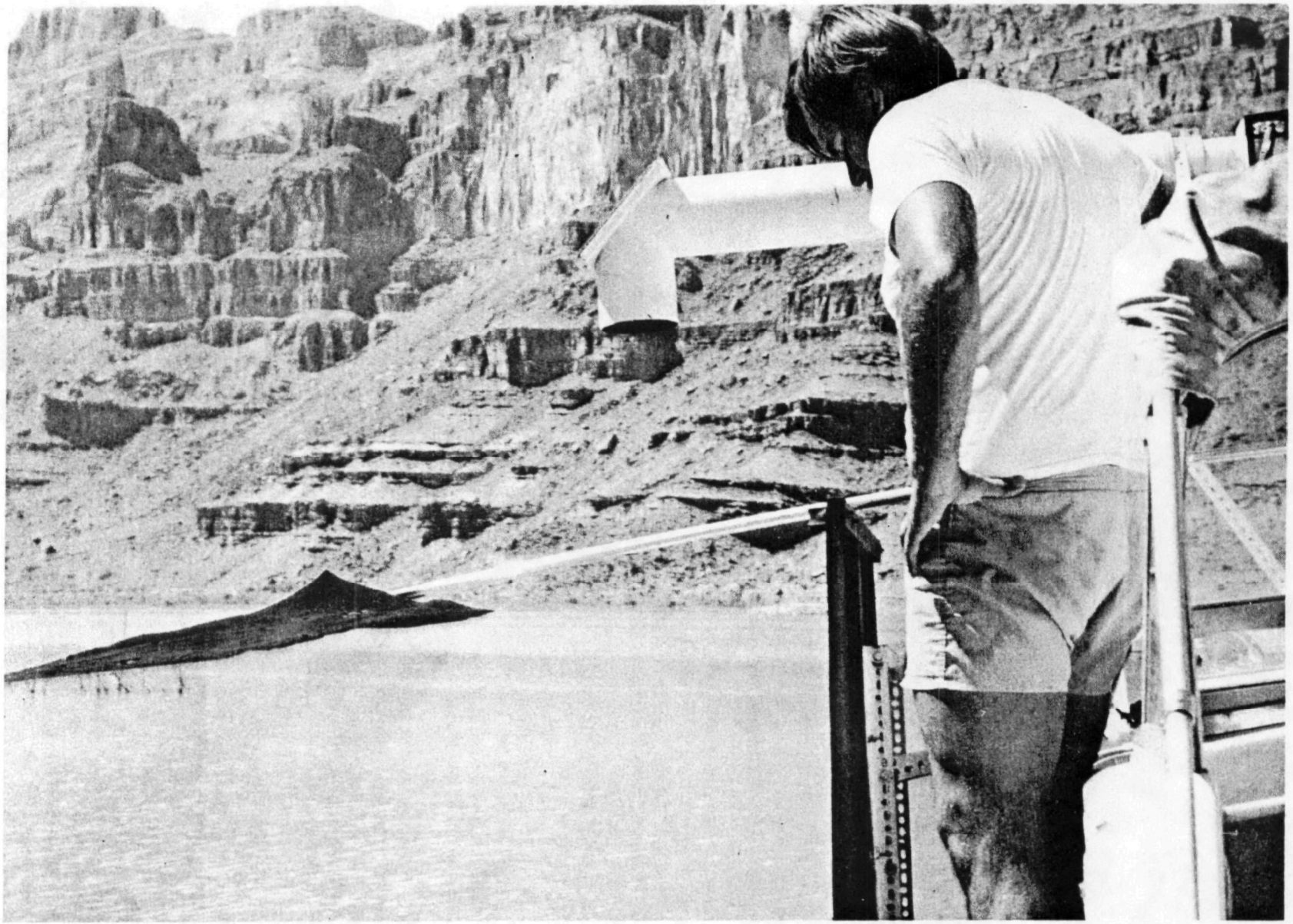

Figure 32. Casting a shadow on the calibration panel.

spectrometer gain position was selected depending on water turbidity. Five complete scans of data were recorded at vertical viewing, 15° fore and aft, and 30° fore and aft.

Water Samples

While the five spectral scans of the water were being recorded two water samples were collected. One sample was from the surface and was collected by dipping into the lake with a bucket. The second sample was taken at the Secchi extinction depth using a Van Dorn sampler. The water samples were stored on ice in 3.8-liter (1-gallon) containers until delivered to the EPA Laboratory in Las Vegas.

Related Field Parameters

For each sample, the top half of the form shown in Figure 33 was completed as a record of conditions at the time. Some of these parameters were specifically needed to accomplish peripheral effects removal while others were of general interest because of their possible effects on the data. Color photographs of sky and water conditions were taken at most sampling stations.

DATA REDUCTION

Spectrometer data were recorded in the field on a strip chart recorder. Manual reading of signal levels from the strip chart and keypunching of these values was required to reduce the data to a computer compatible form.

Figure 34 shows the video channel signals for a typical data set. The signal for the covered aperture case is not shown since it was perfectly flat at 2.0 cm. These data were recorded at Las Vegas Wash, Station L06, on December 17, 1975. The water samples collected here contained 212.5 mg/l of nonfilterable residue which gave a high return from the water. In this case all data were recorded at the low gain setting. Deflection values in centimeters were keypunched along with water sample analysis results and field observations for input into the computer program VOLREF, which calculates volume spectral reflectance according to the method described in Section IV. The computer output for the Figure 34 sample case is shown in Figure 35.

This report contains only this one computer-generated data tabulation as an example. Tabulations of raw data for all 200 samples collected at Lake Mead are too voluminous to include here. Computer printouts like that shown in Figure 35 for all of the Lake Mead data have been delivered to the EPA Technical Monitor as a separate volume.

The data reduction program, VOLREF, was written as part of this project and was run on a CDC 6400 at the Department of Energy (DOE) computer facility. This program has not been formally documented but the comment statements contained within the program listing should provide adequate documentation for purposes of this project. Appendix B is a listing of this program.

MULTISPECTRAL TURBIDITY TECHNIQUES PROJECT
J. O. 71.03 (ROAP 22AEB - task 7)
Field Data Sheet

FIELD OBSERVATIONS

Identification	sample no. 35175-15		date 12/17/75	
	time 1015	PDT	observer R.H.	
Location	general discription Las Vegas Wash			
	grid coordinates ____	N	station no. LO6	
	____	W	depth Surface	m
Conditions	sun elevation 27.2	deg	secchi depth 0.12	m
	sun azimuth 160	deg	sky conditions Clear	
	wind direction 235	deg	boat heading 210	deg
	wind velocity 3.0	m/s	sea state .01	m
	water depth 0.37	m		
Photography	sky photo no. ——		vert water photo no. 1	
	oblique water photo no. 2			
SCS Standards	sun 13		shadow 14	

LABORATORY ANALYSIS REPORT

nonfilt residue (105)	248	mg/l	total residue (105)	3147 mg/l
settleable residue	——	ml/l	filt residue (105)	2899 mg/l
nonsettleable residue	——	mg/l	nonfilt, fixed residue	233 mg/l
nonfilt residue (180)	245	mg/l	color	—— Pt-Co units
filt residue (180)	2817	mg/l	nonfilt, vol residue	12 mg/l
turbidity	70	NTU		

REMARKS

Figure 33. Field observations form filled out at each sampling station.

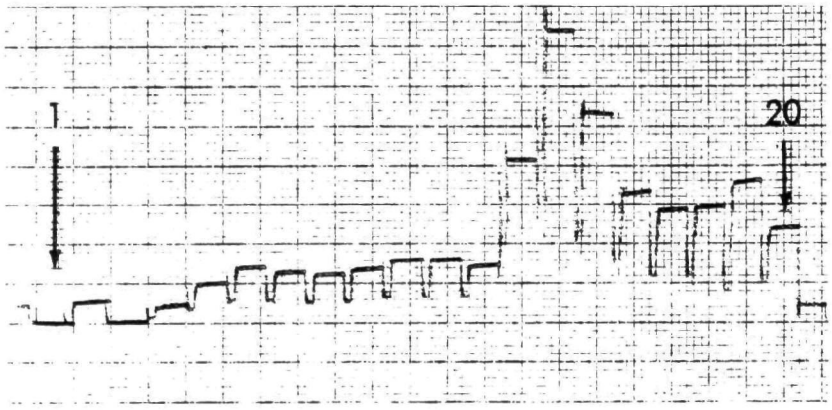

GRAY PANEL

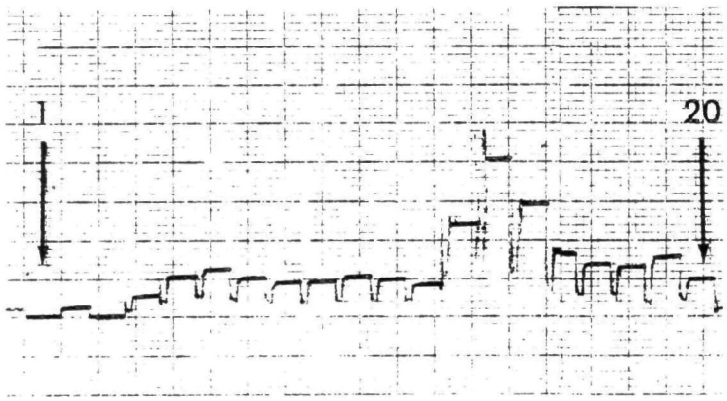

SHADED WHITE PANEL

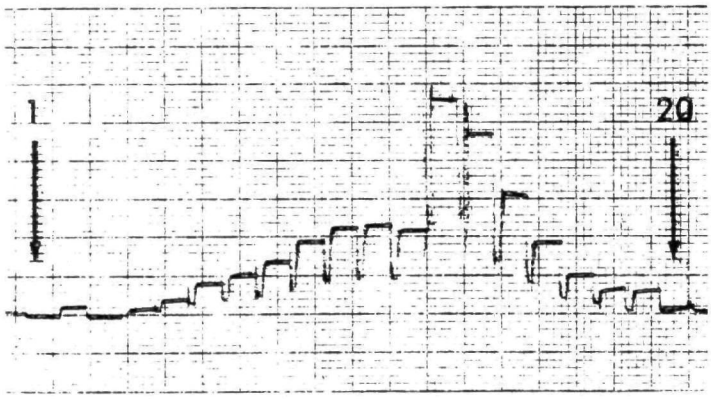

WATER

Figure 34. Spectrometer video outputs as recorded on strip chart for sample 35175-1.

ENVIRONMENTAL PROTECTION AGENCY - EMSL/LV
MULTISPECTRAL TURBIDITY TECHNIQUES STUDY

SAMPLE NUMBER	35175-1			
DATE	12/17/75		SITE	LAS VEGAS WASH
TIME (PDT)	1015		STATION	L06
SKY PHOTO NO.				
VERT. PHOTO NO.	1			
OBL. PHOTO NO.	2		REMARKS-	
SECCHI DEPTH	.1	M		
SEA STATE	1.0	CM		
LOOK ANGLE	0.0	DEG		
BOAT HEADING	210.0	DEG		
SUN ELEVATION	27.2	DEG		
SUN AZIMUTH	160.0	DEG		
WIND DIRECTION	235.0	DEG		
WIND VELOCITY	3.0	M/S		

LABORATORY ANALYSIS REPORT

NONFILT RESIDUE (105)	212.5 MG/L	TOTAL RESIDUE (105)	3102.0 MG/L
FILT RESIDUE (105)	2889.0 MG/L	NONFILT, FIXED RESIDUE	198.5 MG/L
NONFILT RESIDUE (180)	210.0 MG/L	COLOR (PT-CO TEST)	*****
FILT RESIDUE (180)	2815.0 MG/L	NONFILT, VOL RESIDUE	11.5 MG/L
TURBIDITY	60.0 NTU		

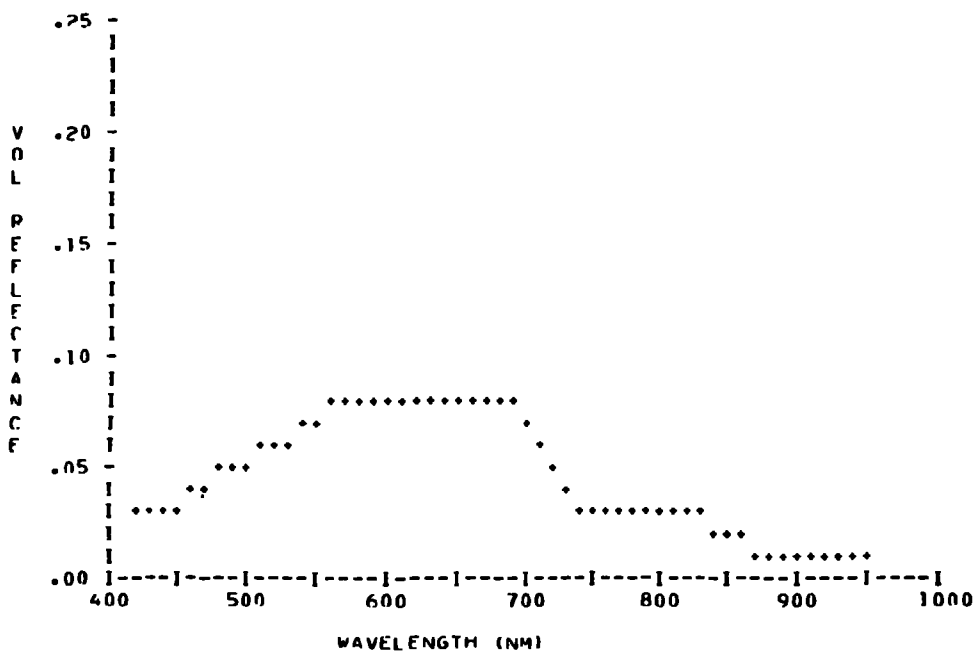

(continued)

Figure 35. Computer printout for the data shown in Figure 34.

SAMPLE NUMBER 35175-1 CONTINUED

	WAVELENGTH	VZ	VG	VE	VW	ALFA	ALFAP	RV
1	343	-0.00	-0.00	-0.00	-0.00	0.00	0.00	0.00
2	377	-0.00	-0.00	-0.00	-0.00	0.00	0.00	0.00
3	385	-0.00	-0.00	-0.00	-0.00	0.00	0.00	0.00
4	415	1.98	2.45	2.56	2.15	5.62	1.07	2.64
5	436	1.98	3.00	3.06	2.79	11.87	1.98	3.12
6	480	1.98	3.42	3.25	2.81	16.98	2.24	4.62
7	517	1.98	3.30	3.01	3.01	17.14	1.80	5.80
8	550	1.98	3.23	2.93	3.37	18.46	1.69	7.35
9	583	1.98	3.39	2.96	3.85	22.82	1.79	8.04
10	620	1.98	3.59	3.06	4.25	27.56	1.99	8.09
11	652	1.98	3.60	3.00	4.33	28.15	1.91	8.21
12	690	1.98	3.45	2.84	4.20	26.32	1.62	8.31
13	703	1.98	6.16	4.41	7.58	80.93	4.56	6.81
14	742	1.98	9.40	6.09	6.69	156.37	7.71	2.91
15	782	1.98	7.33	4.95	5.11	98.80	5.57	3.06
16	829	1.98	5.30	3.66	3.82	64.33	3.15	2.76
17	862	1.98	4.86	3.40	3.00	57.67	2.77	1.67
18	905	1.98	4.96	3.34	2.63	63.96	2.78	.93
19	942	1.98	5.60	3.60	2.62	82.11	3.37	.70
20	984	1.98	4.41	3.00	2.16	55.13	2.12	.25

Figure 35. (Continued)

SECTION VIII

DATA DESCRIPTION

SUSPENDED SEDIMENT CONCENTRATIONS

Water with high concentrations of suspended sediment was not easily found in Lake Mead. Figure 36 is a histogram of nonfilterable residue (105°C) values in the 200 samples collected from the lake. The sediment loads ranged from 0.0 to 1137.0 mg/l but the distribution is heavily weighted toward the low concentration end. It would have been better to have a more uniform distribution of samples over the entire range, but the data collected should be adequate for the intended statistical analysis.

VARIABILITY OF SEDIMENT TYPES

Since an investigation of the transferability of algorithms between sediment types is a major objective of this study, it is necessary to determine if the data set does indeed contain different sediment types. Three different comparisons have been made between data from the five sites. In all comparisons the conclusion reached is that the Lake Mead data is representative of a large variety of sediment types and should, therefore, be well suited for signature transferability study. The specific comparisons are summarized below.

Visual Appearance

Sediment samples were dredged from the lake bottom with the boat anchor at each of the five sites. Visually these samples all appear different. Color tones range from gray for Las Vegas Wash, to yellow-brown for the Muddy River, to dark brown for the Colorado River.

Spectral Reflectance

The silt samples all had higher reflectance when dry than when wet. The samples were moistened to be more representative of what the sediment would look like suspended in water, and the spectral reflectance of the moistened samples was measured. Measurements were made in the laboratory using the field spectrometer to give relative values with respect to Kodak gray cards whose spectral reflectance was known.

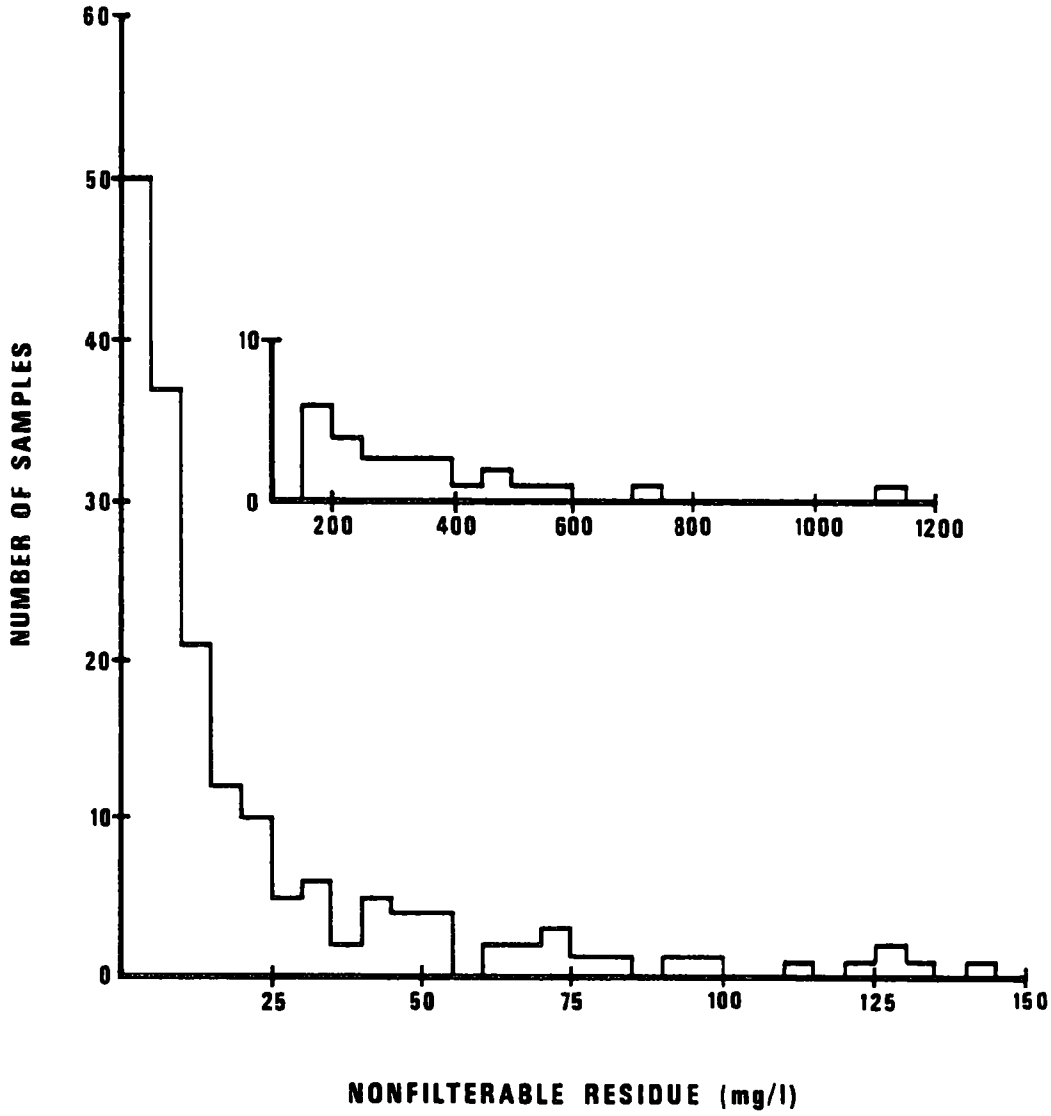

Figure 36. Histogram of nonfilterable residue (105°C) values in the 200 Lake Mead samples.

Figure 37 shows the reflectance curves for the five moistened sediment samples. These curves generally agree with the visual observations, i.e., the gray Las Vegas Wash sample reflectance is flat in the visible range, the darkest colored sample from the Colorado River shows the lowest spectral reflectance, etc. Spectral reflectance curves indicate a diversity of sediment types.

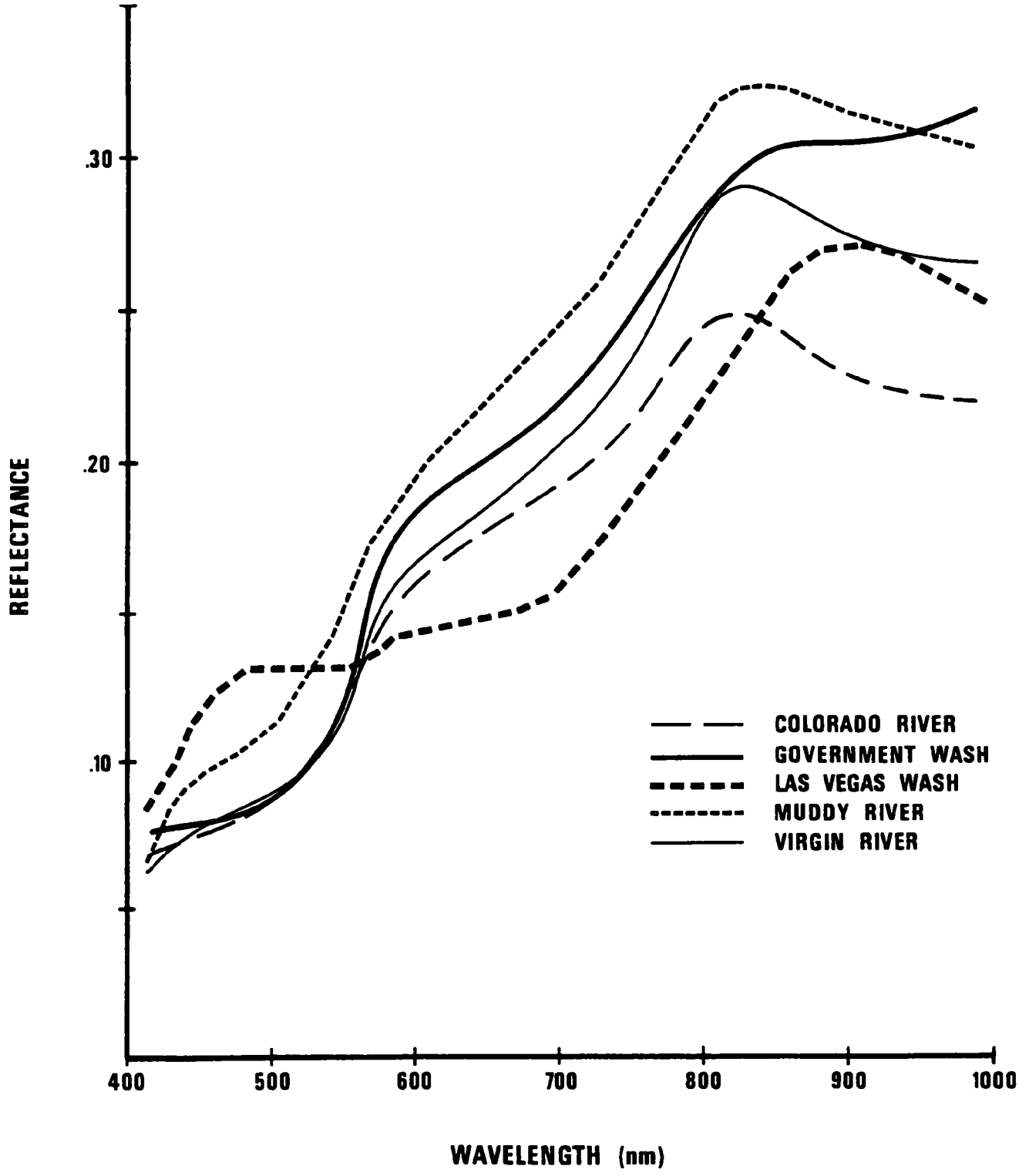

Figure 37. Spectral reflectance curves for the moistened sediment samples.

Scattering Properties

The optical properties of sediment in suspension were compared by relating the laboratory measurements of nonfilterable residue (105°C) to nephelometric turbidity which is a light-scattering measurement. These two parameters are plotted in Figure 38 for all samples in the 50 to 500 mg/l range. No well-defined relationship is apparent in this figure. The uncertainty in laboratory measurements is given by the bars in the center of the graph to show that the scatter in data points cannot be accounted for by instrumental uncertainties. The only conclusion which can be drawn from this graph is that the sediments in the samples are widely varying in scattering properties.

Figure 38 also shows two turbidity vs. residue curves given by previous investigators. Both curves are linear but drastically different in slope. Rosgen (1975) states that the sediment in his study originated from stream bank erosion and consisted of fine sand particles. Scherz and Van Domelen (1975) identify the sediment for their curve as taconite rock flour which consists of extremely fine particles, presumably in the clay particle range. If the difference between the slopes of these lines is primarily the result of particle size, they would seem to represent the extreme cases in the nephelometric turbidity-nonfilterable residue (105°C) relationship. One probably will not find particles smaller than those encountered by Scherz and Van Domelen, and particles larger than those encountered by Rosgen would be too large to remain in suspension. Since the Lake Mead data set contains points in line with each of these curves and others covering the entire area between the lines, it is concluded that, in terms of scattering properties, the data contain sediment variability spanning the entire expected range. However, the number of samples at the clay end of the range is very small which is consistent with the earlier conclusion (page 64) that there was not a significant amount of clay particles in the Lake Mead water samples.

COLOR INTERFERENCES

Water color can be the result of phenomena other than scattering by sediment particles. Color effects from other sources will interfere with estimates of suspended sediment concentration based on water color. The two most common color interferences are thought to result from the presence of tannic acid and small living organism in the water. The choice of sampling sites at Lake Mead was made in the hope that these interfering effects would be present in part of the data so that their significance could be evaluated. The following paragraphs discuss the existence of these two effects in the Lake Mead data.

Tannic Acid

The presence of tannic acid in natural water bodies is the result of the decay of humic material. This compound absorbs blue light resulting in a water color ranging from yellow to reddish-brown depending on the acid concentration.

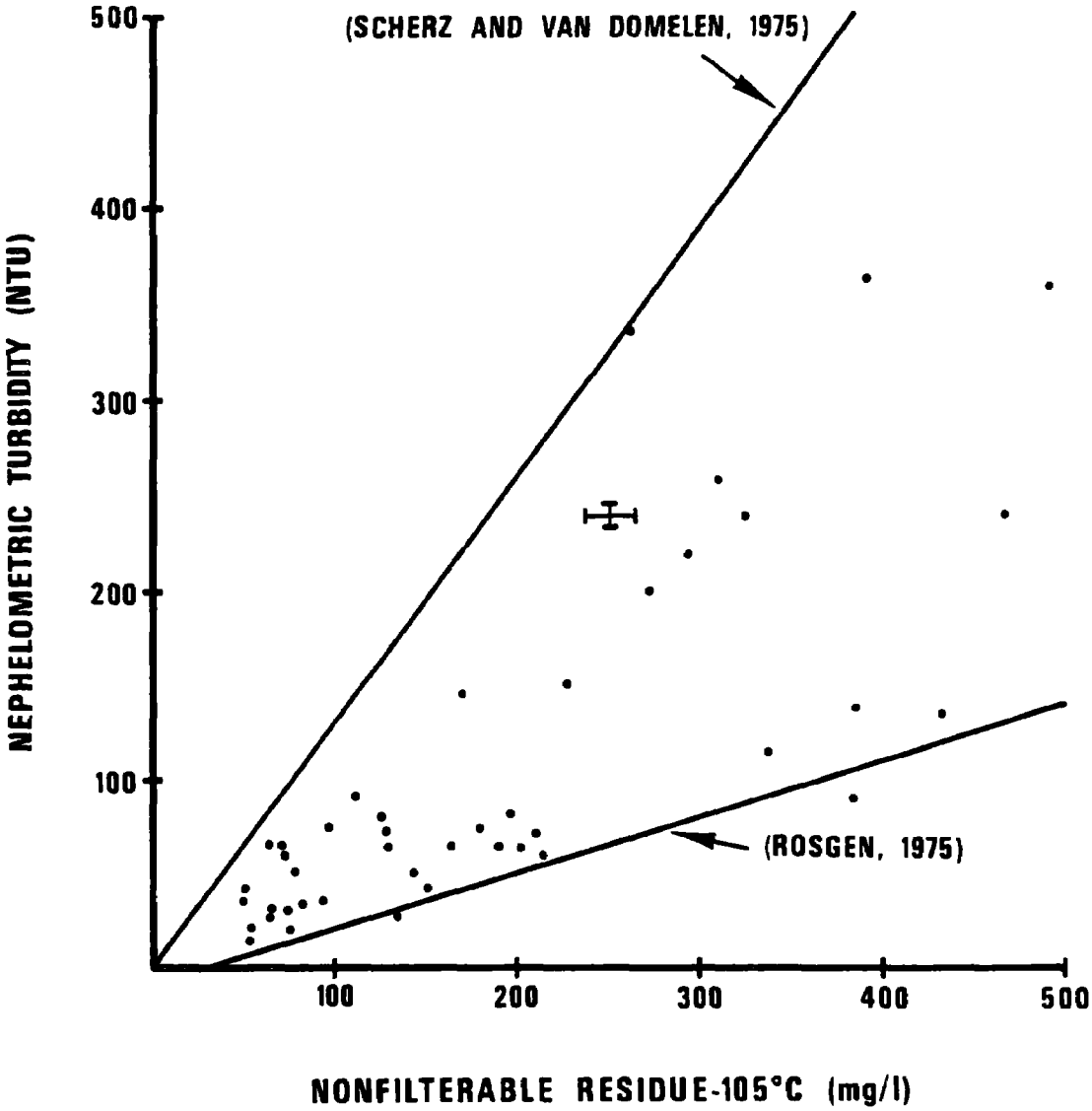

Figure 38. Nonfilterable residue (105°C) vs. nephelometric turbidity for all Lake Mead samples in the 50 to 500 mg/l range.

The platinum-cobalt color test was included in the laboratory analysis of water samples to detect the presence of tannic acid. However, standard methods for this test require a maximum sample hold time of 24 hours, and frequently the color test could not be made within this time. The color test was performed on 70 of the 200 samples collected. Table 8 lists the number of samples tested and the mean color values by site.

TABLE 8. PLATINUM-COBALT COLOR AVERAGES BY SITE

Site	Number Tested	Average Pt-Co Color
Colorado River	0	--
Government Wash	17	10
Las Vegas Wash	15	21
Muddy River	12	14
Virgin River	26	12

A value of 10 Pt-Co units is the detection threshold for this test. There was, therefore, virtually no tannic acid color at four of the five sites. The Las Vegas Wash site had some color but a value of 21 is not thought to be high enough for tannic acid to be considered a significant source of color interference. Tannic acid color interference cannot, therefore, be investigated in the present study.

Living Organisms

Living organisms in the near surface water result in light absorption by chlorophyll, carotenoids, xanthophyll, and various photosynthetic pigments. Figure 39 shows the absorption curve of a natural phytoplankton population. This curve showing strong absorption in the blue and a weaker absorption in the red is typical of chlorophyll-bearing marine organisms.

The water at the Las Vegas Wash and Government Wash sites was visually observed to have a greener appearance than the water at the other three sites. The greener water color is believed to result from a higher concentration of chlorophyll-bearing organisms at these sites. This is to be expected since this part of the lake undoubtedly receives nutrient enrichment from the Las Vegas Wash inflow. Figure 40 shows statistical estimates of the volume spectral reflectance for 0 NTU turbidity water from the Government Wash and Las Vegas Wash sites compared to the same turbidity water at the other three sites. Notice that the Las Vegas and Government Wash curve is more sharply peaked in the green. Presumably this is the result of chlorophyll absorption

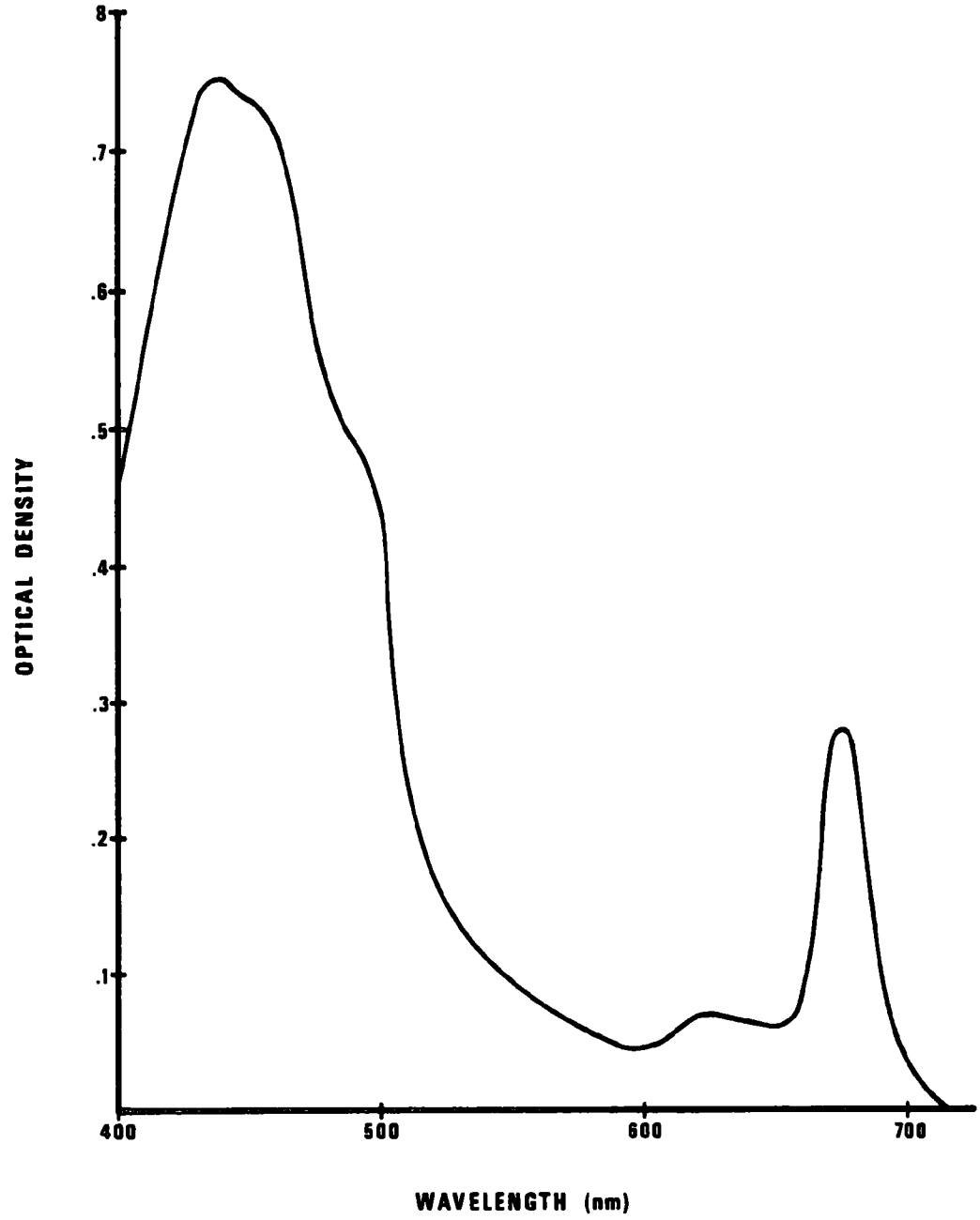

Figure 39. Spectral absorption curve of a natural phytoplankton population.

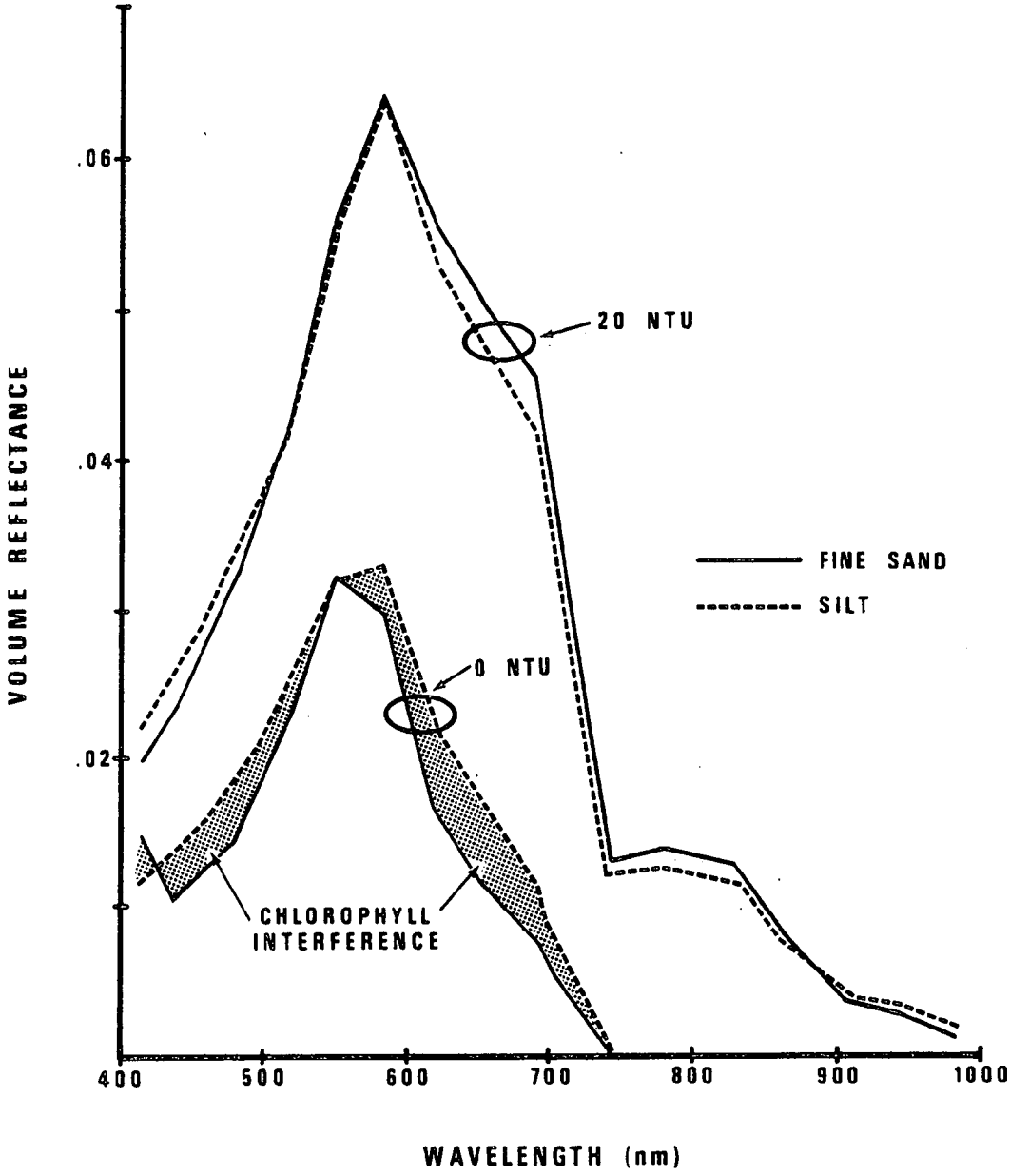

Figure 40. Statistical estimates of volume spectral reflectance for 0 and 20 NTU turbidity levels. Fine sand data are predominantly from Government and Las Vegas Washes; silt data are from the other three sites.

in the blue and red, thus confirming the presence of higher chlorophyll concentrations at these sites.

Spectral reflectance curves for a turbidity of 20 NTU are also shown in Figure 40 for these two cases. With this turbidity the shapes of the curves are almost identical and the chlorophyll absorption is not seen. It is concluded that chlorophyll absorption is a relatively weak effect requiring long path lengths to produce noticeable results. Thus, particle scattering, by reducing the mean path length of light through the water, reduces the chlorophyll absorption effect. Particle scattering is apparently a much stronger effect, predominating over chlorophyll absorption even with relatively low sediment concentrations. Over the range of EPA interest, i.e., greater than 25 mg/l suspended solids, chlorophyll interference is not believed to introduce significant errors in sediment measurements. This statement, of course, would probably not be true if the water body were in a condition of extreme algae bloom, but for typical chlorophyll concentrations only very low turbidity data should be seriously affected.

SECTION IX

DATA ANALYSIS

INTRODUCTION TO DATA ANALYSIS

Analysis of the volume reflectance and associated water sample data from Lake Mead is the focal point of this study. The data acquisition, data reduction, error analysis and other work discussed thus far is all supportive of the data analysis work from which will come answers to the question of feasibility of remote multispectral techniques for monitoring suspended sediments. A brief general discussion outlining the scope and setting the tone for the analysis task is presented here prior to the more detailed analysis results.

A Statistical or an Analytical Approach

There are generally two possible means of seeking a solution to a problem such as the interaction of incident light with a water body and its constituents. With an analytical approach, all of the physical processes involved are mathematically defined, resulting in a model which uniquely describes volume reflectance in terms of measurable physical parameters. The statistical analysis involves gathering a large volume of data, presumably typical of all possible data, in an attempt to find statistical correlation between parameters of interest. The statistical analysis can be conducted apart from any attempt to answer why the correlation exists based on an understanding of the physical processes. Once statistical relationships have been found and defined in terms of confidence intervals, the problem has been statistically solved.

At first glance the analytical solution normally seems the more desirable. However, many problems are so complex that they are amenable only to a statistical solution, and often a statistical solution is sufficient for some application. Such is the case here. The volume reflectance-suspended sediment relationship presents a very complex analytical problem. The statistical approach is much more easily handled and, if properly formulated, statistical analysis is sufficient for purposes of demonstrating feasibility. Thus, the analysis reported here is of a statistical nature. Analytical physical explanations for observed relationships are considered beyond the scope of the present study. Feasibility and signature transferability will be demonstrated on a statistical basis.

Feasibility and Optimality

It is important to consider the difference between demonstrating feasibility and establishing optimality of statistical techniques. The problem of finding optimum statistical algorithms is demonstrated by the data shown in Figure 41. This figure shows six "best fit" curves for relating volume reflectance at 652 nm to nonfilterable residue (105°C) for silt particles in Lake Mead. These curves vary widely and yet each one is a "best fit" according to some definition of "best".

Four of these curves are least-squares second order polynomial fits where the curve is of the form

$$y = a + bx + cx^2 \tag{45}$$

The method of least-squares requires that we minimize χ^2 which is the measure of the goodness of fit.

$$\chi^2 = \frac{\Delta y_i^2}{\sigma_i} = \left[\sigma_i^{-2}(y_i - a - bx_i - cx_i^2)^2\right] \tag{46}$$

where Δy_i is the error in the fit for the i point

σ_i is the weighting factor for the i point

The minimum value of χ^2 can be determined by setting the derivatives of χ^2 with respect to each of the coefficients equal to 0 and solving the resulting simultaneous equations.

Within the framework of the least-squares polynomial technique the choice must be made as to whether reflectance or suspended sediment is to be considered the independent variable. A choice also exists concerning appropriate weighting factors. The two weighting factor selections tried here were $\sigma_i^2 = y_i$, called statistical weighting, and $\sigma_i = 1$, called unweighted. The four possible combinations of independent variable and weighting factors all give different curves in Figure 41 even though each was calculated by the least-squares polynomial technique.

The piecewise linear fit was accomplished by dividing the data into three groups representing three reflectance ranges. A linear least-squares fit was applied to each group with a result quite different from the polynomial curves.

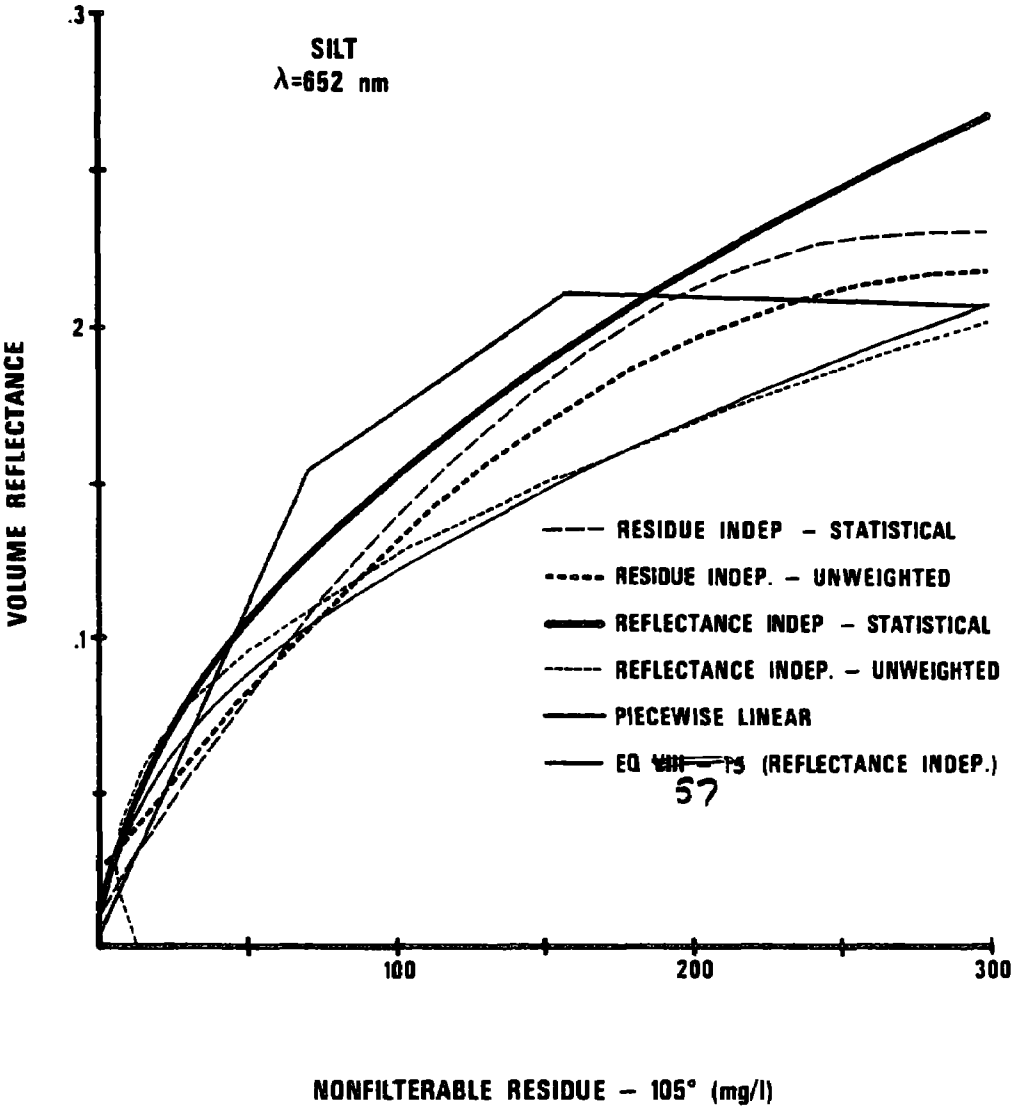

Figure 41. Six "best fit" curves for volume reflectance at 652 nm vs. nonfilterable residue (105°C) for silt-sized particles in Lake Mead.

The last curve, which is different from the previous five, in Figure 41 was calculated using a technique which was ultimately chosen for use in the analysis work reported here. A derivation of this method appears in subsequent discussion.

The best of these "best fits" should be taken as the optimum algorithm for predicting nonfilterable residue values based on water volume reflectance at 652 nm. Best is determined statistical optimality and depends on the data itself, the intended application of the results, and many other factors.

This analysis work does not include an investigation of statistical optimality. Selection of a statistical technique was based on the data and the investigator's previous experience. This method may or may not be optimal, but algorithms need not be optimal in order to demonstrate feasibility, which is the stated objective of this project. Optimality is deferred to in subsequent phases of this study.

VERIFICATION OF THE PARTICLE SIZE HYPOTHESIS

Figure 38 showed a wide variation in the scattering properties of the Lake Mead water samples as indicated by the scatter of points when nephelometric turbidity is plotted against nonfilterable residue. Results by other investigators who were cited in the discussion of Figure 38 led to the hypothesis that particle size is the primary factor determining the scattering properties of suspended sediment.

Although it has just been stated that physical explanations of observed relationships are not the objective of this study, particle size seems to be of such importance that it is imperative that the above hypothesis be verified if possible. The significance of the particle size parameter results from the signature transferability question. If sediment color, composition, texture, etc., are the dominant factors, then the possible variations are infinite and the probability is small that algorithms designed for one site will apply to data from another site. Extensive ground truth would, therefore, be required and the desirability of remote multispectral monitoring would be greatly reduced. However, if particle size is the primary scattering-related parameter, there is a better possibility of signature transferability and minimal ground truth requirements.

Division of the Data Set

If Rosgen's (1975) curve (Figure 38) is taken to be typical of fine sand particles and Scherz and Van Domelen's (1975) curve is typical of clay particles, it would seem reasonable to assume that silt-sized particles would fall on a line between the other two. The 200 Lake Mead data samples were, therefore, divided into three groups tentatively labeled fine sand, silt, and clay depending upon where the nonfilterable residue-nephelometric turbidity point fell with respect to the three lines shown in Figure 42.

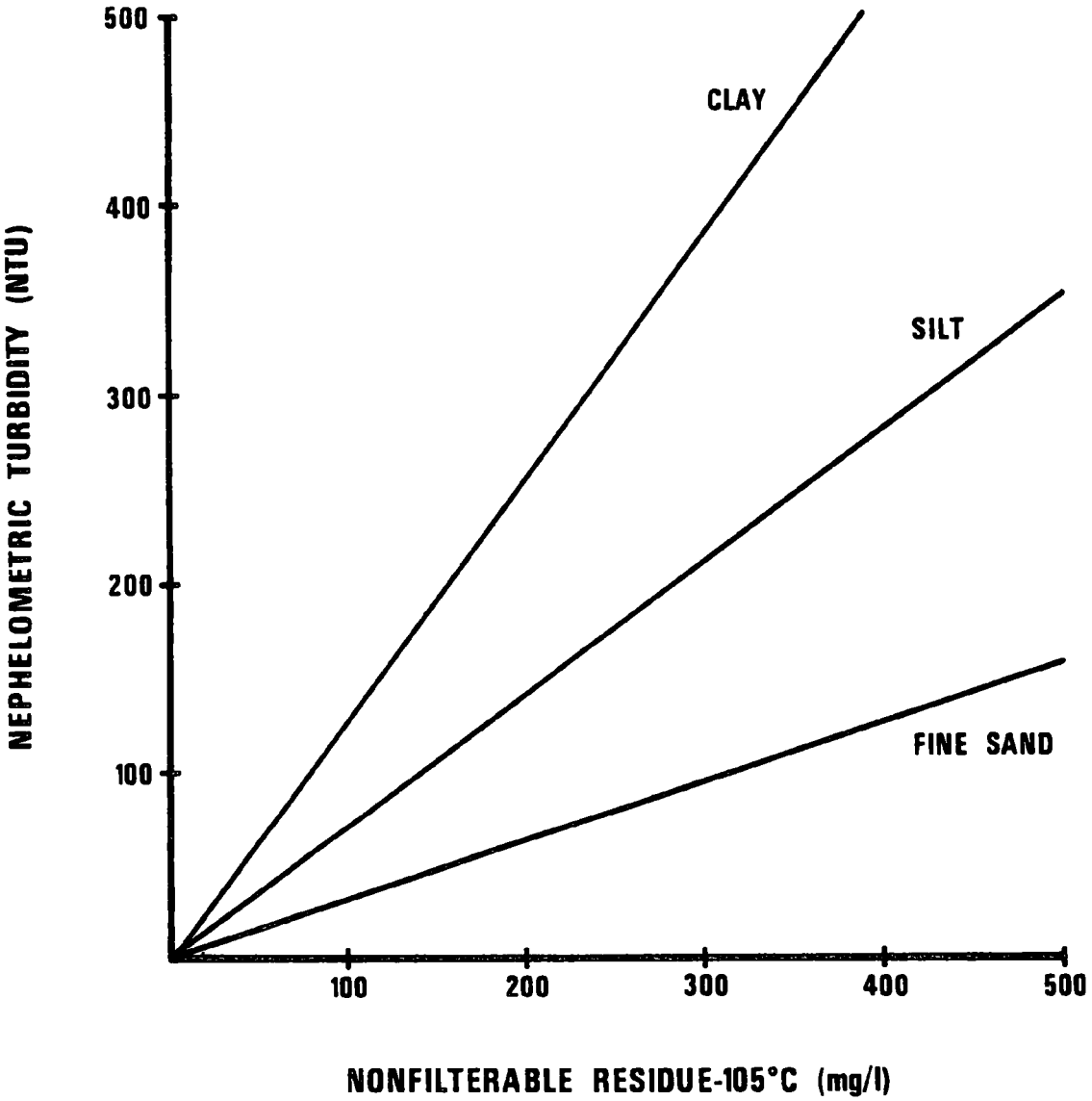

Figure 42. Typical nonfilterable residue-nephelometric turbidity relationships for various particle sizes.

The results of the division are given in Table 9 which shows the number of samples from each site that fell into each category. Notice that the Colorado, Muddy, and Virgin River sites samples fall predominantly into the silt category. Government and Las Vegas Wash samples are predominantly fine sand. Of the 53 samples not falling in the predominant group for their site, 39 contained less than 10 mg/l of nonfilterable residue (105°C). Samples this clean are in the noise level of the laboratory analysis of nonfilterable residues so their failure to agree is not significant. Only 14 samples with meaningful suspended sediment concentrations failed to group with the rest of the samples from their site.

TABLE 9. GROUPING OF SAMPLES BY SITE AND PARTICLE SIZE

	Particle Size		
Site	Clay	Silt	Fine Sand
Colorado River	1	30	9
Government Wash	1	8	31
Las Vegas Wash	0	10	30
Muddy River	4	31	5
Virgin River	11	25	4
Total	17	104	79

The interesting thing about site groupings is that they have no apparent relationship to sediment color. For example, available photography and the sediment spectral reflectance curves (Figure 37) show that the Muddy and Colorado River sites had the highest and lowest reflectances respectively, yet they were grouped together. Visually the Government Wash sample looks most like the Muddy or Virgin River sediment, yet in terms of scattering properties it is associated with the gray colored Las Vegas Wash sample. Therefore, particle size appears to be a more differentiating factor than sediment color.

Particle Size Measurements

Data reported by other investigators suggest the importance of particle size, and division of the Lake Mead data set according to scattering properties tended to support this hypothesis since grouping was not consistent with sediment color. Yet the primary role of particle size had not definitely been proven. It seemed that the particle size hypothesis would be proven only by direct measurement of the size of the particles in the sediment samples taken from the lake bottom at each site.

The EPA laboratory in Las Vegas performed the analysis of Lake Mead water samples but did not have the capability to perform this type of measurement. Sediment samples were, therefore, sent to Battelle Laboratories in Columbus, Ohio, where particle distribution were measured on a Coulter counter. The particle size distribution data are shown in Figures 43 and 44.

Figure 43 shows size distributions from the Muddy, Colorado, and Virgin River samples. These are seen to be quite similar and within the silt particle size range just as had been inferred from the nonfilterable residue-nephelometric turbidity plots. Figure 44 shows size distributions for the two sites which were tentatively identified as fine sand. (The Las Vegas Wash sample is not the same one that came from station L05, but is a sample from station L06 which is closer to the mouth of the wash.) The Las Vegas Wash particles do indeed fall in the fine-sand range; however, the Government Wash sample does not. Several explanations for this could probably be offered. The most reasonable seems to be the fact that prop-wash resuspension was frequently used here to create turbidity when the natural resuspension mechanisms were not present. The prop wash would often create a hole up to a half meter deep in the bottom of the lake, digging into much coarser deposits than would be picked up by the anchor. Our sediment sample is, therefore, possibly not representative of what was suspended in the water.

In spite of the anomalous behavior of the Government Wash sample, the data from the other four samples have sufficiently verified the particle size hypothesis. In summary, the investigation of the particle size question has resulted in the following information.

> Particle size is more important than sediment color in determining scattering properties.
>
> The ratio of nonfilterable residue (105°C) to nephelometric turbidity is a good indicator of particle size. This ratio will typically have the values 3.1, 1.4, and 0.8 for fine sand, silt, and clay respectively.
>
> One of the more valuable pieces of ground truth data from a site to be monitored would be several water samples which could be analyzed to determine the nonfilterable residue-nephelometric turbidity ratio for that site.
>
> Because particle size rather than color is dominant, the prospects look good for some degree of site-to-site signature transferability.

POLYNOMIAL FITS TO RESIDUE/TURBIDITY VS. VOLUME REFLECTANCE

Volume Reflectance-Nonfilterable Residue

Before considering the multispectral problem it is informative to look at single-wavelength relationships. A cursory examination of the data reveals

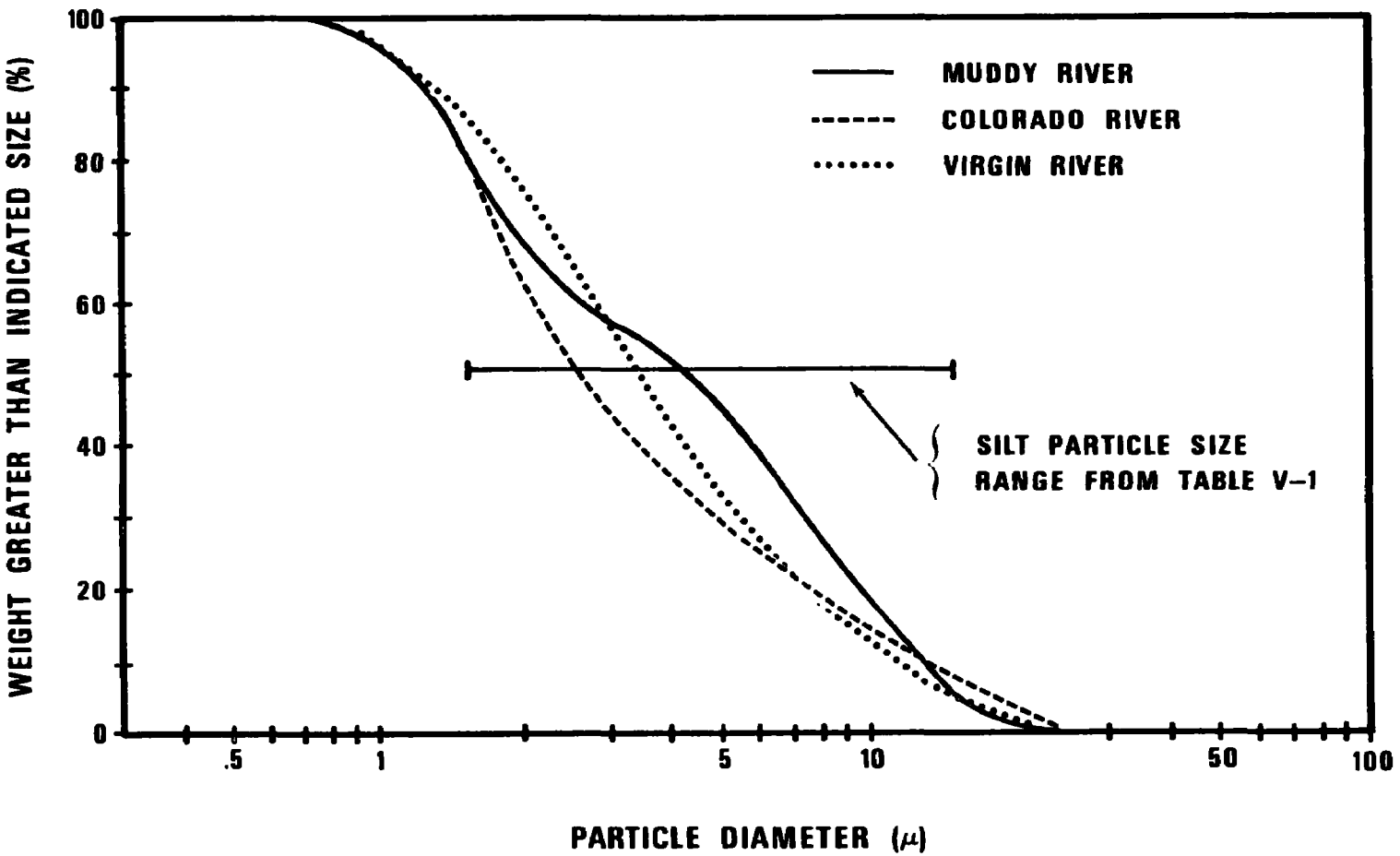

Figure 43. Particle size distribution for Muddy, Virgin, and Colorado River sediment samples.

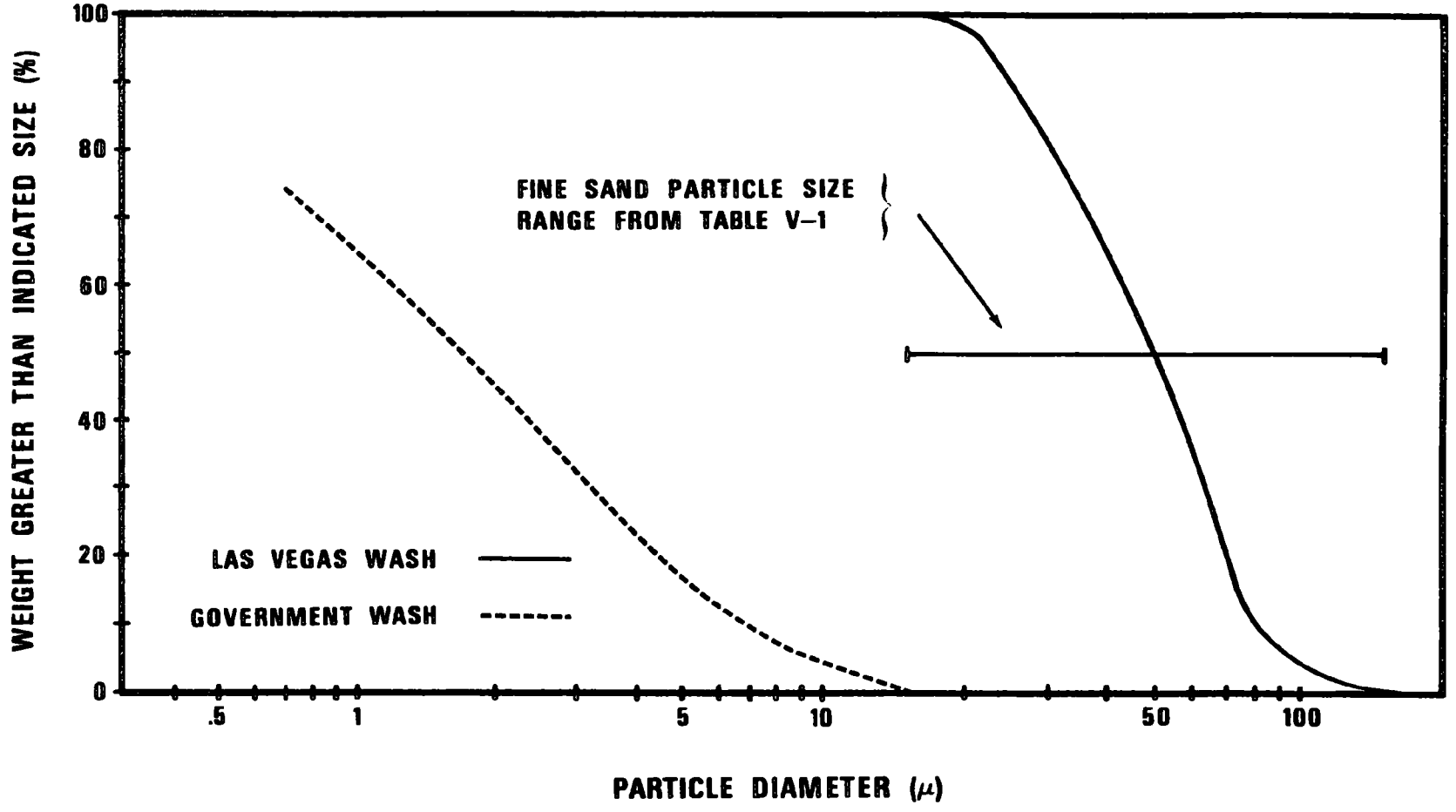

Figure 44. Particle size distribution for Las Vegas and Government Wash sediment samples.

definite nonlinearity. The Fortran subroutine, POLFIT, given by Bevington (1969) was, therefore, used to fit various least-squares polynomials to the data. As has been previously demonstrated, the optimum method of fitting a curve is not always obvious, so several orders of polynomials were considered. The obvious nonlinearity in the data ruled out first-order (linear) polynomials. Polynomials of third or higher orders seemed to be fitting individual data points rather than representing actual reflectance properties. Thus the choice of second-order polynomials seemed most appropriate.

Polynomials were calculated considering reflectance to be the independent variable and also with nonfilterable residue as the independent variable. Both unweighted and statistically weighted fits were investigated. A second-order unweighted least-squares polynomial with nonfilterable residue as the independent variable was chosen as the method of fitting single-wavelength volume reflectance to nonfilterable residue (105°C) in Figures 45 through 48. An equation of the form shown below was fit to each of the data sets grouped by particle size.

$$\rho_w = a_0 + a_1(\text{residue}) + a_2(\text{residue})^2 \qquad (47)$$

Examination of the curves shown here for four selected wavelengths led to the following conclusions.

Reflectance-nonfilterable residue relationships are strongly influenced by particle size.

At visible wavelengths the sensitivity of reflectance to incremental changes in nonfilterable residues decreases with increasing residue values. A point is reached in the vicinity of several hundred milligrams/liter where saturation occurs. Above this point reflectance is insensitive to changes in residue values.

Maximum sensitivity at low sediment concentrations occurs in the red portion of the spectrum.

The near-IR wavelengths are nearly linear and do not show the saturation that appears in the visible. These wavelengths, therefore, have the greatest analytical range.

Since red wavelengths yield maximum sensitivity at low concentrations and near-IR wavelengths yield maximum sensitivity at high concentrations, it becomes apparent that to optimize accuracy over a large analytical range of suspended sediment concentrations, a multispectral approach will be required.

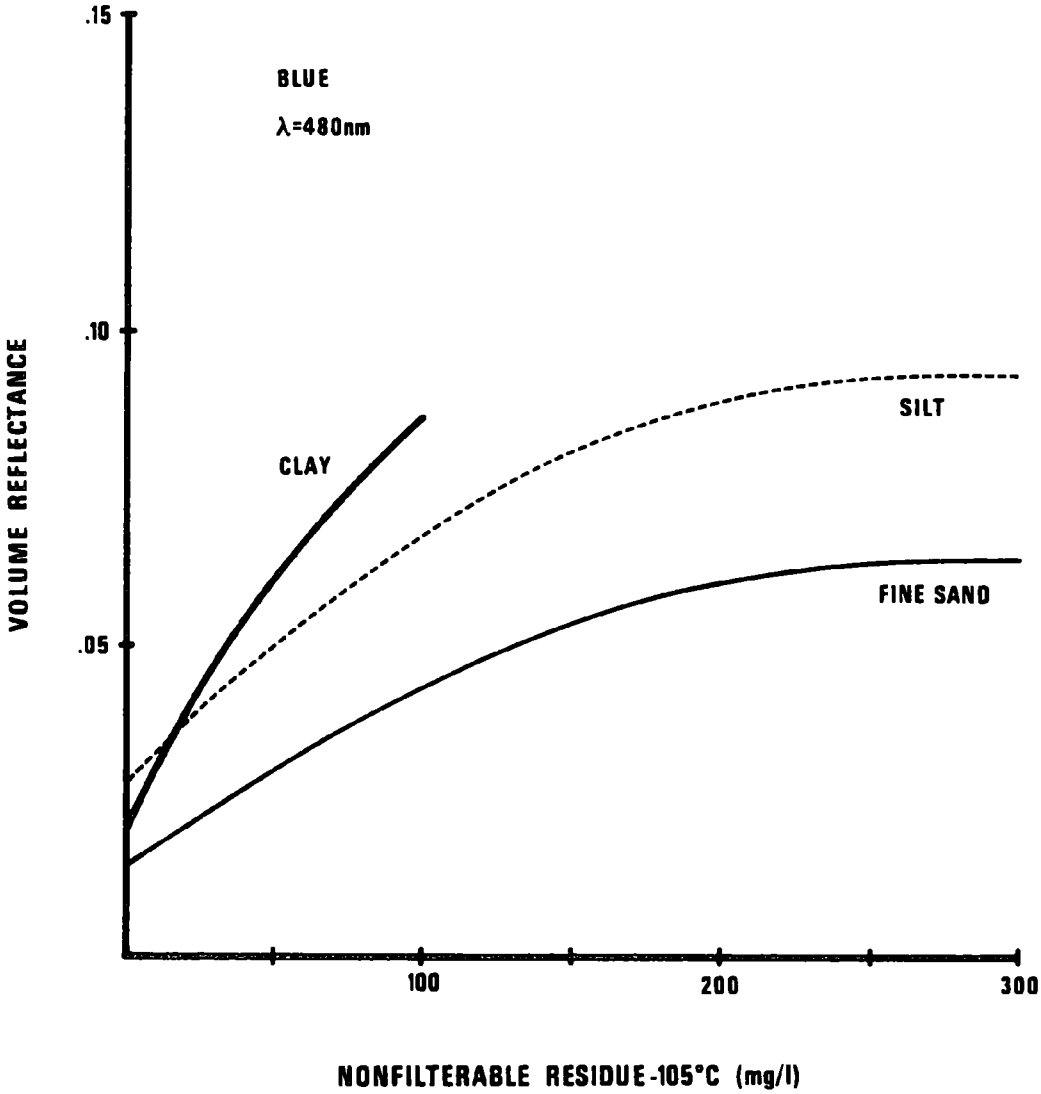

Figure 45. Volume reflectance at 480 nm as a function of nonfilterable residue (105°C).

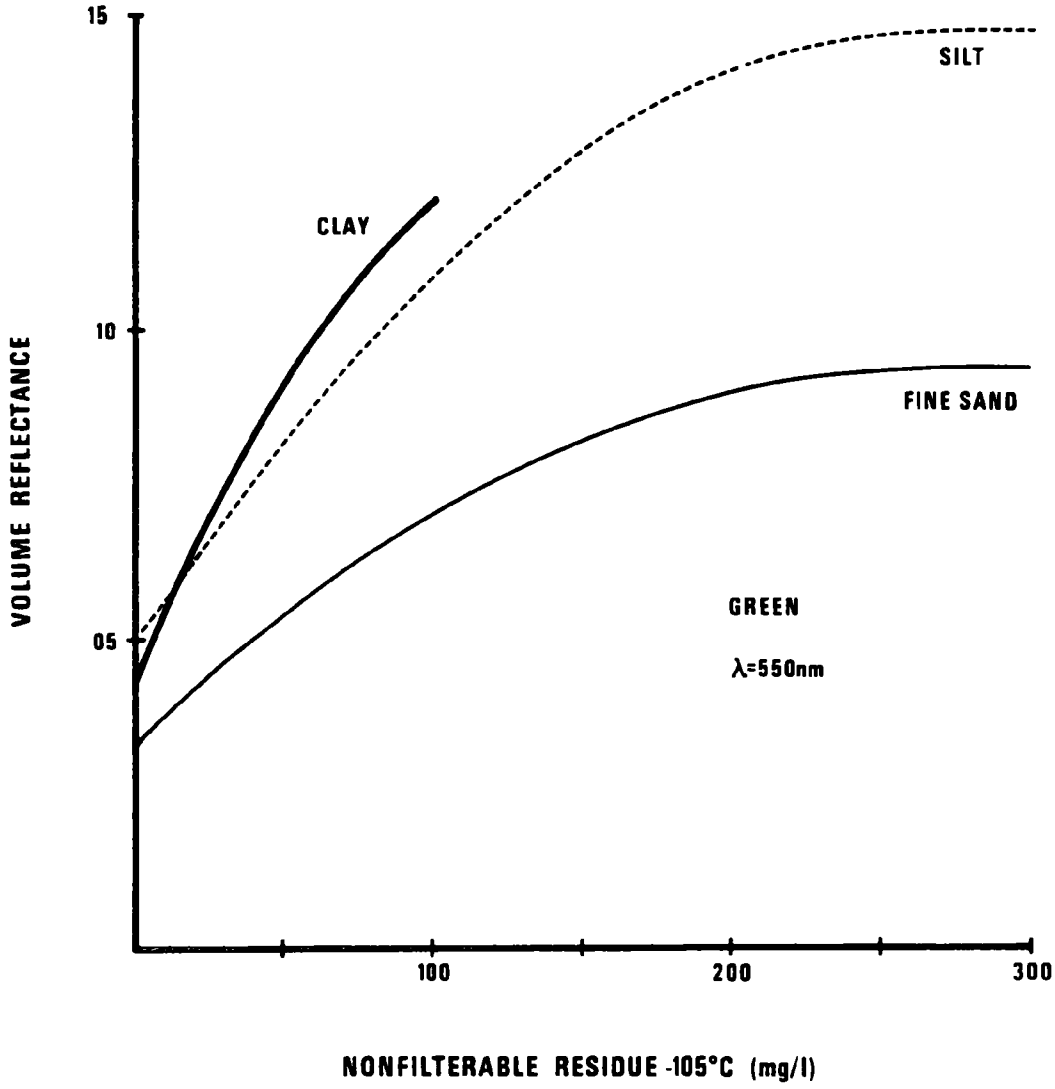

Figure 46. Volume reflectance at 550 nm as a function of nonfilterable residue (105°C).

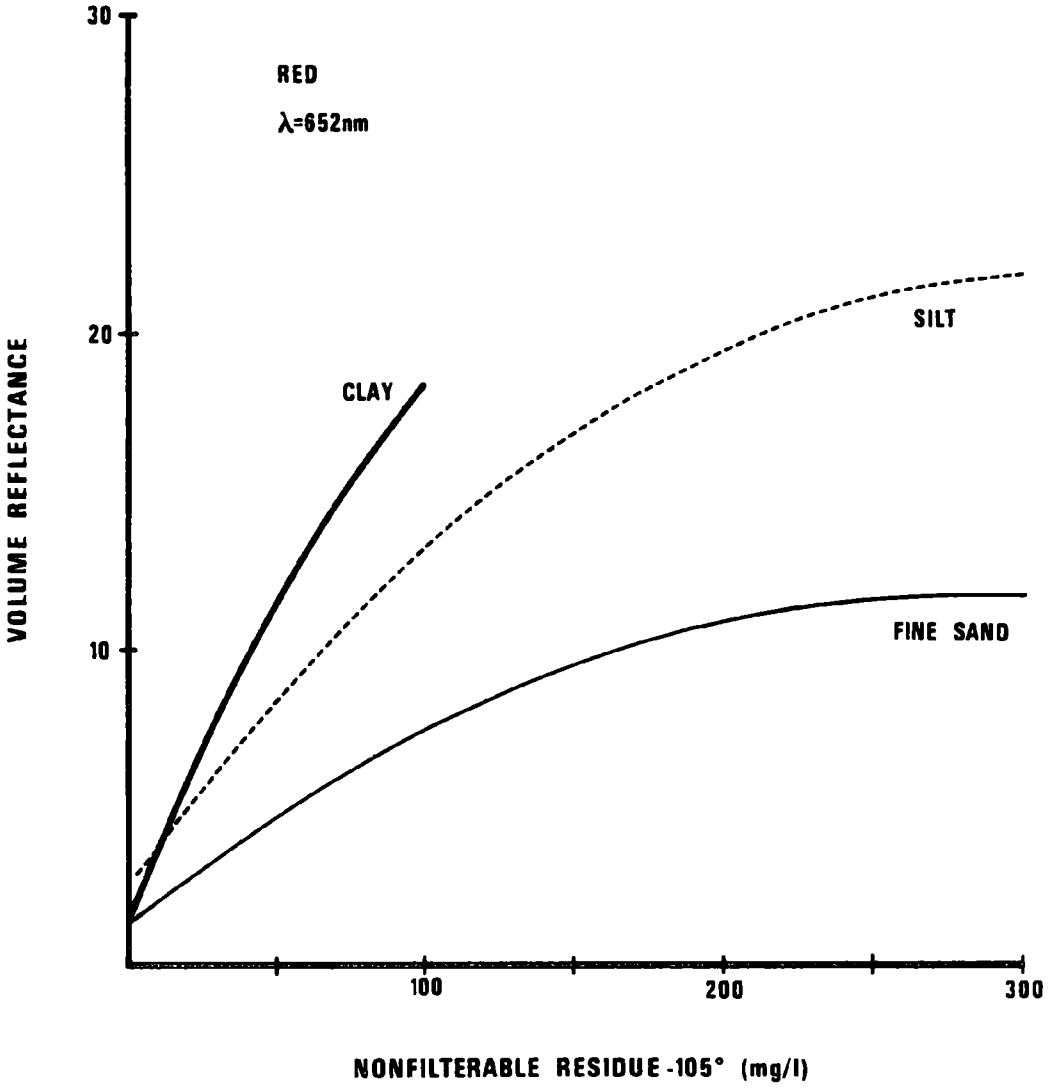

Figure 47. Volume reflectance at 652 nm as a function of nonfilterable residue (105°C).

Volume Reflectance-Nephelometric Turbidity

The same polynomial fitting procedure was used to supply curves for the volume reflectance-nephelometric turbidity relationships. These curves are shown in Figures 49 through 52.

The difference between the turbidity curves and the residue curves is significant. The following conclusions have been drawn from these data.

A reflectance saturation occurs in the nephelometric turbidity relationships at visible wavelengths but not at near-IR

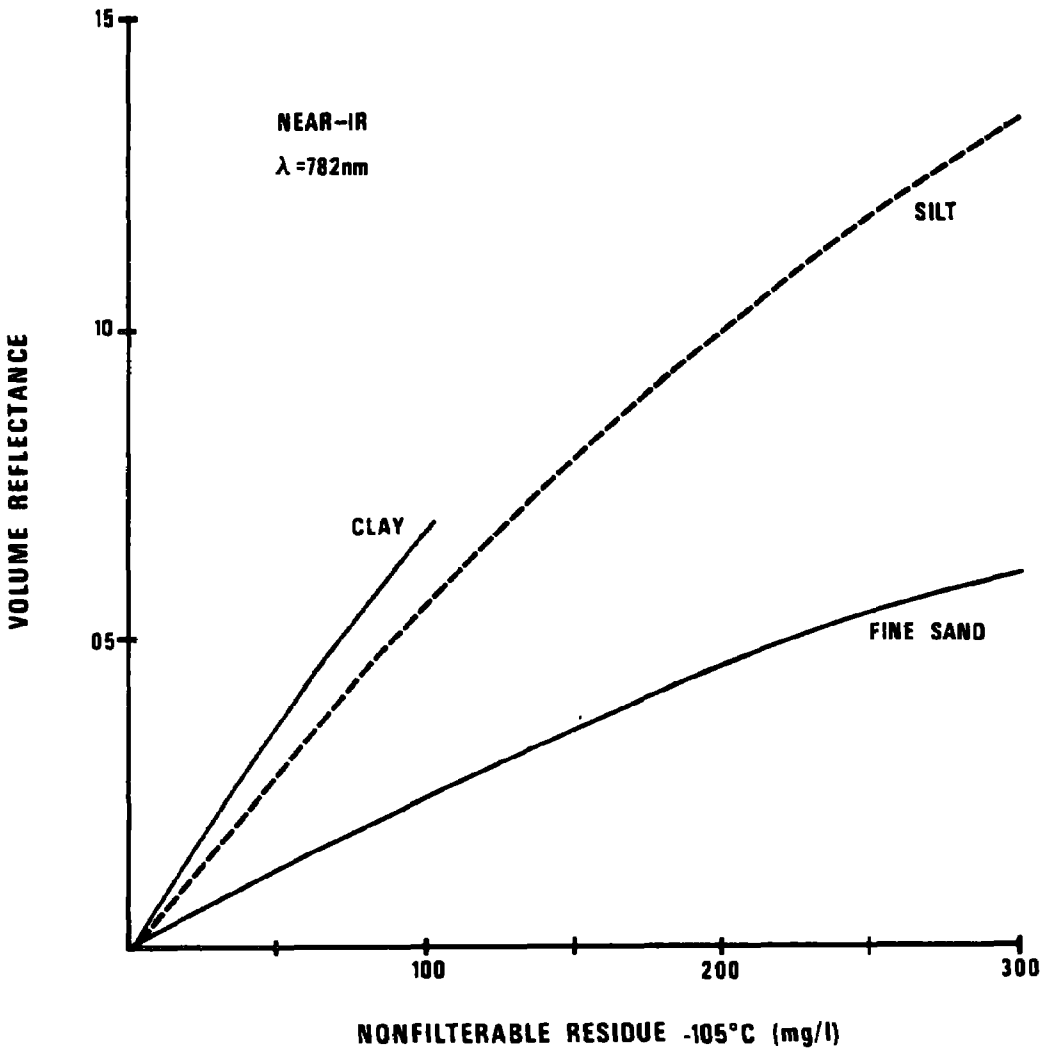

Figure 48. Volume reflectance at 782 nm as a function of nonfilterable residue (105°C).

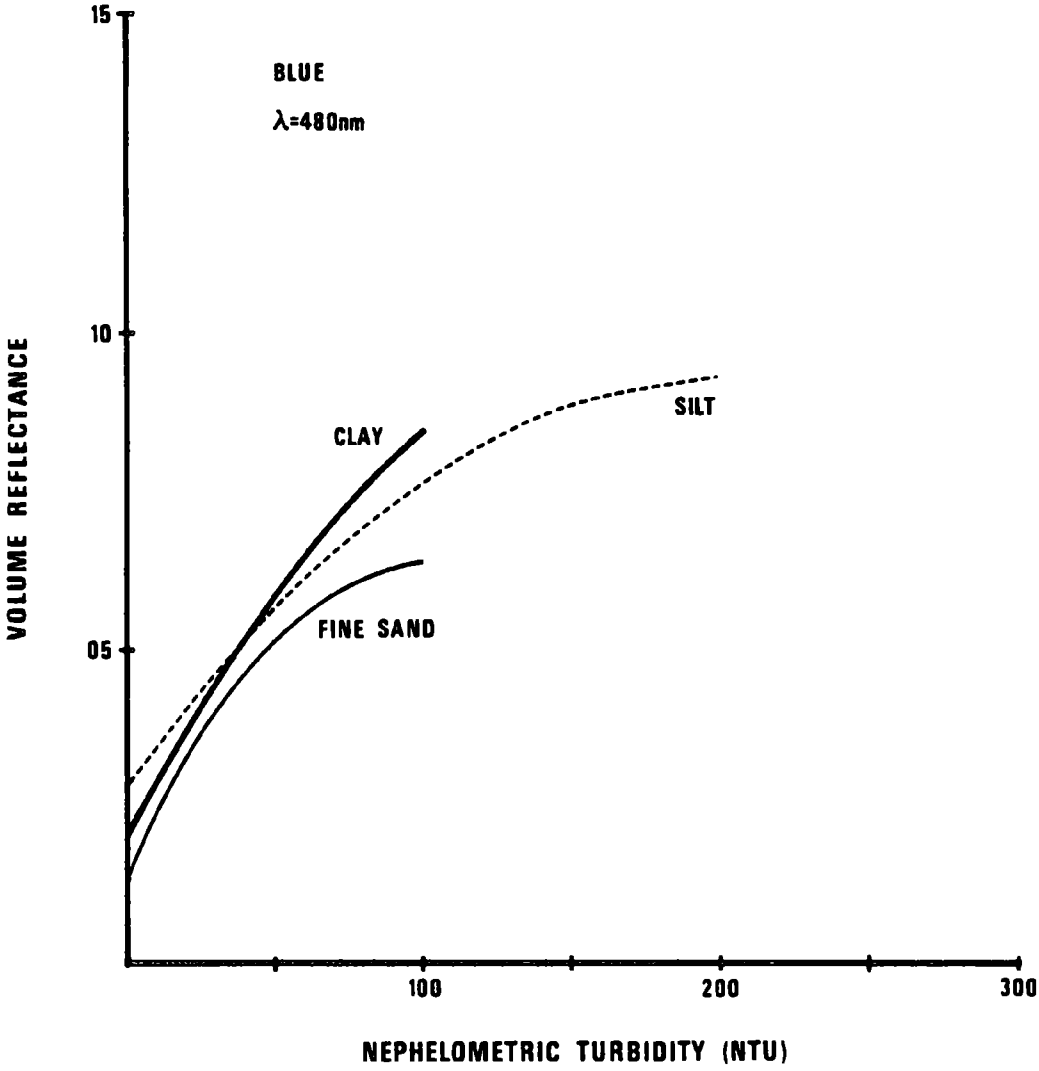

Figure 49. Volume reflectance at 480 nm as a function of nephelometric turbidity.

wavelengths. This result is the same as that observed with nonfilterable residues.

There is much less variability in the turbidity curves resulting from differences in particle size.

Since the turbidity-reflectance relationships are less sensitive to changes in sediment type than are the nonfilterable residue-reflectance relationships, nephelometric turbidity would appear to be a parameter more amenable to remote monitoring than nonfilterable residue.

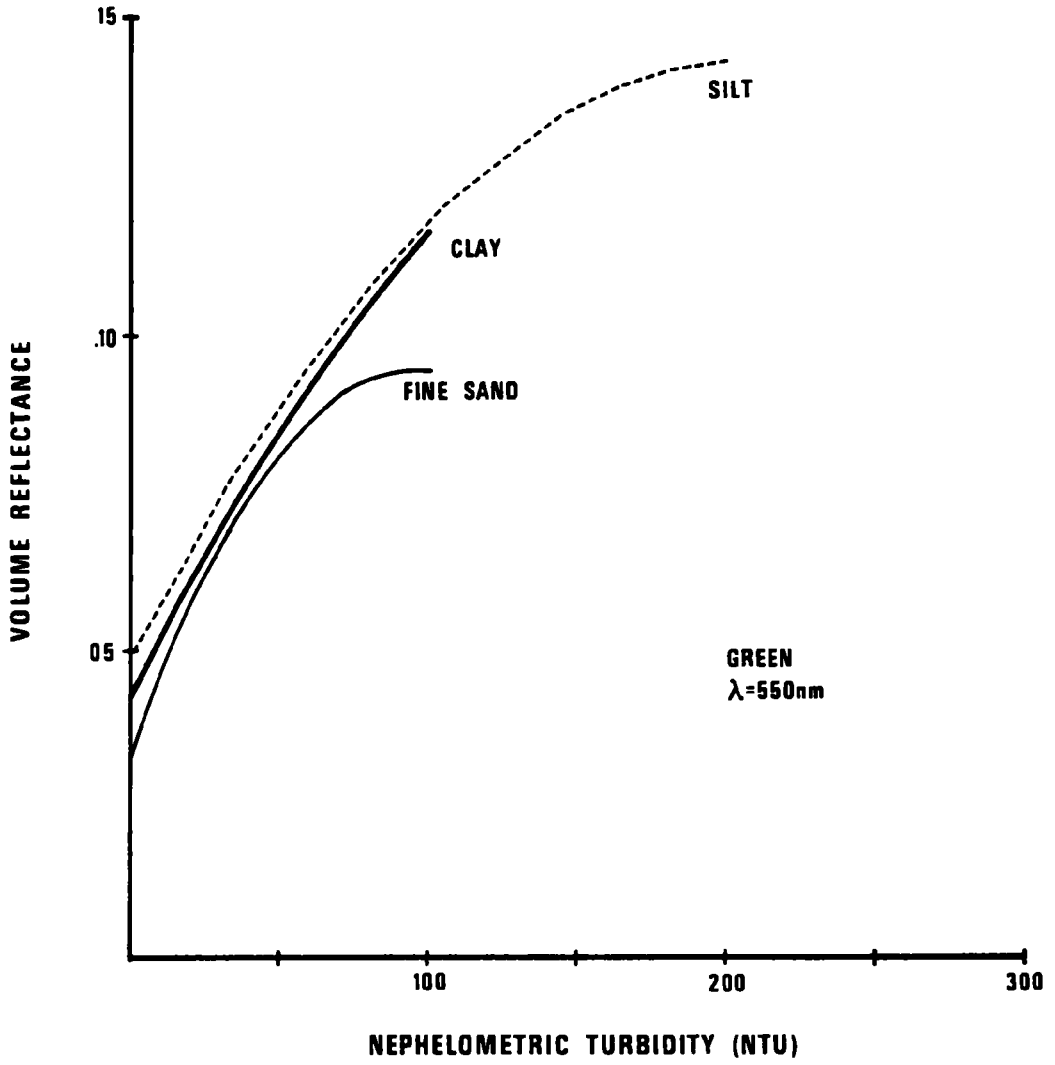

Figure 50. Volume reflectance at 550 nm as a function of nephelometric turbidity.

A STATISTICAL METHOD FOR OBTAINING MULTISPECTRAL QUADRATIC ALGORITHMS

The multispectral approach rather than single wavelength is preferable for the single-wavelength polynomial curves discussed above. Further, it has been shown that the parameters of interest are not linearly related to reflectance in the visible portion of the spectrum. Thus we know that a nonlinear, multivariate, statistical method will be required to obtain good algorithms for predicting residue/turbidity values from volume spectral reflectance. The subroutine POLFIT, which was used to calculate the single-wavelength polynomials, does not handle multivariate data. No other existing software

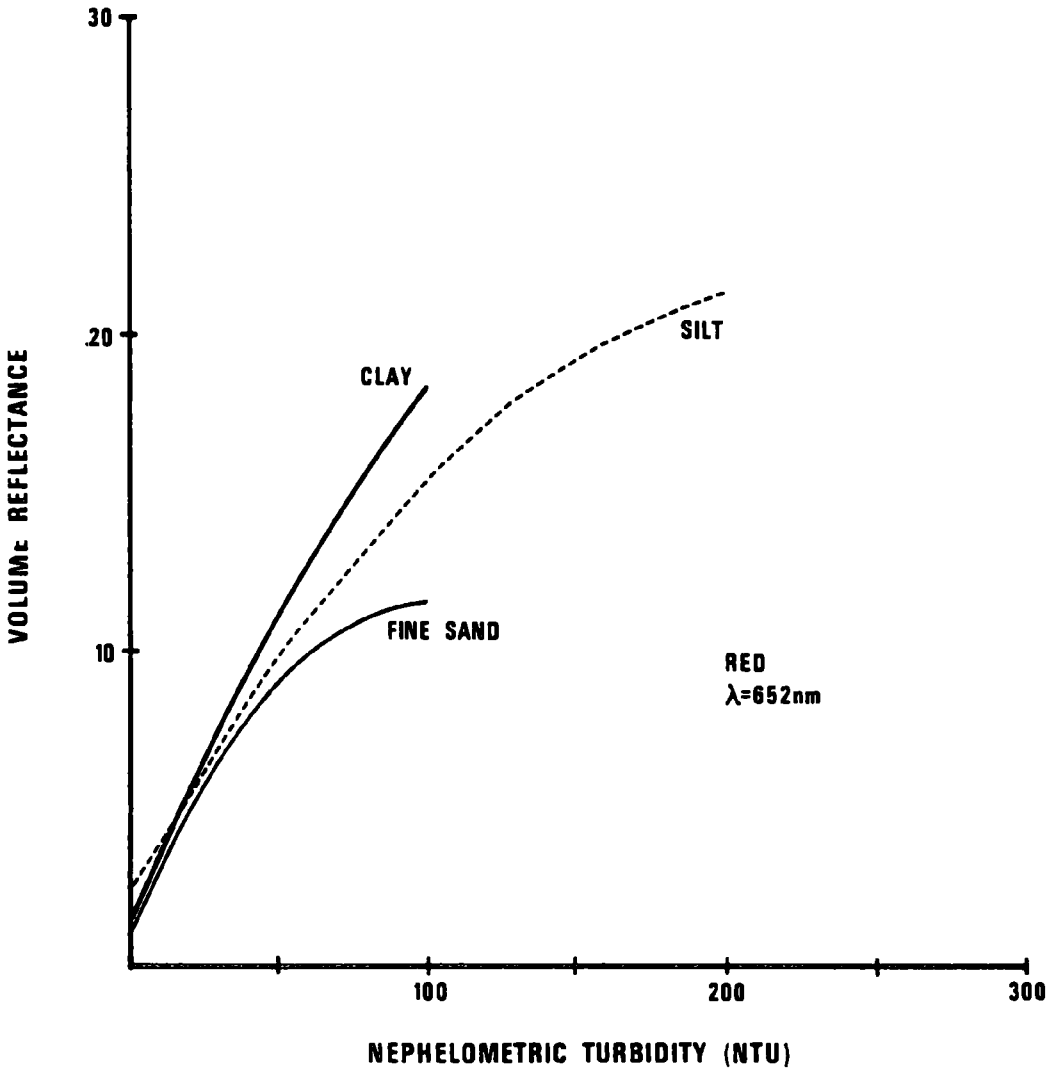

Figure 51. Volume reflectance at 652 nm as a function of nephelometric turbidity.

was available which could be used for nonlinear, multivariate statistical analysis. It was, therefore, necessary to develop this capability as part of this study.

Two approaches to the nonlinear, multivariate problem were considered. The first would be to linearize the parameter of interest in each coordinate of measurement space, and then apply linear analysis to the transformed data. The second approach, and the one followed here, was to develop nonlinear algorithms which operate directly on the raw volume reflectance data.

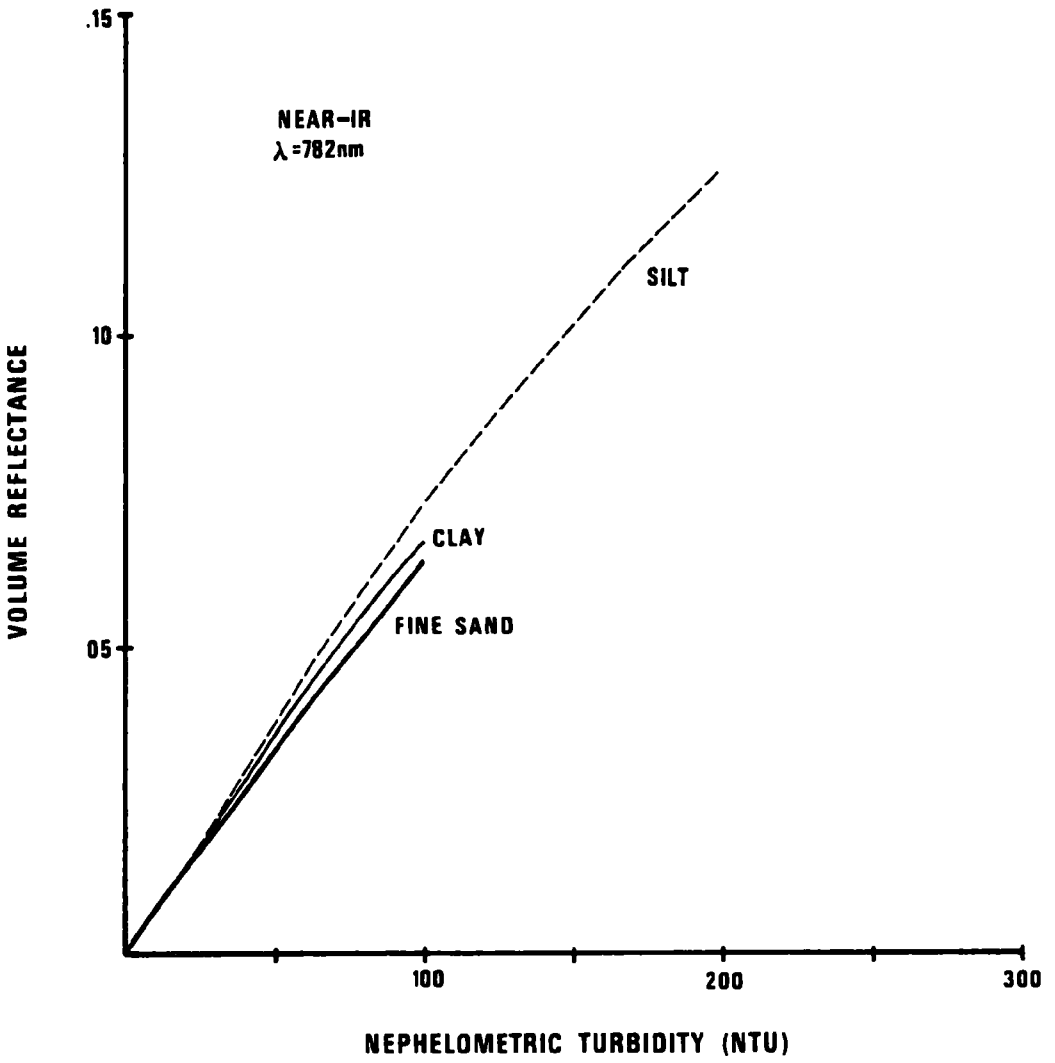

Figure 52. Volume reflectance at 782 nm as a function of nepleometric turbidity.

We need to make a transition now from the physical concept of reflectance spectra to the abstract mathematical concept of multidimensional vector spaces. If we consider K wavelengths simultaneously, the dimensionality of the vector space will be 2K, and a spectrum can be represented by a row vector, X, whose components are the first and second powers of the spectral reflectance values.

$$X \equiv \left(\rho_1, \rho_1^2, \rho_2, \rho_2^2 \ldots, \rho_K, \rho_K^2\right) \tag{48}$$

where ρ_K is the reflectance of k wavelength. Let V be another row vector

$$V \equiv \left[v_1, v_2, v_3, \ldots, v_{2k}\right] \tag{49}$$

called the prediction vector. The prediction, p, of some turbidity related parameter will be given by

$$p = VX^T \tag{50}$$

(The superscript in the above equation denotes transposition.) The problem can now be treated as linear in X although it is actually quadratic in terms of reflectance. If g is the ground truth value of the residue/turbidity parameter of interest, the error, e, in the multispectral prediction is given by

$$e = p - g = VX^T - g \tag{51}$$

We now consider a large number of data vectors which will serve as the training data from which a statistical algorithm will be developed. The nth vector in the training set, X_n, has ground truth value g_n, and the error in the statistical prediction of g_n will be called e_n. The problem is to find the vector V such that

$$\sum_{n=1}^{N} e_n^2 = \text{minimum} \tag{52}$$

where N is the total number of samples in the training set.

The sum of the errors squared is given by

$$\sum_{n=1}^{N} e_n^2 = \sum_{n=1}^{N} VX_n^T X_n V^T - 2\sum_{n=1}^{N} g_n V^T X_n + \sum_{n=1}^{N} g_n^2 \tag{53}$$

The prediction vector which minimizes the sum of the squares of the errors is found by setting $\partial \Sigma e_n^2 / \partial V = 0$. The property of partial derivatives

$$\frac{\partial \Sigma e_n^2}{\partial V} = \sum \frac{\partial e_n^2}{\partial V} \tag{54}$$

allows us to write

$$\frac{\partial \Sigma e_n^2}{\partial V} = 2\left[\sum_{n=1}^{N} X_n^T X_n V^T - \sum_{n=1}^{N} g_n X_n^T\right] = 0 \qquad (55)$$

If summations are replaced by averages nothing is changed mathematically but the notion is simplified allowing the desired V to be given by

$$V^T = \frac{-1}{X_n^T X_n} \frac{}{g_n X_n^T} \qquad (56)$$

Any multispectral algorithm obtained from Equation 56 is constrained to assign the origin of the vector space to a residue/turbidity value of 0. This is not a physically realistic constraint since the Lake Mead data show sediment-free water can have reflectances of five percent or more at some wavelengths. Unweighted second-order polynomials with residue/turbidity as the independent variable, such as those shown previously in Figures 45 through 52, are felt to give the best estimate of volume reflectance for zero suspended sediment. The zero sediment reflectance for the k wavelength, z_k, can be subtracted from ρ_k, to give modified data vectors, X'.

$$X_n' = \left[(\rho_1 - z_1), \rho_1 - z_1)^2, (\rho_2 - z_2), (\rho_2 - z_2)^2, \ldots\right] \qquad (57)$$

If we design a modified V' based on X_n' training data, the result is a statistical algorithm which minimizes Σe_n^2 but which is constrained to a proper zero point.

When applying these V' algorithms to nontraining-set data, z_k's must be subtracted from each data vector. For production processing this subtraction adds computation time reducing the efficiency of the algorithm. Also, we must keep track of z_k values to be used with each algorithm. Rather than do this it is advisable to transform V' back to a form that will be equivalent to V' but which can operate directly on the uncorrected reflectance data. The components of the new prediction vector for this case can be shown to be given by

$$\begin{aligned} v_k &= v_k' - 2v_{k+1}z_k \quad \text{for k odd} \\ v_k &= v_k' \quad \text{for k even} \end{aligned} \qquad (58)$$

and the statistical prediction is then given by

$$p = VX^T + v_o \tag{59}$$

where

$$v_o = \sum_{k=1}^{K} (v'_{2k} z_k^2 - v'_{2k-1} z_k) \tag{60}$$

This technique is developed for multispectral algorithms but for K = 1 the technique reduces to a single-wavelength polynomial fit. Thus all algorithms reported in the remainder of this section, whether they are single-wavelength or multispectral, were obtained according to the method just described.

The Fortran program ALGOR was written to implement this technique on the CDC 6400. This program took as input the cards put out by VOLREF which contained spectral reflectance and water sample analysis results. ALGOR will calculate quadratic multispectral algorithms to predict any of the water sample parameters from any selected combination of wavelengths. Appendix B is a listing of this program.

EVALUATION OF STATISTICAL ALGORITHMS

Detuning by Addition of Random Noise

The most desirable method of evaluating statistical prediction algorithms is to obtain a set of data called a test set which does not include the training set from which the algorithm was designed. Applying an algorithm to the test set gives an independent check on accuracy. By collecting 200 samples at Lake Mead, it was hoped that there would be enough data to provide for separate, statistically significant training and test sets. However, the small number of samples with high sediment concentrations made it impossible to divide the data in this manner and still maintain the statistical significance of both sets at high concentrations. Thus, it is necessary to evaluate accuracy by applying algorithms back to the training sets.

Accuracy evaluations based on the training set generally tend to give values which are too low unless the set is very large. This happens because the algorithm is "fine-tuned" to the training set and operates on nuances peculiar to the training set that are not representative of the data in general. An algorithm fine-tuned to a training set in this manner will not do nearly as well when applied to an independent test set.

Since the accuracy evaluations here must be done with the training set, it is desirable to make a correction to prevent misleadingly low accuracy

estimates. One way to do this is to corrupt the training set data by adding a certain amount of random noise. This has the effect of preventing the algorithm from being too finely tuned. It is not necessary to actually generate and add random noise since the same effect can be achieved by simply increasing the diagonal elements of the matrix $X_n^T X_n$.

To demonstrate this random noise effect, the 40 Muddy River samples were divided into two halves. A six-wavelength algorithm was designed from the half consisting of the even numbered samples with varying amounts of random noise added. These algorithms were applied to the half of the data containing the odd numbered samples as well as back to the even numbered training set. Accuracies for these two cases have been plotted in Figure 53 as a function of noise added. It is seen here that without random noise the training set evaluation of accuracy is very good and the test set is poor. As noise is added, the two accuracy methods begin to converge and the training set accuracy evaluation becomes more representative of what an independent test set evaluation shows. Two percent random noise was, therefore, added to "detune" all of the algorithms reported in the remainder of this section.

Method of Reporting Accuracies

When algorithms are applied to training set data, what is the best way to express the resulting errors? Errors are associated with samples with residue/turbidity values ranging from zero to several hundred. A simple root mean square (rms) error calculation is not too meaningful because of the large range. A 10 mg/l error in a value of 200 mg/l is small but a 10 mg/l error in a value of 5 mg/l is large. It seems more desirable to express errors as a function of ground truth values. It was decided to report algorithm accuracies in this report by putting ground truth and absolute value of error data into the subroutine POLFIT in order to fit unweighted second-order polynomials. This procedure gives a least-squares fit to the absolute value of the errors. This is not necessarily identical to a standard deviation. Since the error analysis results were expressed in standard deviations, the error analysis is not expected to correspond numerically with least-squares fits to absolute values. However, even though the two error expressions may not be numerically equivalent, they should correspond in principle. For example, if the error analysis showed errors for the IR wavelengths to be 50 percent smaller than those in the visible, the algorithm error evaluation for these two cases should show approximately the same 50 percent difference.

SINGLE CHANNEL ALGORITHMS FOR VERIFICATION OF ERROR ANALYSIS RESULTS

The analysis of errors in the 200 Lake Mead samples was summarized by Figure 27 which showed expected errors at red (652 nm) and near-IR (782 nm) wavelengths. An important analysis task was to actually design algorithms to predict nonfilterable residues and nephelometric turbidities from volume reflectances at these two wavelengths. If the algorithms agree with the error analysis results, it would tend to verify both the error analysis procedures and also the statistical methods used in designing algorithms.

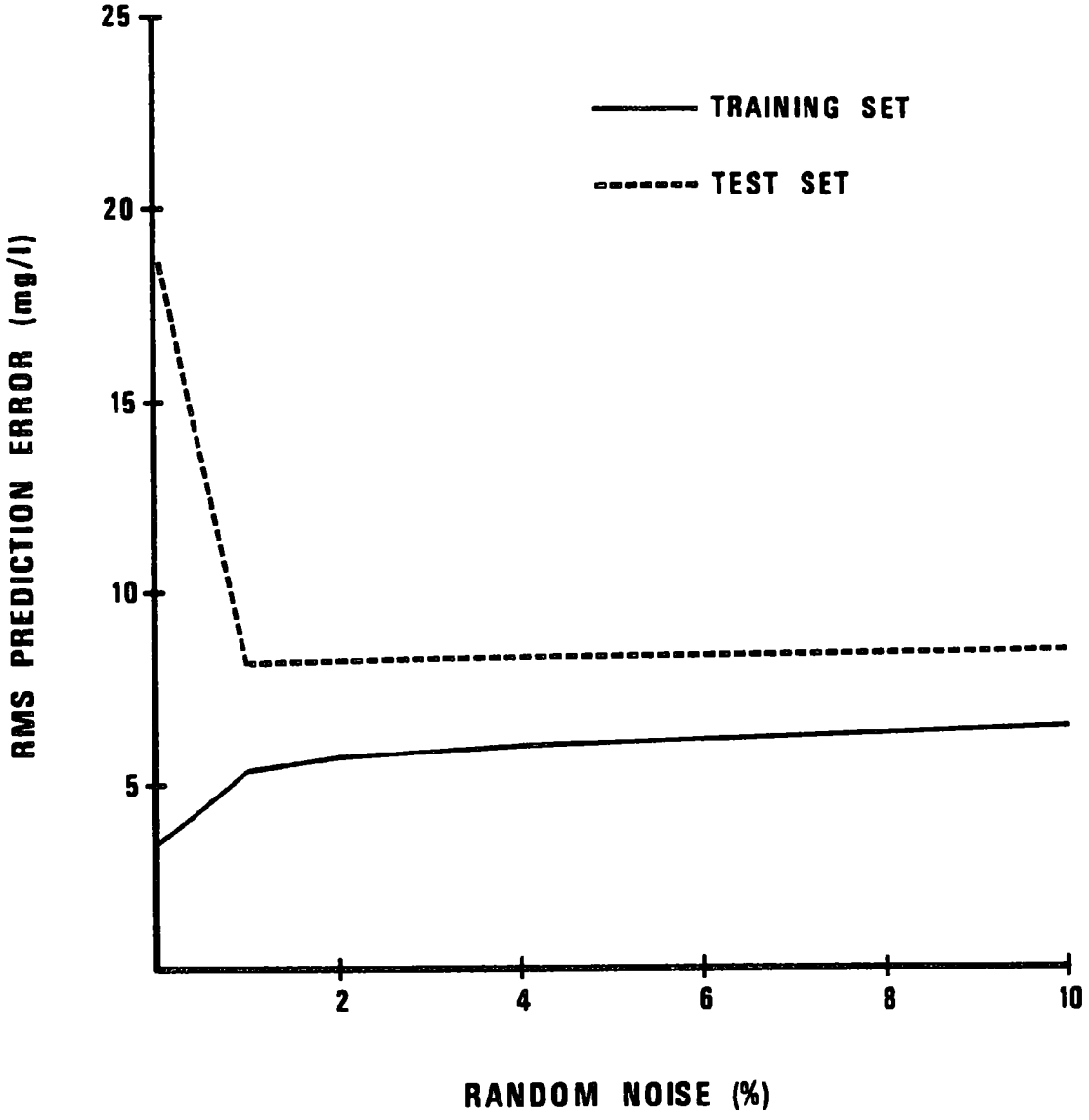

Figure 53. Effects of random noise addition on training set and test set accuracy evaluations.

Separate algorithms were designed for silt and fine sand particle sizes, but the errors for the two cases were combined in calculating the polynomial fit to the absolute value of the errors. Table 10 contains the coefficients for these single-wavelength algorithms.

TABLE 10. SINGLE-WAVELENGTH ALGORITHMS - PARTICLE SIZE KNOWN

Wavelength	Particle Size	Parameter	v_0	v_1	v_2
652	Silt	NTU	3.0	-291.0	6826
652	Fine Sand	NTU	-8.8	772.1	-880.4
782	Silt	NTU	0.0	1070	4453
782	Fine Sand	NTU	0.0	1692	-4806
652	Silt	mg/l	-0.1	-195.7	8142
652	Fine Sand	mg/l	-28.0	2493	-4910
782	Silt	mg/l	0.0	1519	5343
782	Fine Sand	mg/l	0.0	5316	-19305

These algorithms were applied to the Lake Mead data polynomials fit to the absolute value of the errors with the result shown in Figure 54. Comparison of Figures 54 and 27 shows a strong resemblance between the error analysis results and the actual performance of the single-wavelength algorithms. Note the following specific points of comparison.

> The error analysis predicted about 55 percent larger errors for the red wavelength than for the near-IR wavelength at ground truth values of 200. Actual algorithms for red data had 65 percent larger errors than did the near-IR algorithms.
>
> The error analysis predicted that in the near-IR turbidity prediction errors would be 26 percent smaller than residue errors at ground truth values of 200. Actual algorithms resulted in 25 percent smaller errors for turbidity.
>
> The error analysis results contained a crossover at a ground truth value of 50 between the red NTU and mg/l curves. The actual algorithms have this same crossover.

This type of agreement seems to establish the validity of both the error analysis and the statistical algorithms.

In comparing these two figures notice that although the principal features are similar, the magnitudes of the errors differ by about 30 percent. This is not surprising since numerical differences could occur for the following reasons.

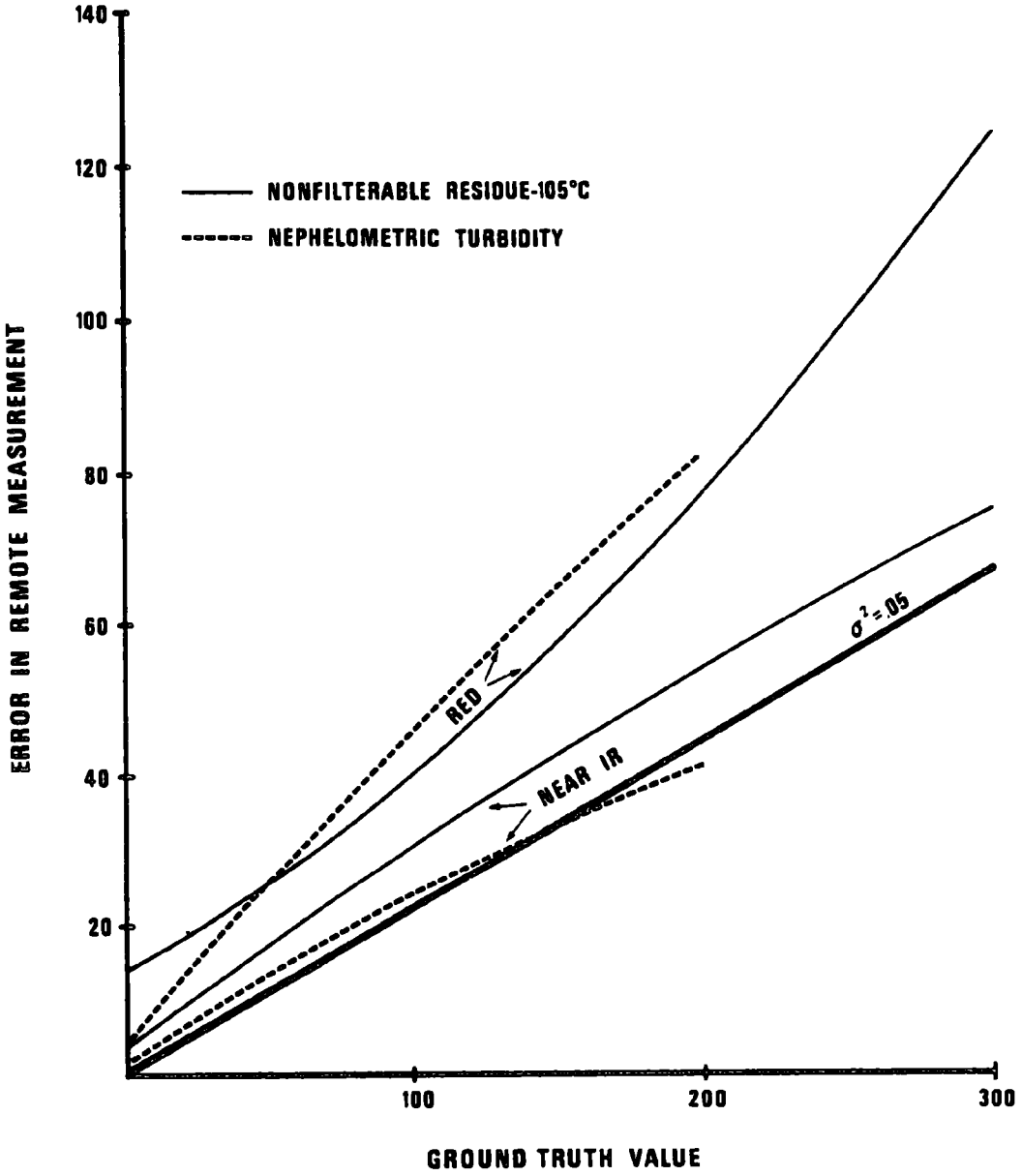

Figure 54. Uncertainties in remote measurements based on red or near-IR volume reflectance.

One figure shows standard deviations; the other figure shows a least-squares fit to the absolute value of the errors.

The error analysis did not include variability of the sediment types which would contribute to the measured errors of actual algorithms.

Random noise has been added in the design of the algorithms to degrade their accuracy.

Another interesting feature of Figure 54 is the upward curvature of the curve representing errors in nonfilterable residue predictions based upon the red wavelength. This apparently results from saturations in the visible wavelengths which leaves reflectance insensitive to changes in sediment concentration above about 200 mg/l (see Figure 54).

MULTISPECTRAL ALGORITHMS

The data analysis reported thus far has shown that volume reflectance at visible wavelengths gives the best sensitivity to sediment changes at low concentrations, but saturation occurs above about 200 mg/l. The near-IR reflectance does not saturate but lacks sensitivity at low concentrations. Thus to optimize both analytical range and sensitivity a multispectral approach has been suggested. The program ALGOR was, therefore, used to generate and evaluate 2, 6, and 10-wavelength multispectral quadratic algorithms for prediction of nephelometric turbidity and nonfilterable residue (105°C).

The data set was divided into clay, silt, and fine sand subsets as previously described, and algorithms were generated for the silt and fine sand cases. (The clay subset was not used because its 17 samples were not enough to be statistically significant.) The algorithms were applied back to the training sets to evaluate accuracy, but the errors for the silt and fine sand cases were combined before performing the error fit calculation. Thus accuracies reported here are representative of what would be expected if the particle size is known for a monitoring site.

Tables 11 through 14 contain the coefficients of the multispectral algorithms. The least-squares fits to the absolute values of the algorithm errors are shown in Figures 55 and 56 for the nonfilterable residue and nephelometric turbidity algorithms respectively. Also shown in these figures for sake of comparison are the near-IR single-wavelength algorithm results from Figure 54. The determination of which wavelengths were to be used in the multispectral algorithms resulted from a rather arbitrary selection by the investigator. Selection was not made according to any specific mathematical criteria.

Notice that at low turbidities the expected improvement of the two-wavelength algorithm over the near-IR algorithm is not present. This is a characteristic of the data set and not a general result. The reason for this can be seen from the error analysis (Figures 21 and 23) which show that the

TABLE 11. MULTISPECTRAL ALGORITHM COEFFICIENTS*
FINE SAND - NONFILTERABLE RESIDUE (105°C)

Wavelength (nm)	2λ Algorithm	6λ Algorithm	10λ Algorithm
415			95.99/-6329
436			
480			-240.3/16128
517		-434.0/964.6	
550			279.0/-9770
583		542.9/-8396	163.9/-4333
620			384.7/-189.8
652	1327/-13051	1001/-4030	
690			654.3/-9407
703		1207/-10269	862.8/-3442
742			2401/-226.8
782	4208/6204	2516/9475	
829			1837/10584
862		1338/8828	
905			-734.8/40652
942			
984			
v_o	-13.53	-16.40	-14.67

* Coefficients in each column are given in the format first-order coefficient/second-order coefficient.

TABLE 12. MULTISPECTRAL ALGORITHM COEFFICIENTS*
SILT - NONFILTERABLE RESIDUE (105°C)

Wavelength (nm)	2λ Algorithm	6λ Algorithm	10λ Algorithm
415			31.06/743.5
436			
480			-213.9/5251
517		-141.9/730.4	
550			25.98/-1804
583		458.4/-4580	438.6/-4836
620			219.8/-2638
652	354.7/-2058	263.4/-547.4	
690			314.2/715.3
703		290.6/-517.3	228.4/-303.6
742			899.3/5491
782	1496/6089	1129/6922	
829			542.0/226.9
862		978.7/7342	
905			1583/-11175
942			
984			
v_0	-7.26	-16.54	-18.01

* Coefficients in each column are given in the format first-order coefficient/second-order coefficient.

TABLE 13. MULTISPECTRAL ALGORITHM COEFFICIENTS*
FINE SAND - NEPHELOMETRIC TURBIDITY

Wavelength (nm)	2λ Algorithm	6λ Algorithm	10λ Algorithm
415			84.06/-3316
436			
480			-89.67/3536
517		-253.9/2905	
550			-40.80/-766.7
583		221.5/-2820	74.66/-1404
620			134.7/175.7
652	450.6/-3480	286.4/-1339	
690			220.2/-2344
703		383.2/-2278	260.8/-1129
742			656.6/-928.1
782	1179.6/2873	724.0/5039	
829			368.2/-1307
862		279.1/-1237	
905			339.8/33043
942			
984			
v_o	-4.76	-5.05	-4.07

* Coefficients in each column are given in the format first-order coefficient/second-order coefficient.

TABLE 14. MULTISPECTRAL ALGORITHM COEFFICIENTS*
SILT - NEPHELOMETRIC TURBIDITY

Wavelength (nm)	2λ Algorithm	6λ Algorithm	10λ Algorithm
415			11.17/83.96
436			
480			106.9/-1073
517		-35.38/1075	
550			-198.5/2090
583		299.9/-3919	281.1/-4179
620			115.6/123.7
652	138.4/-179.8	144.1/1006	
690			174.2/-258.6
703		174.8/300.9	134.6/-51.81
742			614.9/5113
782	822.0/5338	602.1/4162	
829			330.9/2003
862		399.5/-1354	
905			418.2/-6144
942			
984			
v_0	-3.43	-11.77	-9.49

* Coefficients in each column are given in the format first-order coefficient/second-order coefficient.

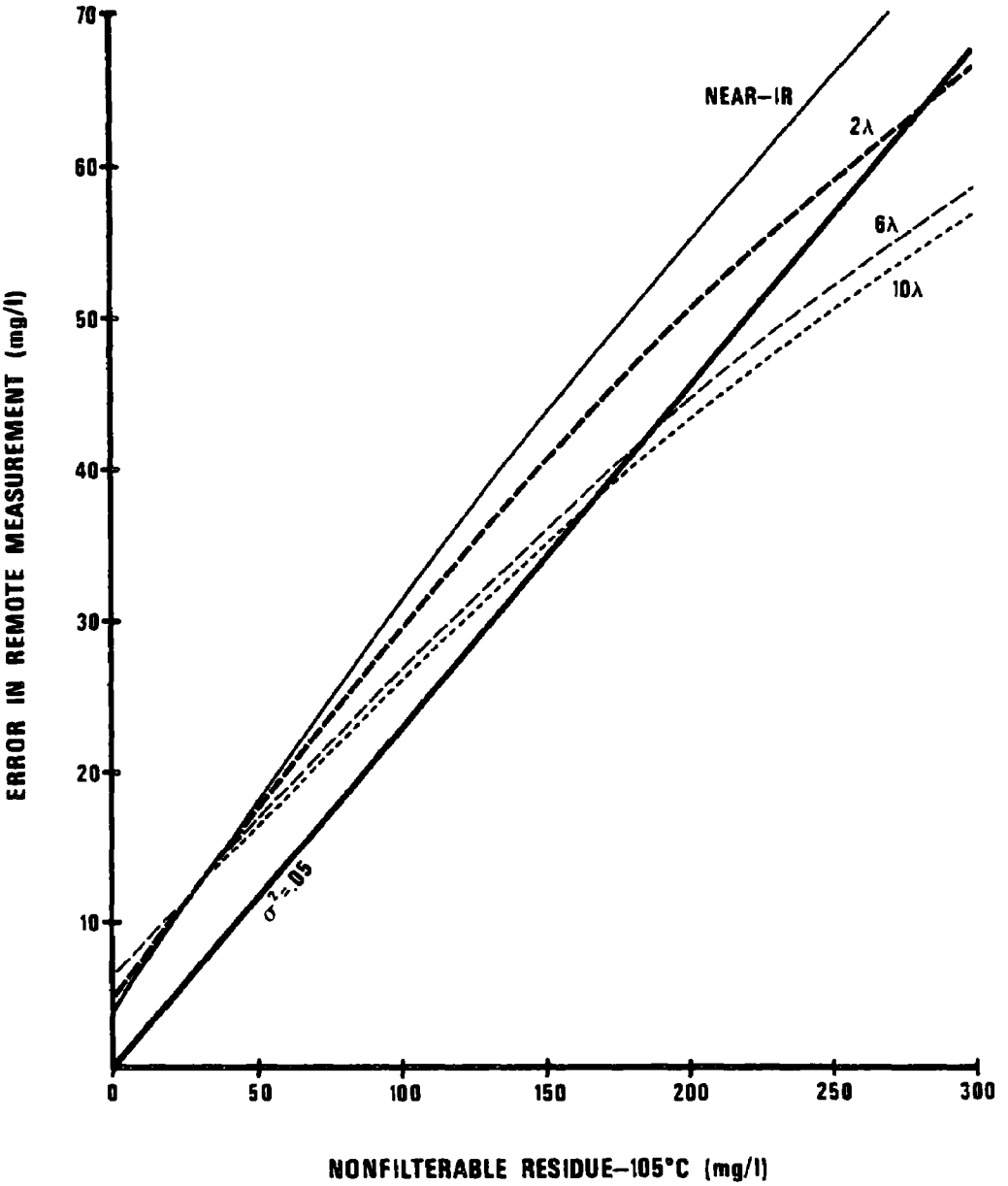

Figure 55. Accuracies of multispectral algorithms for predicting nonfilterable residue (105°C).

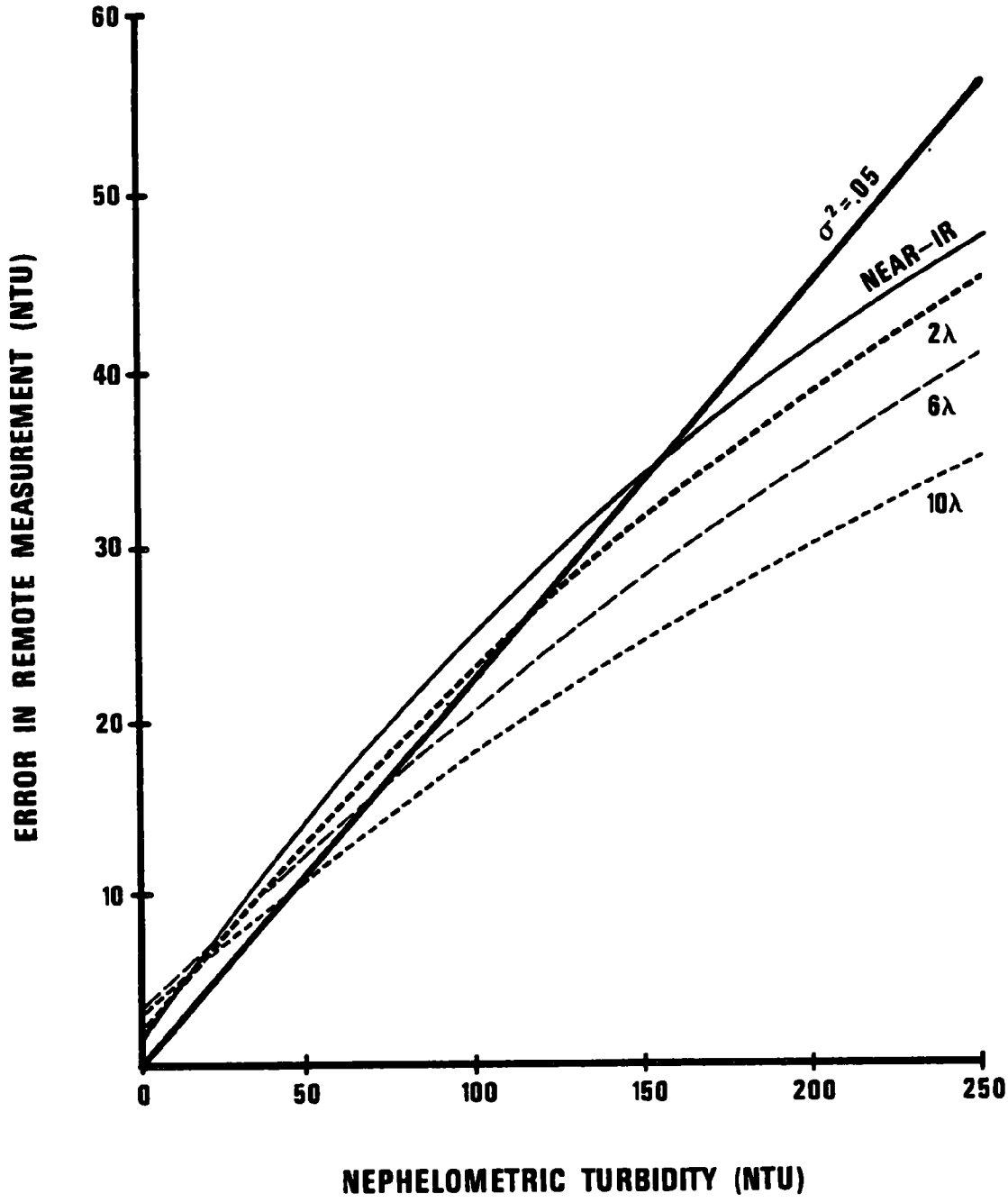

Figure 56. Accuracies of multispectral algorithms for predicting nephelometric turbidity.

red wavelength, which is supposed to be the source of the accuracy improvement, has rather large instrumental uncertainties. With an improved spectrometer, more of the expected advantage of the two-wavelength algorithm would be realized.

Study of the multispectral results leads to the following conclusions.

As the number of wavelengths is increased the accuracy improvement is not dramatic.

Since spectral reflectance curves of the sediment samples (Figure 37) were lacking any spectral fine structure, the improvement resulting from added wavelengths is thought to be the result of a $\sqrt{N}$ reduction of random noise rather than the result of better resolution of sediment signatures.

Sensor and data processing costs both go up rapidly with increasing numbers of wavelengths. A trade-off between cost and accuracy is, therefore, involved in deciding how many wavelengths to use. It is expected that the best choice will generally be in the range of two to four wavelengths. Accuracy improvements resulting from more wavelengths will probably not be great enough to justify the additional costs.

Nephelometric turbidity can be predicted from volume spectral reflectance with more accuracy than nonfilterable residue (105°C). For example, Figure 55 shows the 10-wavelength prediction of a nonfilterable residue of 250 mg/l has an uncertainty of ±50.4 mg/l for a variance of 0.041. The same sample, if it consisted of silt-sized particles, would have a nephelometric turbidity of 180 NTU. According to Figure 56 a 10-wavelength prediction of this value would have an uncertainty of ±28 NTU for a variance of 0.025.

Even with a multispectral system it is not expected that an accuracy of $\sigma^2 = 0.05$ will be possible all the way down to 25 mg/l. However, one should be able to come quite close to achieving EPA's desired accuracy.

SIGNATURE TRANSFERABILITY

The single-wavelength and multispectral algorithms have demonstrated that volume reflectance can be related to suspended sediment concentration with accuracies approaching EPA's requirements. Thus part of the feasibility question has been answered. Signature transferability is the other basic issue to be addressed in order to completely demonstrate feasibility. Is each monitoring site or sediment type a unique case, or is there some commonality between sites and sediment types which would permit multispectral monitoring without extensive ground truth?

Thus far the analysis results have indicated that the factor of commonality for nonfilterable residue is particle size, and that nephelometric turbidity-volume reflectance signatures may be transferable without any a priori knowledge. An additional analysis task was undertaken to further substantiate these conclusions. Algorithms designed from silt data were applied to fine sand data with the intent that the accuracy of these misapplied algorithms would be an indicator of signature transferability.

Only samples with nonfilterable residue (105°C) values in the range 0 to 50 mg/l were used in this step. The higher concentration ranges were ignored because the relatively few samples there raised some question as to statistical significance. The silt subset contained 86 samples in the 0- to 50-mg/l range which were used as the training set for six-wavelength algorithms for nonfilterable residue and nephelometric turbidity. Tables 15 and 16 contain the coefficients of these algorithms. These two algorithms were applied back to the silt training set to estimate their accuracy which is shown in Figure 57.

The fine sand subset contained 55 samples in the 0- to 50-mg/l range to which the algorithms of Tables 15 and 16 were also applied. The accuracy of the silt algorithms misapplied to the fine sand data is also shown in Figure 57. Notice that misapplying algorithms in the nonfilterable residue case resulted in large errors. Therefore, it is further demonstrated that signature transferability in this parameter will not be possible unless particle size is known. However, misapplication of the nephelometric turbidity algorithm results in virtually no increase in errors. Thus nephelometric turbidity exhibits a good probability of signature transfer. For purposes of remote monitoring nephelometric turbidity would, therefore, have to be considered a more desirable indicator of suspended sediment.

UNIVERSAL NEPHELOMETRIC TURBIDITY ALGORITHMS

It has been concluded that if suspended sediment is expressed in units of nephelometric turbidity, volume reflectance signatures are invariant between sediment types. Therefore, the final analysis step would be to combine clay, silt, and fine sand subsets and design nephelometric turbidity algorithms which would presumably be of universal applicability regardless of sediment type.

Three universal algorithms have been developed. Two are single-wavelength algorithms operating on volume reflectance at the red (652 nm) and near-IR (782 nm) wavelengths. The third is a two-wavelength algorithm operating on both of these wavelengths. These wavelengths were selected because they roughly correspond to bands obtainable by densitometric analysis of color-infrared photography, and they also correspond to LANDSAT bands 5 and 6. Thus other investigators using these types of sensors might find these algorithms of interest, and if volume reflectance can be derived from their data, these investigators may provide data of value in verifying the conclusions that have led to these algorithms.

Table 17 contains the coefficients of the universal nephelometric turbidity algorithms and Figure 58 shows their expected accuracies.

TABLE 15. MULTISPECTRAL ALGORITHM - NONFILTERABLE RESIDUE (0 TO 50 mg/l SILT)

Wavelength (nm)	First-Order Coefficient	Second-Order Coefficient
517	-47.91	471.3
583	11.74	-437.1
652	132.6	-196.8
703	287.6	-1104
782	938.8	-15307
862	1059	-11564
v_0	-4.53	

TABLE 16. MULTISPECTRAL ALGORITHM - NEPHELOMETRIC TURBIDITY (0 TO 40 NTU SILT)

Wavelength (nm)	First-Order Coefficient	Second-Order Coefficient
517	-13.36	-17.59
583	-7.43	-63.56
652	86.54	-677.6
703	213.0	-787.1
782	858.6	-257.7
862	620.5	-262.77
v_0	-3.05	

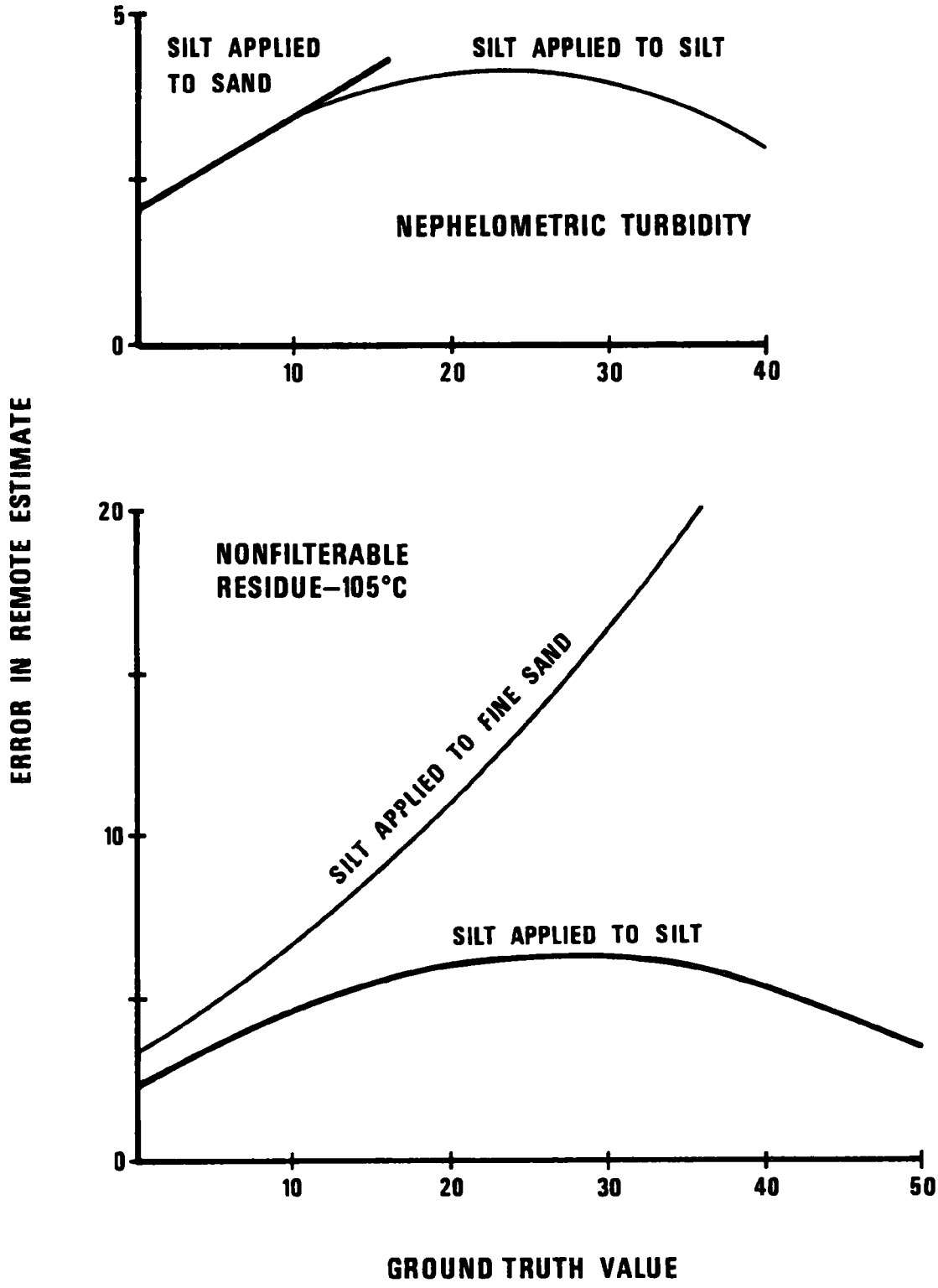

Figure 57. Comparison between accuracies of correct and misapplied six-wavelength algorithms.

TABLE 17. UNIVERSAL NEPHELOMETRIC TURBIDITY ALGORITHMS

Type	Wavelength (nm)	v_0	First-Order Coefficient	Second-Order Coefficient
Single-wavelength	652	-4.38	33.96	5352
Single-wavelength	782	0.0	1181	4062
Two-wavelength	652		233.7	-1384

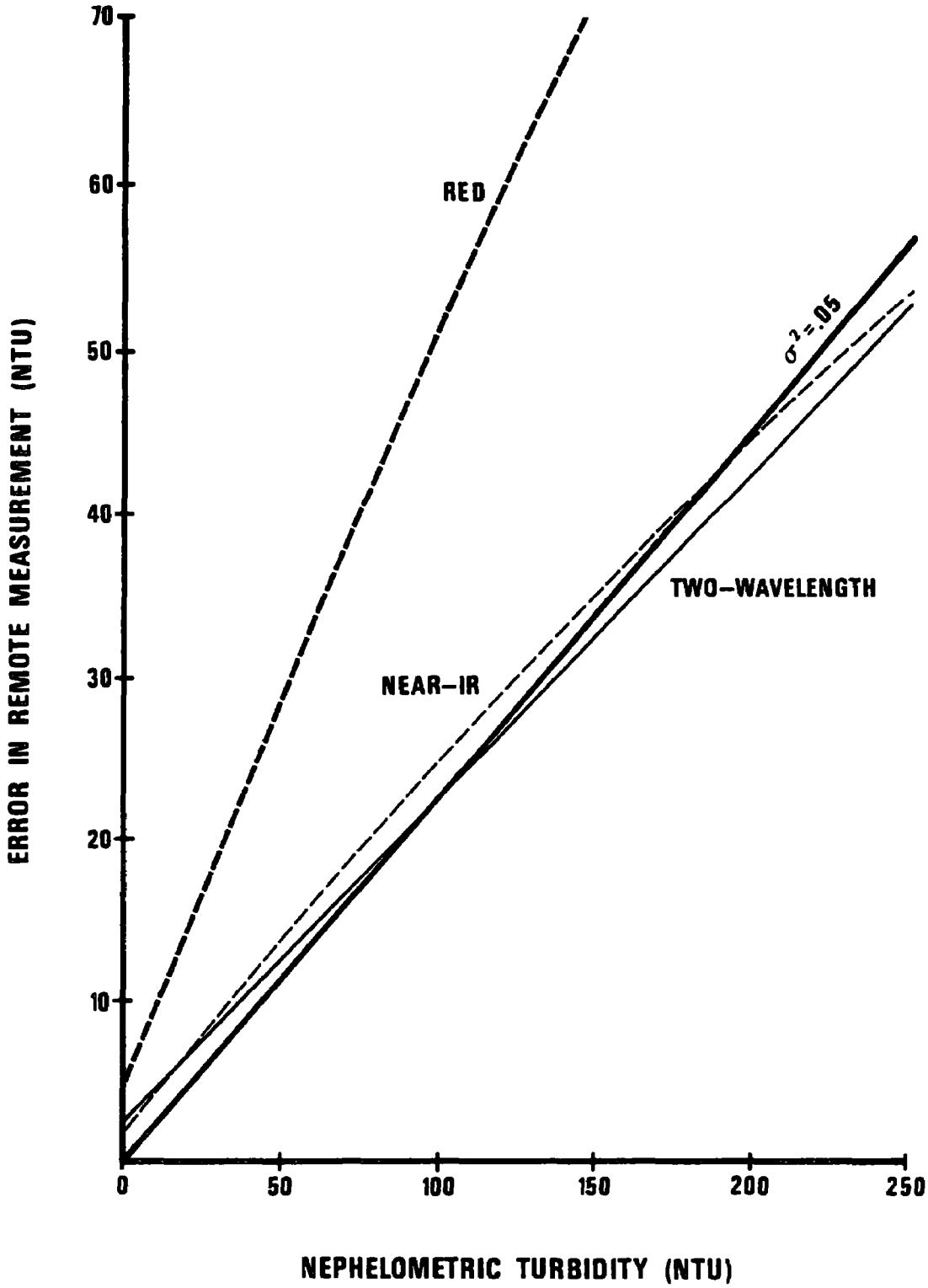

Figure 58. Expected accuracy of universal nephelometric turbidity algorithms.

SECTION X

REFERENCES

American Society for Testing and Materials, 1973. Annual Book of ASTM Standards, Part 23, Water; Atmospheric Analysis, ASTM, Philadelphia, Pennsylvania.

Bevington, P., 1969. Data Reduction and Error Analysis for the Physical Sciences, McGraw-Hill.

Blanchard, B. J., and R. W. Leamer, 1973. American Water Resources Association, Proceedings, 17:339.

Bowker, D., P. Fleischer, W. G. Whitte, T. A. Gosink and W. J. Hanna, 1975. "An Investigation of the Waters In the Lower Chesapeake Bay Area", Proceedings of the Tenth International Symposium on Remote Sensing of Environment.

Cox, C., and W. Munk, 1956. "Slopes of the Sea Surface Deduced from Photographs of Sun Glitter", Bull. Scripps Institute Oceanography University of California, 6:401-488.

Encyclopedia of Industrial Chemical Analysis, 1966. Ed. Snell and Hilton, Interscience Publishers, Volume 3.

European Inland Fisheries Advisory Board (EIFAB), 1965. Working Party on Water Quality Criteria for European Freshwater Fish. Report on finely divided solids and inland fisheries. Air Water Pollution 9 (3):151-163.

Goldman, C., 1974. "Limnological Studies and Remote Sensing of the Upper Truckee River Sediment Plume in Lake Tahoe, California-Nevada" Remote Sensing of Environment. American Elsevier Publishing Co., Inc., 3, 49-67.

Grum, F., and G. Luckey, 1968. "Optical Sphere Paint and Working Standard of Reflectance", Applied Optics, Volume 7, Number 11.

Jerlov, N., 1968. Optical Oceanography, Elsevier Publishing Company.

Klemas, V., D. S. Bartlett, W. D. Philpot, G. R. Davis and R. H. Rogers, 1974. "Correlation of Coastal Water Turbidity and Current Circulation with ERTS-1 and Skylab Imagery", Proceedings of the Ninth International Symposium on Remote Sensing of Environment. Ann Arbor, Michigan.

Klooster, S., and J. Scherz, 1974. "Water Quality in Photographic Analysis", Photogrammetric Engineering XL-8, 927-935.

Kritikos, H., L. Yorinks and H. Smith, 1974. "Suspended Solids Analysis Using ERTS-A Data", Remote Sensing of Enviroment, 3, 69-78.

Laursen, E., and E. Silverston, 1976. "On Sediment Transport Through the Grand Canyon", Proceedings of the Third Federal Inter-Agency Sedimentation Conference.

Lillesand, T., 1973. "Use of Aerial Photography to Quantitatively Estimate Water Quality Parameters in Surface Water Mixing Zones", PhD Thesis, University of Wisconsin.

Lillesand, T., F. L. Scarpace and J. P. Clapp, 1975. "Water Quality in Mixing Zones", Photogrammetric Engineering and Remote Sensing.

Moon, P., and D. Spencer, 1942. "Illumination from a Nonuniform Sky", Illumination Engineering, Volume 37.

Novotny, J., 1975a. "Summary Report - Job Order 30.02 Spectrometer Modification and Checkout", Lockheed Electronics Co., Inc., Technical Memo #EAL-TM-006.

Novotny, J., 1975b. "Job Order 30.02 - Spectrometer Development and Checkout", Lockheed Electronics Co., Inc.

Piech, K., and J. Walker, 1971. "Aerial Color Analysis of Water Quality", Journal Survey and Mapping Division, Proceedings A.S.C.E., Volume 97, Number SU^2.

Pionke, H., and B. Blanchard, 1975. "The Remote Sensing of Suspended Sediment Concentration of Small Impoundments", Water, Air, and Soil Pollution, 4, 19-32.

Pijanowski, B., 1975. "The Meaning and Measurement of Turbidity", Proceedings - International Conference on Environmental Sensing and Assessment, Las Vegas, Nevada.

National Oceanic Instrumentation Center, NOIC Turbidity Workshop, 1974, Washington, D. C.

Ritchie, J., J. Roger McHenry, F. R. Schiebe and R. B. Wilson, 1974. "The Relationship of Reflected Solar Radiation and the Concentration of Sediment in the Surface Water of Reservoirs", Proceedings of the Third Annual Remote Sensing of Earth Resources Conference, Tullahoma, Tennessee.

Rosgen, D., 1975. "The Use of Color Infrared Photography for the Determination of Suspended Sediment Concentrations and Source Areas", U.S. Forest Service, Fort Collins, Colorado.

Scherz, J., and J. Van Domelen, 1975. "Water Quality Indicators Obtainable from Aircraft and LANDSAT Images and Their Use in Classifying Lakes", Proceedings of the Tenth International Symposium on Remote Sensing of Environment, Ann Arbor, Michigan.

Sekera, Z., 1957. "Polarization of Skylight", in Handbuch der Physik, Springer, Berlin.

American Public Health Association (APHA), 1971. Standard Methods for the Examination of Water and Wastewater, 13th edition, APHA, AWWA, WPCF.

U.S. Department of Interior (USDI), 1959. "Study and Interpretation of the Chemical Characteristics of Natural Water", U.S. Geological Survey Water Supply Paper 1473, USGPO, Washington, D. C.

U.S. Environmental Protection Agency (U.S. EPA), undated. Memorandum from D. S. Barth, EMSL/LV Director to Richard Johnson.

U.S. Environmental Protection Agency (U.S. EPA), 1973. "Methods for Identifying and Evaluating the Nature and Extent of Nonpoint Sources of Pollutants", EPA-430/9-73-014.

U.S. Environmental Protection Agency (U.S. EPA), 1975. "Remote Sensing Instrumentation Criteria: For Monitoring Sediments and Salinity in Surface Waters", EPA-600/0-75-004.

APPENDIX A

METRIC CONVERSION TABLE

Non-metric Unit	Multiply by	Metric Unit
feet (ft)	0.3048	meters (m)
gallon (gal)	3.8	liters (l)
miles (mi)	1.609	kilometers (km)

APPENDIX B

VOLREF

PROGRAM LISTING

```
      PROGRAM VOLREF (INPUT,OUTPUT,TAPE5=INPUT,TAPE6=OUTPUT,PUNCH)
C
C     ****** ****.*****************************************************
C
C THIS PROGRAM TAKES AS INPUT PUNCHED CARDS CONTAINING SPECTROMETER DATA
C RECORDED ON STRIP CHARTS IN THE FIELD AND CALCULATES WATER VOLUME SPECTRAL
C REFLECTANCE.  THE PERIPHERAL EFFECTS MASKING TRUE VOLUME REFLECTANCE ARE
C REMOVED BY THE SCS TECHNIQUE DEVELOPED BY PIECH AND WALKER (1972)
C
C     ******************************************************************
C
C THIS PROGRAM IS INTENDED FOR USE WITH THE EPA EMSL/LV SPECTROMETER
C WHICH SAMPLES 20 WAVELENGTHS.  THUS, DIMENSIONS OF ARRAYS ARE SET
C ACCORDINGLY.
C
      DIMENSION ALFA(20),ALFAP(20),LAMBDA(20),R(20,14),SITE(2)
      DIMENSION VZ(20),VG(20),PAR(11),COM(8),VE(20),VW(20),VES(20)
      DIMENSION LABEL(7),DATA(6),A(29,7),ASTOR(29),VWS(20),VGS(20)
      INTEGER COLBL,A,BLANK,ASTOR
      DATA NCH/20/
      DATA BLANK/'          '/
C
C ENTER VALUES OF REFLECTANCE STANDARDS
C
C NO. 1 FLAT WHITE ENAMEL - BRAND UNKNOWN
C
      DATA (R(I,1),I=1,20) /0.7,0.7,0.7,0.7,0.7,0.705,0.71,0.72,0.72,0.7
     12,0.72,0.73,0.73,0.72,0.72,0.7,0.68,0.65,0.65,0.635/
C
C NO. 2 ZYNOLYTE SPEED-E-NAMEL GRAY METAL PRIMER (0427)
C
      DATA (R(I,2),I=1,20)/0.23,0.23,0.23,0.23,0.23,0.23,0.23,0.227,0.22
     11,0.213,0.205,0.192,0.189,0.178,0.163,0.154,0.145,0.13,0.125,0.125
     2/
C
C NO. 3 KRYLON GRAY PRIMER (NO. 2 RECOATED)
C
      DATA (R(I,3),I=1,20)/.04,.056,.094,.114,.112,.105,.09,.08,.073,.06
     14,.062,.059,.059,.054,.057,.056,.054,.05,.047,.045/
C
C NO. 4 KRYLON FLAT WHITE ENAMEL (NO.1 RECOATED)
C
      DATA (R(I,4),I=1,20) /0.7,0.7,0.7,0.7,0.7,0.72,0.74,0.745,0.73,0.7
     115,0.71,0.71,0.705,0.705,0.705,0.7,0.69,0.65,0.65,0.635/
C
C NO. 3 AND NO. 4 LOST OVERBOARD
C
C NO. 5 KRYLON FLAT WHITE ENAMEL (NEW AL SHEET - SOME AL SHOWING THROUGH PAIN
C
C NO. 6 KRYLON GRAY PRIMER    (OVER PREVIOUS FLAT BLACK)
C
      DATA (R(I,6),I=1,20)/.04,.056,.094,.1,.097,.085,.076,.07,.066,.062
     1,.06,.055,.053,.052,.054,.05,.047,.045,.043,.042/
C
C NO. 7 KRYLON GRAY PRIMER (NO. 6 RECOATED)
C
      DATA (R(I,7),I=1,20)/.04,.056,.094,.107,.103,.092,.083,.076,.072,.
```

```
     1.071,.067,.065,.064,.058,.059,.06,.057,.052,.049,.046/
C
C NO. 8 KRYLON FLAT WHITE ENAMEL (NO. 5 RECOATED)
C
C NO. 9 KRYLON GRAY PRIMER (NO. 7 RECOATED)
C
      DATA (R(I,9),I=1,20)/.04,.056,.094,.11,.109,.103,.095,.09,.087,.08
     14,.08,.073,.071,.066,.069,.067,.064,.06,.057,.056/
C
C NO. 10 KRYLON FLAT WHITE ENAMEL (NO. 8 RECOATED)
C
C NO. 11 KRYLON GRAY PRIMER (NO. 9 RECOATED)
C
      DATA (R(I,11),I=1,20)/.04,.056,.094,.106,.102,.093,.081,.076,.073,
     1.069,.067,.065,.064,.06,.063,.061,.06,.056,.053,.053/
C
C NO. 12 ZYNOLYTE SPEED-E-NAMEL FLAT WHITE (0377) (OVER NO. 10)
C
C NO. 13 KRYLON GRAY PRIMER (NO. 11 RECOATED)
C
      DATA (R(I,13),I=1,20)/.04,.056,.094,.099,.102,.101,.092,.081,.074,
     1.07,.069,.067,.062,.057,.065,.062,.06,.056,.053,.053/
C
C NO. 14 KRYLON FLAT WHITE ENAMEL (NO. 12 RECOATED)
C
      DATA (R(I,14),I=1,20)/.74,.74,.76,.768,.774,.803,.81,.797,.776,.76
     18,.755,.753,.755,.755,.755,.755,.725,.692,.68,.68/
C
C ENTER WAVELENGTHS IN NANOMETERS WHICH THE SPECTROMETER SAMPLES
C
      DATA LAMBDA/343,377,385,415,436,480,517,550,583,620,652,690,703,74
     12,782,829,862,905,942,984/
C
C ENTER AXES AND LABELS FOR SPECTRAL PLOTS
C
      DATA A(26,1)/'    .00 I--'/,A(26,2)/'--I----I--'/,A(26,7)/'--I----I
     1  '/
      DATA A(27,1)/'       400 '/,A(27,2)/'       500 '/,A(27,3)/'       60
     10 '/,A(27,4)/'       700 '/,A(27,5)/'       800 '/,A(27,6)/'       90
     20 '/,A(27,7)/'      1000'/
      DATA A(29,1)/'           '/,A(29,2)/'           '/,A(29,3)/'    WAVE
     1LE'/,A(29,4)/'NGTH (NM) '/,A(29,5)/'           '/,A(29,6)/'
     2  '/,A(29,7)/'           '/
      DATA A(1,1)/'   .25 -  '/,A(2,1)/'       I  '/,A(6,1)/'V  .20 -  '
     1/,A(7,1)/'O      I  '/,A(8,1)/'L      I  '/,A(10,1)/'R      I  '/,
     2A(11,1)/'E  .15 -  '/,A(12,1)/'F      I  '/,A(14,1)/'E      I  '/,
     3A(15,1)/'C      I  '/,A(16,1)/'T  .10 -  '/,A(17,1)/'A      I  '/,
     4A(18,1)/'N      I  '/,A(21,1)/'   .05 -  '/
C
C ENTER DATA CARD RECOGNITION LABELS
C
      DATA LABEL/'ID        ','COVERED   ','SUN       ','SHADOW    ','WA
     1TER     ','LAB       ','END       '/
      DO 3007 I=1,20
      R(I,5)=R(I,4)
      R(I,10)=R(I,4)
      R(I,12)=R(I,4)
```

```
C300? P(I,2)=P(I,4)
C
C SETUP PRINT ARRAY WITH INFORMATION NOT ENTERED VIA DATA STATEMENTS
C
      DO 21 I=3,5
   21 A(I,1)=A(2,1)
      DO 22 I=22,25
   22 A(I,1)=A(2,1)
      DO 23 I=1,7
   23 A(28,I)=BLANK
      A(9,1)=A(2,1)
      A(13,1)=A(9,1)
      A(19,1)=A(15,1)
      A(20,1)=A(14,1)
      A(26,3)=A(26,2)
      A(26,4)=A(26,2)
      A(26,5)=A(26,2)
      A(26,6)=A(26,2)
      DO 15 I=1,29
   15 ASTOP(I)=A(I,1)
C
C BEGIN READING DATA CARDS
C
 2000 READ(5,100) CDLBL,ALPHA,DATA
  100 FORMAT(2A10,6F10.0)
C
C IF CARD LABEL READS 'END' TERMINATE PROCESSING
C
      IF(CDLBL.EQ.LABEL(7)) GO TO 777
C
C IF CARD LABEL READS 'WATER' READ WATER DATA AND PROCESS
C
      IF(CDLBL.EQ.LABEL(5)) GO TO 2
      GO TO 1
    2 READ(5,101) VW
  101 FORMAT(8F10.0)
      THETA=DATA(1)
      GO TO 1000
C
C IF CARD LABEL READS 'COVERED' READ DATA REPPRESENTING ZERO ENERGY INPUT TBS
C GO BACK AND READ ANOTHER CARD
C
    1 IF(CDLBL.EQ.LABEL(2)) GO TO 7
      GO TO 8
    7 READ(5,101) VZ
      SKYREF=DATA(1)
      GO TO 2000
C
C IF CARD LABEL READS 'SUN' READ IN DATA FOR REFLECTANCE STANDARD IN SUNLIGH
C THEN GO BACK AND READ ANOTHER CARD
C
    8 IF(CDLBL.EQ.LABEL(3)) GO TO 9
      GO TO 10
    9 READ(5,101) VG
      X=DATA(1)
      NREFSN=IFIX(X)
      GO TO 2000
```

```
C IF CARD LABEL READS 'SHADOW' READ DATA FOR REFLECTANCE STANDARD SHADED
C SUNLIGHT THEN GO BACK AND READ ANOTHER CARD
C
   10 IF(COLBL.EQ.LABEL(4)) GO TO 11
      GO TO 12
   11 READ(5,101) VE
      X=DATA(1)
      VREFSH=IFIX(X)
      GO TO 2000
C
C IF CARD LABEL READS 'LAB' READ IN LABORATORY ANALYSIS RESULTS THEN GO
C BACK AND READ ANOTHER CARD
C
   12 IF(COLBL.EQ.LABEL(6)) GO TO 13
      GO TO 14
   13 READ(5,101) PAR
      GO TO 2000
C
C IF CARD LABEL READS 'ID' READ IN SAMPLE IDENTIFICATION AND OTHER
C RELATED INFORMATION AND THEN GO BACK AND READ ANOTHER CARD
C
   14 IF(COLBL.EQ.LABEL(1)) GO TO 4
      GO TO 2000
    4 READ(5,102) DATE,TIME,PHI,SI,CSTATE,SECCHI,HEAD
  102 FORMAT(2A10,12F5.0)
      SAMPNO=ALPHA
      READ(5,107) WINDIR,W,SFOTO,VWFOTO,OWFOTO,SITE,STAT
  107 FORMAT(2F10.0,6A10)
      READ(5,103) COM
  103 FORMAT(8A10)
      GO TO 2000
C
C PROCESSING OF WATER SPECTRUM BEGINS HERE
C
 1000 CONTINUE
C
C WRITE OUT ALL ID AND LABORATORY DATA FOR THIS SAMPLE
C
      WRITE(6,104)
  104 FORMAT(1H1////41X,41HENVIRONMENTAL PROTECTION AGENCY - EMSL/LV/41X
     1,40HMULTISPECTRAL TURBIDITY TECHNIQUES STUDY//)
      WRITE(6,105) SAMPNO,DATE,SITE,TIME,STAT,SFOTO,VWFOTO,OWFOTO
  105 FORMAT(14H SAMPLE NUMBER,6X,A10//5H DATE,15X,A10,40X,4HSITE,6X,2A1
     10/11H TIME (PDT),9X,A10,40X,7HSTATION,13X,A10/14H SKY PHOTO NO.,6X
     2,A10/16H VERT. PHOTO NO.,4X,A10/15H OBL. PHOTO NO.,5X,A10,40X,8HRE
     3MARKS-)
      WRITE(6,106) SECCHI,COM(1),COM(2),COM(3),COM(4),CSTATE,COM(5),COM(
     16),COM(7),COM(8),THETA,HEAD,PHI,SI,WINDIR,W
  106 FORMAT(13H SECCHI DEPTH,7X,F10.1,2H M,48X,4A10/10H SEA STATE,10X,F
     110.1,3H CM,47X,4A10/11H LOOK ANGLE,9X,F10.1,4H DEG/13H BOAT HEADIN
     2G,7X,F10.1,4H DEG/14H SUN ELEVATION,6X,F10.1,4H DEG/12H SUN AZIMUT
     3H,8X,F10.1,4H DEG/15H WIND DIRECTION,5X,F10.1,4H DEG/14H WIND VELO
     4CITY,6X,F10.1,4H M/S/)
      WRITE(6,108) PAR(1),PAR(7),PAR(8),PAR(9)
  108 FORMAT(27H LABORATORY ANALYSIS REPORT//10X,21HNONFILT RESIDUE (105
     1),8X,F6.1,5H MG/L,20X,19HTOTAL RESIDUE (105),10X,F6.1,5H MG/L/10X,1
```

```
     2HHFILT RESIDUE (105),11X,F6.1,5H MG/L,20X,22HNONFILT. FIXED RESIDU
     3E,7X,F5.1,5H MG/L)
      WRITE(6,109) PAR(4),PAR(10),PAR(5),PAR(11),PAR(6)
  109 FORMAT(10X,21HNONFILT RESIDUE (180),9X,F5.1,5H MG/L,20X,18HCOLOR (
     1PT-CO TEST),12X,F5.1,5X  /10X,19HFILT RESIDUE (180),11X,F6.1,5H MG
     2/L,20X,20HNONFILT. VOL RESIDUE,10X,F5.1,5H MG/L /10X,9HTURBIDITY,2
     31X,F5.1,4H NTU)
C
C SAVE SOME INFORMATION NEEDED LATER
C
      DO 6 I=1,20
      VWS(I)=VW(I)
      VES(I)=VE(I)
    6 VGS(I)=VG(I)
C
C CALCULATE PORTION OF AVAILABLE SKY NOT COVERED BY SUN SHIELD
C
      XKE=0.97-((80.0-PHI)*0.005)
C
C CALCULATE TRANSMITTANCE AND REFLECTANCE OF WIND ROUGHENED SURFACE
C FOR DIFFUSE SKYLIGHT
C
      CALL SKY (W,SKYTRN,SKYREF)
C
C CALCULATE TRANSMITTANCE OF WIND ROUGHENED SURFACE FOR SUNLIGHT
C
      DELANG=SI-WINDIR
      DELANG=ABS(DELANG)
      IF(DELANG.GT.180.0) DELANG=360.0-DELANG
      CALL SURTRN (W,DELANG,PHI,TRANS1,2)
C
C CALCULATE TRANSMITTANCE OF WIND ROUGHENED SURFACE FOR UPWELLING LIGHT
C AT ANGLE OF OBSERVATION
C
      DELANG=HEAD-WINDIR
      DELANG=ABS(DELANG)
      IF(DELANG.GT.180.0) DELANG=360.0-DELANG
      IF(THETA.LT.0.01) DELANG=180.0-DELANG
      THETA=ABS(THETA)
      X=90.0-THETA
      CALL SURTRN (W,DELANG,X,TRANS2,1)
C
C LOOP ON WAVELENGTHS CALCULATING VOLUME SPECTRAL REFLECTANCE
C
      DO 20 I=1,20
C
C CONVERT SHADE DATA RECORDED ON HIGH REFLECTANCE STANDARD TO WHAT IT WOULD
C HAVE BEEN IF THE LOW REFLECTANCE STANDARD HAD BEEN USED INSTEAD
C
      RATIO=R(I,NREFSN)/R(I,NREFSH)
      VE(I)=RATIO*(VE(I)-VZ(I))
C
C CALCULATE APPROXIMATE ALPHA
C
      ALFA(I)=(VG(I)-VZ(I))/R(I,NREFSN)
C
C CALCULATE ALPHA PRIME
```

```
      VG(I)=VG(I)-VZ(I)
      IF(VG(I).LT.0.001) GO TO 30
      ALFAP(I)=(ALFA(I)*VE(I))/(XKE*VG(I))
      GO TO 31
   30 ALFAP(I)=0.0
C
C CORRECT APPROXIMATE ALPHA
C
   31 ALFA(I)=TRANS2*((TRANS1*ALFA(I))+((SKYTRN-TRANS1)*ALFAP(I)))
      IF(ALFA(I).LT.0.001) GO TO 32
C
C CALCULATE WATER VOLUME SPECTRAL REFLECTANCE
C
      VW(I)=(VW(I)-(SKYREF*ALFAP(I))-VZ(I))/ALFA(I)
      GO TO 20
   32 VW(I)=0.0
      ALFA(I)=0.0
   20 CONTINUE
      DO 24 I=1,3
   24 VW(I)=0.0
C
C LOAD REFLECTANCE VALUES INTO PLOT ARRAY
C
      CALL PLTARY (VW,A)
C
C PRINT OUT PLOT OF SPECTRUM
C
      WRITE(6,111)
  111 FORMAT(/)
      DO 3 I=1,29
      WRITE(6,112) (A(I,J),J=1,7)
  112 FORMAT(1X,7A10)
    3 CONTINUE
C
C PUNCH OUT DATA ON CARDS
C
      PUNCH 120,SAMPNO,PAR(1),PAR(8),PAR(4),PAR(5),PAR(6),PAR(7),PAR(9),
     1PAR(10),PAR(11)
  120 FORMAT(A10,9F7.1)
      PUNCH 121,VW
  121 FORMAT(10F8.4)
C
C PRINT TABULATION OF ALL RAW DATA AND INTERMEDIATE RESULTS
C
      WRITE(6,113) SAMPNO
  113 FORMAT(15H1SAMPLE NUMBER ,A10,10H CONTINUED///)
      WRITE(6,114)
  114 FORMAT(11H WAVELENGTH,8X,2HVZ,14X,2HVG,14X,2HVE,14X,2HVW,13X,4HALF
     1A,11X,5HALFAP,13X,2HRV//)
      DO 5 I=1,20
      VW(I)=VW(I)*100.0
      WRITE(6,115) I,LAMBDA(I),VZ(I),VGS(I),VES(I),VWS(I),ALFA(I),ALFAP(
     1I),VW(I)
  115 FORMAT(1X,I2,I6,4X,F10.2,6X,F10.2,6X,F10.2,6X,F10.2,6X,F10.2,6X,F1
     10.2,6X,F10.2)
    5 CONTINUE
```

```
C
C ERASE SPECTRAL DATA FROM PLOT ARRAY
C
      DO 15 I=1,29
   15 A(1,I)=ASTOR(I)
C
C GO BACK AND READ IN MORE DATA CARDS
C
      GO TO 2000
C
C
C WRITE PROCESSING TERMINATED MESSAGE
C
  777 WRITE(6,110)
  110 FORMAT(45H1END CARD ENCOUNTERED - PROCESSING TERMINATED)
      STOP
      END
```

```
      SUBROUTINE SURTRN(W,DELANG,PHI,TRANS,UORD)
C
C ******************************************************************
C
C THIS SUBROUTINE CALCULATES THE TRANSMITTANCE OF THE AIR-WATER INTERF
C GIVEN WIND VELOCITY AND LOOK ANGLE WITH RESPECT TO THE HORIZON AND W
C DIRECTION
C
C ******************************************************************
C
C       IS THE WIND VELOCITY IN M/SEC - SUPPLIED BY CALLING PROGRAM
C
C     DELANG IS THE HORIZONTAL ANGLE IN DEGREES BETWEEN SUN AZIMUTH AN
C     POINTING UPWIND - SUPPLIED BY THE CALLING PROGRAM
C
C     PHI IS THE SUN ELEVATION IN DEGREES ABOVE THE HORIZON - SUPPLIED
C     CALLING PROGRAM
C
C     TRANS IS THE CALCULATED SURFACE TRANSMITTANCE - RETURNED TO THE
C     CALLING PROGRAM
C
C     UORD IS A FLAG INDICATING WHETHER CALCULATION IS FOR UPWELLING
C     (UORD=1) OR DOWNWELLING (UORD=2) LIGHT
C
C ******************************************************************
C
      INTEGER UORD
      DELANG=DELANG/57.29578
      PHI=PHI/57.29578
      ZENITH=1.5707963-PHI
C
C CALCULATE CROSS- AND UPWIND INCREMENTS TO ADD TO ANGLES TO ACCOUNT F
C NONPERPENDICULAR INCIDENCE
C
      X=COS(DELANG)/TAN(PHI)
      DANGU=ATAN(X)
      X=SIN(DELANG)/TAN(PHI)
      DANGC=ATAN(X)
C
C CALCULATE VALUES FOR SIGU AND SIGC
C
      SIGU=((0.003+(0.00512*W))/2.0)**0.5
      SIGC=SIGU
C
C
C LOOP ON ETA (UPWIND 'STANDARDIZED' SLOPE COMPONENT)
C
      ETA=-3.2
      PSUM=0.0
      SUM=0.0
      DO 1 J=1,31
      ETA=ETA+0.2
      XI=-3.2
C
C CALCULATE UPWIND COMPONENT OF TOTAL SLOPE (WIND + SUN EFFECTS)
C
      Y=ETA*SIGU
```

```
      ANGU=ATAN(Y)
      ANGU=ANGU+DANGU
      SLU=TAN(ANGU)
C
C LOOP ON XI (CROSSWIND 'STANDARDIZED' SLOPE COMPONENT) - BECAUSE OF
C SYMMETRY IN CROSSWIND DIRECTION, ONLY ONE HALF OF THE FUNCTION MUST B
C EVALUATED
C
      DO 2 K=1,15
      XI=XI+0.2
C
C EVALUATE CROSSWIND COMPONENT OF TOTAL SLOPE (WIND + SUN EFFECTS)
C
      Z=XI*SIGC
      ANGC=ATAN(Z)
      ANGC=ANGC+DANGC
      SLC=TAN(ANGC)
C
C OBTAIN THE PROBABILITY OF THIS SLOPE COMPONENT COMBINATION
C
      CALL PROB (XI,ETA,W,P,SIGU,SIGC)
C
C CALCULATE SLOPE OF WATER SURFACE
C
      X=((Y*Y)+(Z*Z))**0.5
      X=ATAN(X)
      AREA=1.0/COS(X)
C
C CHECK FOR INCIDENCE ANGLES GREATER THAN + OR - PI/2
C
      IF(ANGU.GT.1.5707963.OR.ANGU.LT.-1.5707963) GO TO 3
      IF(ANGC.GT.1.5707963.OR.ANGC.LT.-1.5707963) GO TO 3
C
C EVALUATE TOTAL SLOPE (WIND + SUN EFFECTS)
C
      SLOPE=((SLU*SLU)+(SLC*SLC))**0.5
C
C OBTAIN REFLECTANCE FOR THIS SLOPE
C
      THETA=ATAN(SLOPE)
      CALL ROES(THETA,REF)
C
C SUM REFLECTANCES WEIGHTED BY THE PROBABILITY OF EACH TIMES THE COSINE
C OF THE INCIDENCE ANGLE TIMES THE AREA
C
      SINJ=SIN(THETA)/1.3333
      XJ=ASIN(SINJ)
      IF(UORD.EQ.1) X=COS(XJ)
      IF(UORD.EQ.2) X=COS(THETA)/COS(XJ)
      SUM=SUM+ ((1.0-REF)*X*P*AREA)
      IF(UORD.EQ.1) PSUM=PSUM+(P*COS(THETA)*AREA)
C
C ADD OTHER HALF OF PROBABILITY FUNCTION
C
    3 ANGC=ANGC-DANGC
      ANGC=-ANGC+DANGC
      IF(ANGU.GT.1.5707963.OR.ANGU.LT.-1.5707963) GO TO 4
```

```
      IF(ANGC.GT.1.5707963.OR.ANGC.LT.-1.5707963) GO TO 4
      SLC=TAN(ANGC)
      SLOPE=((SLU*SLU)+(SLC*SLC))**0.5
      THETA=ATAN(SLOPE)
      CALL ROES (THETA,REF)
      SINJ=SIN(THETA)/1.3333
      XJ=ASIN(SINJ)
      IF(UORD.EQ.1) X=COS(XJ)
      IF(UORD.EQ.2) X=COS(THETA)/COS(XJ)
      SUM=SUM+ ((1.0-REF)*X*P*AREA)
C
C SUM PROBABILITIES SINCE DISTRIBUTION FUNCTION IS UNNORMALIZED
C
      IF(UORD.EQ.1) PSUM=PSUM+(P*COS(THETA)*AREA)
    4 IF(UORD.EQ.2) PSUM=PSUM+(P*2.0)
    2 CONTINUE
C
C BECAUSE OF DOUBLING FOR SYMMETRY, THE ABOVE LOOP DID NOT INCLUDE THE
C CASE. CALCULATE VALUES FOR THIS CASE AND ADD TO SUMS
C
      CALL PROB (0.0,ETA,W,P,SIGU,SIGC)
      IF(ANGU.GT.1.5707963.OR.ANGU.LT.-1.5707963) GO TO 1
      SLC=TAN(DANGC)
      SLOPE=((SLU*SLU)+(SLC*SLC))**0.5
      THETA=ATAN(SLOPE)
      CALL ROES(THETA,REF)
      X=ATAN(Y)
      AREA=1.0/COS(X)
      SINJ=SIN(THETA)/1.3333
      XJ=ASIN(SINJ)
      IF(UORD.EQ.1) X=COS(XJ)
      IF(UORD.EQ.2) X=COS(THETA)/COS(XJ)
      SUM=SUM+((1.0-REF)*X*P*AREA)
      IF(UORD.EQ.1) PSUM=PSUM+(P*COS(THETA)*AREA)
    1 IF(UORD.EQ.2) PSUM=PSUM+P
C
C CALCULATE FACTOR TO NORMALIZE PROBABILITY DISTRIBUTION FUNCTION
C
      XNORM=1.0/PSUM
      IF(UORD.EQ.2) XNORM=XNORM/COS(ZENITH)
C
C NORMALIZE SUM OF THE REFLECTANCES
C
      SUM=SUM*XNORM
C
C CALCULATE SURFACE TRANSMITTANCE
C
      TRANS=SUM
      PHI=PHI*57.29578
      DELANG=DELANG*57.29578
      RETURN
      END
```

```
      SUBROUTINE PLTAPY (VW,A)
C
C     ****** A ******************************************************
C
C  THIS SUBROUTINE LOADS REFLECTANCE VALUES INTO THE APPROPRIATE LOCATIONS IN
C  AN ARRAY TO BE PRINTED TO FORM THE PLOT OF SPECTRAL REFLECTANCE.
C  POINTS ARE ENTERED AT 10 NM INTERVALS WITH LINEAR INTERPOLATION SUPPLYING
C  THE VALUES WHERE ACTUAL MEASUREMENTS DO NOT EXIST.  VALUES BELOW 0.0
C  AND ABOVE 0.25 ARE TRUNCATED.
C
C     ****** A ******************************************************
C
C     VW IS THE ARRAY CONTAINING REFLECTANCE VALUES FROM THE CALLING PROGRAM
C
C     A IS THE PRINT ARRAY RETURNED TO THE CALLING PROGRAM
C
C     ****** A ******************************************************
C
      DIMENSION VW(20),A(29,7)
      DIMENSION POINT(10)
      DIMENSION EVW(58)
      INTEGER A,POINT,BLANK
      DATA BLANK/'          '/
      DATA POINT(1)/67777777777777777779/
      DATA POINT(2)/77677777777777777773/
      DATA POINT(3)/77776777777777777773/
      DATA POINT(4)/77777767777777777773/
      DATA POINT(5)/77777777677777777773/
      DATA POINT(6)/77777777767777777773/
      DATA POINT(7)/77777777777677777773/
      DATA POINT(8)/77777777777767777773/
      DATA POINT(9)/77777777777777767773/
      DATA POINT(10)/77777777777777777673/
C
C     BLANK OUT PREVIOUS DATA IN A
C
      DO 4 I=2,7
      DO 4 J=1,25
    4 A(J,I)=BLANK
C
C     PERFORM LINEAR INTERPOLATION TO EXPAND ORIGINAL REFLECTANCE VALUES
C     INTO 58 VALUES AT 10 NM INTERVALS
C
      J=-2
      EVW(1)=0.0
      EVW(2)=VW(4)
      EVW(3)=VW(4)+((VW(5)-VW(4))/2.0)
      EVW(4)=VW(5)
      EVW(5)=VW(5)+((VW(6)-VW(5))/4.0)
      EVW(6)=VW(5)+((VW(6)-VW(5))/2.0)
      EVW(7)=VW(5)+((VW(6)-VW(5))/1.333)
      EVW(8)=VW(6)
      EVW(9)=VW(6)+((VW(7)-VW(6))/4.0)
      EVW(10)=VW(6)+((VW(7)-VW(6))/2.0)
      EVW(11)=VW(6)+((VW(7)-VW(6))/1.333)
      EVW(12)=VW(7)
      EVW(13)=VW(7)+((VW(8)-VW(7))/3.0)
```

```
      EVW(14)=VW(7)+((VW(8)-VW(7))/1.5)
      EVW(15)=VW(8)
      EVW(16)=VW(8)+((VW(9)-VW(8))/3.0)
      EVW(17)=VW(8)+((VW(9)-VW(8))/1.5)
      EVW(18)=VW(9)
      EVW(19)=VW(9)+((VW(10)-VW(9))/4.0)
      EVW(20)=VW(9)+((VW(10)-VW(9))/2.0)
      EVW(21)=VW(9)+((VW(10)-VW(9))/1.333)
      EVW(22)=VW(10)
      EVW(23)=VW(10)+((VW(11)-VW(10))/3.0)
      EVW(24)=VW(10)+((VW(11)-VW(10))/1.5)
      EVW(25)=VW(11)
      EVW(26)=VW(11)+((VW(12)-VW(11))/4.0)
      EVW(27)=VW(11)+((VW(12)-VW(11))/2.0)
      EVW(28)=VW(11)+((VW(12)-VW(11))/1.333)
      EVW(29)=VW(12)
      EVW(30)=VW(13)
      EVW(31)=VW(13)+((VW(14)-VW(13))/4.0)
      EVW(32)=VW(13)+((VW(14)-VW(13))/2.0)
      EVW(33)=VW(13)+((VW(14)-VW(13))/1.333)
      EVW(34)=VW(14)
      EVW(35)=VW(14)+((VW(15)-VW(14))/4.0)
      EVW(36)=VW(14)+((VW(15)-VW(14))/2.0)
      EVW(37)=VW(14)+((VW(15)-VW(14))/1.333)
      EVW(38)=VW(15)
      EVW(39)=VW(15)+((VW(16)-VW(15))/5.0)
      EVW(40)=VW(15)+((VW(16)-VW(15))/2.5)
      EVW(41)=VW(15)+((VW(16)-VW(15))/1.667)
      EVW(42)=VW(15)+((VW(16)-VW(15))/1.25)
      EVW(43)=VW(16)
      EVW(44)=VW(16)+((VW(17)-VW(16))/3.0)
      EVW(45)=VW(16)+((VW(17)-VW(16))/1.5)
      EVW(46)=VW(17)
      EVW(47)=VW(17)+((VW(18)-VW(17))/2.5)
      EVW(48)=VW(17)+((VW(18)-VW(17))/2.5)
      EVW(49)=VW(17)+((VW(18)-VW(17))/1.667)
      EVW(50)=VW(17)+((VW(18)-VW(17))/1.25)
      EVW(51)=VW(18)
      EVW(52)=VW(18)+((VW(19)-VW(18))/3.0)
      EVW(53)=VW(18)+((VW(19)-VW(18))/1.5)
      EVW(54)=VW(19)
      EVW(55)=VW(19)+((VW(20)-VW(19))/4.0)
      EVW(56)=VW(19)+((VW(20)-VW(19))/2.0)
      EVW(57)=VW(19)+((VW(20)-VW(19))/1.333)
      EVW(58)=VW(20)
C
C     LOAD EXPANDED REFLECTANCE ARRAY INTO PRINT ARRAY
C
      IDY=1
      IS=8
      DO 5 I=1,58
      X=(EVW(I)*100.0)+0.5
      IVW=X
      IF(IVW.GT.25) IVW=25
      IF(IVW.LT.0) IVW=0
      IDX=26-IVW
      IS=IS+1
```

```
      IF(IS.GT.10) IDY=IDY+1
      IF(IS.GT.10) IS=1
      IF(IDX.EQ.25) GO TO 5
      A(IDX,IDY)=A(IDX,IDY).AND.POINT(IS)
    5 CONTINUE
      RETURN
      END
```

```
      SUBROUTINE SKY (W,SKYTRN,SKYREF)
C
C   ****************************************************************************
C
C THIS SUBROUTINE CALCULATES THE TRANSMISSION OF LIGHT ACROSS THE AIR-WATER
C INTERFACE AS A FUNCTION OF WIND VELOCITY.  THE REFLECTANCE OF
C SKYLIGHT IS ALSO CALCULATED
C
C   ****************************************************************************
C
C       W IS WIND VELOCITY IN METERS/SECOND SUPPLIED BY THE CALLING PROGRAM
C
C       SKYTRN IS THE SKYLIGHT TRANSMISSION FACTOR RETURNED TO THE CALLING PR
C
C       SKYREF IS THE SKYLIGHT REFLECTANCE RETURNED TO THE CALLING PROGRAM
C
C   ****************************************************************************
C
      IF(SKYREF.LT.0.0001) GO TO 1
      GO TO 2
    1 SKYREF=0.0266
      IF(W.GT.0.5) SKYREF=0.02
    2 IF(W.GT.5.0) SKYTRN=1.133+(0.0006*(W-5.0))
      IF(W.LE.5.0) SKYTRN=1.122+(0.0022*W)
      RETURN
      END
```

```
      SUBROUTINE ROES(THETA,REF)
C
C ************************************************************
C
C THIS SUBROUTINE CALCULATES THE REFLECTANCE OF THE AIR-WATER INTERFACE
C FOR UNPOLARIZED LIGHT USING FRESNEL'S EQUATION AND ASSUMING N = 1.333
C
C ************************************************************
C
C     THETA IS THE ANGLE OF INCIDENCE IN RADIANS MEASURED WITH RESPECT TO THE
C     SURFACE NORMAL - SUPPLIED BY THE CALLING PROGRAM
C
C     REF IS THE CALCULATED SURFACE REFLECTANCE - RETURNED TO CALLING PROGRAM
C
C ************************************************************
C
      REAL I,J,IPJ,IMJ
      IF(THETA.LT.0.0174533) GO TO 1
      I=THETA
      SI=SIN(I)
      SJ=SI/1.3333
      J=ASIN(SJ)
      IPJ=I+J
      IMJ=I-J
      SSIPJ=SIN(IPJ)*SIN(IPJ)
      SSIMJ=SIN(IMJ)*SIN(IMJ)
      TSIPJ=TAN(IPJ)*TAN(IPJ)
      TSIMJ=TAN(IMJ)*TAN(IMJ)
      REF=0.5*((SSIMJ/SSIPJ)+(TSIMJ/TSIPJ))
      GO TO 777
    1 REF=0.0204082
  777 RETURN
      END
```

```
      SUBROUTINE PROB (XI,ETA,W,P,SIGU,SIGC)
C
C ****. ***********************************************************
C
C THIS SUBROUTINE CALCULATES THE PROBABILITY OF OCCURANCE OF A GIVEN SEA
C SLOPE WHEN WIND VELOCITY IS KNOWN. THE CALCULATION IS BASED ON A GENERALI
C PROBABILITY DISTRIBUTION FUNCTION
C THIS APPROACH IS BASED ON THE WORK OF COX AND MUNK (1956)
C
C ****. ***********************************************************
C
C     XI AND ETA ARE THE 'STANDARDIZED' CROSS- AND UPWIND SLOPE COMPONENTS
C     SUPPLIED BY THE CALLING PROGRAM
C
C     W IS THE WIND VELOCITY IN M/SEC - SUPPLIED BY THE CALLING PROGRAM
C
C     P IS THE CALCULATED PROBABILITY (UNNORMALIZED) - RETURNED TO THE
C     CALLING PROGRAM
C
C     CALCULATED FROM WIND VELOCITY AND RETURNED TO THE CALLING PROGRAM
C
C ***********************************************************************
C
C CALCULATE THE SLOPE STANDARD DEVIATIONS FOR CROSS- AND UPWIND DIRECTIONS
C
      SIGC=((0.003+(0.00512*W))/2.0)**0.5
      SIGU=SIGC
C
C CALCULATE THE INDIVIDUAL TERMS IN THE PROBABILITY DISTRIBUTION FUNCTION
C
      A=0.15915/(SIGU*SIGC)
      B=-0.5*((XI*XI)+(ETA*ETA))
C
C CALCULATE PROBABILITY
C
      P=A*(2.71828**B)
  777 RETURN
      END
```

APPENDIX C

ALGOR

PROGRAM LISTING

```
      PROGRAM ALGOR(INPUT,OUTPUT,TAPE5=INPUT,TAPE6=OUTPUT,PUNCH)
C
C ***********************************************************************
C
C THIS PROGRAM TAKES AS INPUT PUNCHED CARDS OUTPUT BY VOLREF WHICH
C CONTAIN WATER VOLUME REFLECTANCE AND WATER SAMPLE ANALYSIS DATA.
C FROM THIS DATA MULTISPECTRAL QUADRATIC ALGORITHMS ARE CALCULATED TO
C PREDICT ANY OF THE SAMPLE ANALYSIS PARAMETERS FROM SELECTED WAVELENGTHS
C
C ***********************************************************************
C
C THIS PROGRAM IS INTENDED FOR USE WITH DATA GENERATED BY THE EPA EMSL/LV
C SPECTROMETER WHICH SAMPLES 20 WAVELENGTHS. THUS DIMENSIONS OF ARRAYS ARE
C SET ACCORDINGLY
C
C THE MAXIMUM TRAINING SET SIZE IS 200
C
      DOUBLE PRECISION COV
      DIMENSION COV(57,57),PHI(40),IUSE(40),DATA(40,200),V(41),COM(8)
      DIMENSION VP(40)
      DIMENSION GT(200,9),ZTUR(20)
      DATA END/'END       '/
      XNS=0.0
C
C READ IN PARAMETERS FOR THIS RUN
C
      READ(5,96) NC,XNOISE,IPAR,IPUNCH
   96 FORMAT(I10,F10.0,2I10)
      READ(5,95) (IUSE(I),I=1,40,2)
   95 FORMAT(20I4)
      NC=NC*2
      DO 80 I=1,40,2
      IF(IUSE(I).EQ.0) GO TO 150
      J=I+1
      IUSE(I)=(IUSE(I)*2)-1
      IUSE(J)=IUSE(I)+1
   80 CONTINUE
  150 READ(5,94) ZTUR
   94 FORMAT(10F8.0)
      READ(5,98) COM
   98 FORMAT(8A10)
      WRITE(6,97) COM
   97 FORMAT(1H1,8A10//13H SAMPLES USED/)
C
C LOOP ON SAMPLES READING IN TRAINING SET DATA
C
      DO 1 I=1,200
      READ(5,99) SAMPNO,(GT(I,J),J=1,9)
   99 FORMAT(A10,9F7.0)
      IF(SAMPNO.EQ.END) GO TO 405
      XNS=XNS+1.0
      WRITE(6,120) SAMPNO
  120 FORMAT(1X,A10)
      READ(5,100) (DATA(N,I),N=1,40,2)
  100 FORMAT(10F8.0)
C
C SUBTRACT ZERO TURBIDITY REFLECTANCE VALUES AND SQUARE DATA
```

```
C
      L=0
      DO 1 J=1,40,2
      K=J+1
      L=L+1
      DATA(J,I)=DATA(J,I)-ZTUP(L)
      DATA(K,I)=DATA(J,I)*DATA(J,I)
    1 CONTINUE
C
C CLACULATE MATRIX X TRANSPOSE X AND VECTOR XG
C
  405 NS=XNS
      DO 300 I=1,NS
      DO 3 J=1,NC
      DO 3 K=1,NC
      L=IUSE(J)
      M=IUSE(K)
    3 COV(J,K)=COV(J,K)+(DATA(L,I)*DATA(M,I))
      DO 4 L=1,NC
      M=IUSE(L)
    4 PHI(L)=PHI(L)+(GT(I,IPAR)*DATA(M,I))
  300 CONTINUE
C
C ADD RANDOM NOISE BY EXPANDING DIAGONAL ELEMENTS
C
      X=1.0+XNOISE
      DO 404 II=1,40
  404 COV(II,II)=COV(II,II)*X
C
C INVERT X TRANSPOSE X MATRIX
C
      CALL MATINV(COV,NC,DET)
C
C CALCULATE COEFFICIENTS V PRIME
C
      DO 6 I=1,NC
      DO 6 J=1,NC
    6 VP(I)=VP(I)+(COV(I,J)*PHI(J))
C
C CONVERT V PRIME TO V WHICH OPERATES ON UNCORRECTED DATA
C
      DO 7 I=1,40,2
      J=I+1
      K=(IUSE(I)+1)/2
      IF(K.EQ.0) GO TO 9
      V(J)=VP(J)
    7 V(I)=VP(I)-(2.0*VP(J)*ZTUR(K))
    9 DO 8 I=1,40,2
      J=I+1
      K=(IUSE(I)+1)/2
      IF(K.EQ.0) GO TO 13
    8 V(41)=V(41)+(VP(J)*ZTUR(K)*ZTUR(K))-(VP(I)*ZTUR(K))
C
C WRITE OUT COEFFICIENT VECTOR V
C
   13 WRITE(6,301)
  301 FORMAT(14H1WEIGHT VECTOR//)
```

```
      WRITE(6,112) V
  112 FORMAT(8E15.8/)
      WRITE(6,113)
  113 FORMAT(1H1)
C
C APPLY ALGORITHM TO TRAINING SET DATA
C
      WRITE(6,102)
  102 FORMAT(25H TRAINING SET REPORT CARD//10X,12HGROUND TRUTH,10X,18HRE
     1MOTE MEASUREMENT,13X,5HERROR/)
      ERRTOT=0.0
      DO 10 I=1,NS
      P=0.0
      DO 11 J=1,NC
      L=IUSE(J)
   11 P=P+(VP(J)*DATA(L,I))
      ERR=P-GT(I,IPAR)
C
C WRITE AND PUNCH TRAINING SET ERROR DATA
C
      WRITE(6,110) GT(I,IPAR),P,ERR
  110 FORMAT(12X,F7.2,17X,F7.2,17X,F7.2)
      IF(IPUNCH.EQ.0) GO TO 310.
      PUNCH 121,GT(I,IPAR),P,ERR
  121 FORMAT(3F10.2)
  310 ERRTOT=ERRTOT+(ERR*ERR)
   10 CONTINUE
C
C CALCULATE AND WRITE RMS PREDICTION ERROR FOR TRAINING SET
C
      ERRTOT=ERRTOT/XNS
      ERRTOT=SQRT(ERRTOT)
      WRITE(6,111) ERRTOT
  111 FORMAT(1X,///10H RMS ERROR,10X,F6.2)
      STOP
      END
```

```
      SUBROUTINE MATINV(ARRAY,NORDER,DET)
      DOUBLE PRECISION ARRAY,AMAX,SAVE,A,B,C
      DIMENSION ARRAY(57,57),IK(57),JK(57)
   10 DET=1.0
   11 DO 100 K=1,NORDER
C
C FIND LARGEST ELEMENT ARRAY(I,J) IN REST OF MATRIX
C
      AMAX=0.0
   21 DO 30 I=K,NORDER
      DO 30 J=K,NORDER
      A=DABS(AMAX)
      B=ARRAY(I,J)
      C=DABS(B)
   23 IF(A-C) 24,24,30
   24 AMAX=ARRAY(I,J)
      IK(K)=I
      JK(K)=J
   30 CONTINUE
C
C INTERCHANGE ROWS AND COLUMNS TO PUT AMAX IN ARRAY(K,K)
C
   31 IF(AMAX) 41,32,41
   32 DET=0.0
      GO TO 140
   41 I=IK(K)
      IF(I-K) 21,51,43
   43 DO 50 J=1,NORDER
      SAVE=ARRAY(K,J)
      ARRAY(K,J)=ARRAY(I,J)
   50 ARRAY(I,J)=-SAVE
   51 J=JK(K)
      IF(J-K) 21,61,53
   53 DO 60 I=1,NORDER
      SAVE=ARRAY(I,K)
      ARRAY(I,K)=ARRAY(I,J)
   60 ARRAY(I,J)= -SAVE
C
C ACCUMULATE ELEMENTS OF INVERSE MATRIX
C
   61 DO 70 I=1,NORDER
      IF(I-K) 63,70,63
   63 ARRAY(I,K)= -ARRAY(I,K)/AMAX
   70 CONTINUE
   71 DO 80 I=1,NORDER
      DO 80 J=1,NORDER
      IF(I-K) 74,80,74
   74 IF(J-K) 75,80,75
   75 ARRAY(I,J)=ARRAY(I,J)+ARRAY(I,K)*ARRAY(K,J)
   80 CONTINUE
   81 DO 90 J=1,NORDER
      IF(J-K) 83,90,83
   83 ARRAY(K,J)=ARRAY(K,J)/AMAX
   90 CONTINUE
      ARRAY(K,K)=1.0/AMAX
  100 DET=DET*AMAX
C
```

```
C RESTORE ORDERING OF MATRIX
C
  101 DO 130 L=1,NORDER
      K=NORDER-L+1
      J=IK(K)
      IF(J-K) 111,111,105
  105 DO 110 I=1,NORDER
      SAVE=ARRAY(I,K)
      ARRAY(I,K)=-ARRAY(I,J)
  110 ARRAY(I,J)=SAVE
  111 I=JK(K)
      IF(I-K) 130,130,113
  113 DO 120 J=1,NORDER
      SAVE=ARRAY(K,J)
      ARRAY(K,J)=-ARRAY(I,J)
  120 ARRAY(I,J)=SAVE
  130 CONTINUE
  140 RETURN
      END
```

TECHNICAL REPORT DATA

(Please read Instructions on the reverse before completing)

1 REPORT NO	2.	3 RECIPIENT'S ACCESSION NO
EPA-600/4-80-019		

4 TITLE AND SUBTITLE	5 REPORT DATE
MULTISPECTRAL TECHNIQUES FOR REMOTE MONITORING OF SEDIMENT IN WATER: A feasibility investigation	March 1980
	6. PERFORMING ORGANIZATION CODE

7. AUTHOR(S)	8. PERFORMING ORGANIZATION REPORT NO
Ronald J. Holyer	

9 PERFORMING ORGANIZATION NAME AND ADDRESS	10. PROGRAM ELEMENT NO.
Lockheed Electronics Company, Inc. 4220 S. Maryland Parkway Suite 120 Las Vegas, Nevada 89109	1HD620
	11. CONTRACT/GRANT NO.

12 SPONSORING AGENCY NAME AND ADDRESS	13. TYPE OF REPORT AND PERIOD COVERED
U.S. Environmental Protection Agency--Las Vegas, NV Office of Research and Development Environmental Monitoring Systems Laboratory Las Vegas, Nevada 89114	14. SPONSORING AGENCY CODE EPA/600/07

15. SUPPLEMENTARY NOTES

NTIS-Only distribution

16. ABSTRACT

A data acquisition and analysis program has been undertaken to demonstrate the feasibility of remote multispectral techniques for monitoring suspended sediment concentrations in natural water bodies. Two hundred surface albedo measurements (400 to 1,000 nanometers) were made at Lake Mead with coincident water sampling for laboratory analysis. Water volume spectral reflectance was calculated from the recorded surface albedo, and volume reflectance-suspended sediment relationships were investigated. Statistical analysis has shown that quantitative estimates of nonfilterable residue (105°C) and nephelometric turbidity can be made from volume spectral reflectance data with sufficient accuracy to make the multispectral technique feasible for sediment monitoring.

17 KEY WORDS AND DOCUMENT ANALYSIS

a DESCRIPTORS	b IDENTIFIERS/OPEN ENDED TERMS	c COSATI Field/Group
remote sensing turbidity spectroscopy suspended sediment water quality	Lake Mead multispectral techniques	08 H 13 B 14 B 20 F

18. DISTRIBUTION STATEMENT	19 SECURITY CLASS *(This Report)*	21 NO OF PAGES
RELEASE TO PUBLIC	UNCLASSIFIED	174
	20 SECURITY CLASS *(This page)*	22 PRICE
	UNCLASSIFIED	

EPA Form 2220-1 (9-73)

INSTRUCTIONS

1. **REPORT NUMBER**
Insert the EPA report number as it appears on the cover of the publication.

2. **LEAVE BLANK**

3. **RECIPIENTS ACCESSION NUMBER**
Reserved for use by each report recipient.

4. **TITLE AND SUBTITLE**
Title should indicate clearly and briefly the subject coverage of the report, and be displayed prominently. Set subtitle, if used, in smaller type or otherwise subordinate it to main title. When a report is prepared in more than one volume, repeat the primary title, add volume number and include subtitle for the specific title.

5. **REPORT DATE**
Each report shall carry a date indicating at least month and year. Indicate the basis on which it was selected *(e.g., date of issue, date of approval, date of preparation, etc.)*.

6. **PERFORMING ORGANIZATION CODE**
Leave blank.

7. **AUTHOR(S)**
Give name(s) in conventional order *(John R. Doe, J. Robert Doe, etc.)*. List author's affiliation if it differs from the performing organization.

8. **PERFORMING ORGANIZATION REPORT NUMBER**
Insert if performing organization wishes to assign this number.

9. **PERFORMING ORGANIZATION NAME AND ADDRESS**
Give name, street, city, state, and ZIP code. List no more than two levels of an organizational hirearchy.

10. **PROGRAM ELEMENT NUMBER**
Use the program element number under which the report was prepared. Subordinate numbers may be included in parentheses.

11. **CONTRACT/GRANT NUMBER**
Insert contract or grant number under which report was prepared.

12. **SPONSORING AGENCY NAME AND ADDRESS**
Include ZIP code.

13. **TYPE OF REPORT AND PERIOD COVERED**
Indicate interim final, etc., and if applicable, dates covered.

14. **SPONSORING AGENCY CODE**
Leave blank.

15. **SUPPLEMENTARY NOTES**
Enter information not included elsewhere but useful, such as: Prepared in cooperation with, Translation of, Presented at conference of, To be published in, Supersedes, Supplements, etc.

16. **ABSTRACT**
Include a brief *(200 words or less)* factual summary of the most significant information contained in the report. If the report contains a significant bibliography or literature survey, mention it here.

17. **KEY WORDS AND DOCUMENT ANALYSIS**
(a) DESCRIPTORS - Select from the Thesaurus of Engineering and Scientific Terms the proper authorized terms that identify the major concept of the research and are sufficiently specific and precise to be used as index entries for cataloging.

(b) IDENTIFIERS AND OPEN-ENDED TERMS - Use identifiers for project names, code names, equipment designators, etc. Use open-ended terms written in descriptor form for those subjects for which no descriptor exists.

(c) COSATI FIELD GROUP - Field and group assignments are to be taken from the 1965 COSATI Subject Category List. Since the majority of documents are multidisciplinary in nature, the Primary Field/Group assignment(s) will be specific discipline, area of human endeavor, or type of physical object. The application(s) will be cross-referenced with secondary Field/Group assignments that will follow the primary posting(s).

18. **DISTRIBUTION STATEMENT**
Denote releasability to the public or limitation for reasons other than security for example "Release Unlimited." Cite any availability to the public, with address and price.

19. & 20. **SECURITY CLASSIFICATION**
DO NOT submit classified reports to the National Technical Information service.

21. **NUMBER OF PAGES**
Insert the total number of pages, including this one and unnumbered pages, but exclude distribution list, if any

22. **PRICE**
Insert the price set by the National Technical Information Service or the Government Printing Office, if known.